QUANTITATIVE RISK ASSESSMENT OF A MARINE RISER: AN INTEGRATED APPROACH

MUDDASSIR NAZIR


CENTRE FOR NFLD. STUDIES
MEMORIAL UNIVERSITY
OF NEWFOUNDLAND

QUANTITATIVE RISK ASSESSMENT OF A MARINE RISER: AN INTEGRATED APPROACH

by

©Muddassir Nazir

A thesis submitted to the

School of Graduate Studies

in partial fulfillment of the

requirements for the degree of

Doctor of Philosophy

Faculty of Engineering and Applied Science

Memorial University of Newfoundland

December, 2007

St. John's Newfoundland Canada

Abstract

This work presents an integrated risk assessment methodology for structural failure of a marine riser and the consequent release of oil causing ecological risks to marine life.

A simple, but efficient methodology for fatigue reliability assessment of a vertical top-tensioned rigid riser is proposed. The fatigue damage response is considered as a narrow-band Gaussian stationary random process with a zero mean for the short-term behavior. However, non-linearity in a response associated with Morison-type wave loading is accounted for by using a factor, which is the ratio of expected damage according to a non-linear probability distribution to the expected damage according to a linear method of analysis. Long-term non-stationary response is obtained by summing up a large number of short-term stationary responses. Uncertainties associated with both strength and stress functions of the limit state are quantified by a lognormal distribution. A closed form reliability analysis is carried out, which is based on the limit state function formulated in terms of Miner's cumulative damage rule. The results thus obtained are compared with the well-documented lognormal format of reliability analysis based on time to fatigue failure. The validity of selecting a lognormal hazard rate function for fatigue life is discussed. A Monte Carlo simulation technique is also used as a reliability assessment method. A simple algorithm is used to reduce the large uncertainty associated with direct sampling. Uncertainty arises in the direct sampling technique because of using a small number of simulations in calculating small failure probabilities. A worked example is included to show the practical riser design problem based on reliability analysis.

As a part of the ecological risk assessment, a fugacity-based methodology is presented to predict the multimedia fate of spilled oil in a marine environment. A level IV (dynamic) fugacity-based methodology coupled with weathering processes is presented. A two-compartment system, comprised of water and sediment, is used to explore the fate of oil. During a spill, oil is entrained into the water column due to natural dispersion, which is considered as the primary input source to the water compartment. Direct input to the sediment compartment is assumed negligible. However, the water column acts as a source to the sediment compartment. Unlike the conventional multimedia modelling approach, the impact area is not predefined; rather the oil slick spreading process determines the contaminated area growth. Naphthalene is used as an indicator for oil. To demonstrate the application of the proposed methodology, simulations for a batch spill scenario of Statfjord oil are also presented. The current study suggests that the water compartment response to the chemical input is faster than the sediment compartment. The major fate processes identified are advection and volume growth in water and sediment, respectively.

The current study has used the U.S. EPA ecological risk assessment (ERA) framework to estimate the effects on marine life due to underwater release of oil and gas from a broken riser. This approach combines the hydrodynamics of underwater blowout, weathering algorithms, and multimedia fate and transport to measure the exposure

concentration. Uncertainties related to multimedia input parameters are incorporated in the analysis. The 95th percentile of the exposure concentration ($EC_{95\%}$) is taken as the representative exposure concentration (as a conservative value). A bootstrapping method is utilized to characterize $EC_{95\%}$ and associated uncertainty. Toxicity data available in the literature are used to calculate the 5th percentile of the 'predicted no observed effect concentration' ($PNEC_{5\%}$) using bootstrapping. The risk is characterized based on the cumulative distribution of risk quotient (RQ), which is defined as the ratio of $EC_{95\%}$ to $PNEC_{5\%}$.

This thesis describes a probabilistic basis for the ERA, which is essential from risk management and decision making viewpoints. Two case studies of underwater oil and gas mixture release, and oil release with no gaseous mixture, are used to show the systematic implementation of the methodology, elements of ERA, and the probabilistic method in assessing and characterizing the risk.

Acknowledgements

I would like to extend my deep gratitude to my supervisors Dr. Faisal Khan, Dr. Paul Amyotte and Dr. Rehan Sadiq for their guidance, help, and support throughout the course of my Ph.D. degree. Without their untiring and selfless cooperation I would have never been able to achieve the present level of understanding and the quality of my research work.

I am thankful to Dr. Mahmoud Haddara for his willingness to serve as a member of the thesis committee.

I gratefully acknowledge the financial support from my supervisory committee and the school of graduate studies, Memorial University of Newfoundland.

I express my thanks to the faculty members who have imparted in me valuable knowledge while doing my graduate courses.

I thank my parents for their wholehearted support, encouragement and blessings. They have very kindly supported me morally during my hectic study hours.

Finally, I am personally indebted to my friends for providing me with pleasant and friendly living while staying at St. Johns. Thank you all.

Table of Contents

List of Figures

List of Tables

List of Symbols[1]

A	constant derived from distillation data
A_C	asphaltene content
A_S	area of slick
A_{Sp}	area of spill associated with source strength
a	crack size, parameter used in Equation (2.41)
B	constant derived from distillation data
BF	bio-available fraction
$\hat{B}$	ratio of actual stress to estimated stress; Equation (3.3)
B_{WX}	effective diffusivity
b	empirical material constant as used in the S-N approach, local radius of the plume element
b_G	plume radius following the Gaussian distribution at the exit
C	confidence level, material property used in Equations (2.29) and (2.31), concentration
$COV(x_i, x_j)$	covariance
CV	coefficient of variation
C_A	added mass coefficient
C_D	drag coefficient
C_M	hydrodynamic inertia coefficient
C_W	water column concentration
C_b	rotational stiffness of the riser base
C_i	concentration of a compound constituting the oil
C_3	final fraction water content
C_4	a constant $\in$ [1, 10]; where 1 is for light substances such as gasoline, and 10 is for crude oils.
C^s	aqueous solubility
c	empirical material constant as used in the S-N approach

$\hat{c}$	variable material property
D	various transport processes as defined in Table 4.3
$D(t)$	accumulated damage
D_a	fraction of sea surface dispersed per hour
D_b	faction of the dispersed oil not returning to the slick
d	parameter used in Equation (2.41), diameter of riser
d_r	depth of oil release
E	Young's modulus of elasticity
EC	exposure concentration
$EC_{95\%}$	the 95th percentile of exposure concentration
$E[\ ]$	expectation of a variable
$F(z,t)$	fluid force per unit length (Morison-type wave loading)
F_E	volume fraction evaporated
F_I	inertia force per unit length, as defined in Equation (3.10)
F_D	drag force per unit length, as defined in Equation (3.11)
F_i	non-normal cumulative distribution of random variables X_i
f	fugacity
$f(b,K)$	ratio of non-linear to linear expected fatigue damages as defined in Equation (3.18)
f_i	density of random variables X_i
G	performance/ limit state function, volumetric flow rate
GOR	gas to oil rato
g	gravitational acceleration
$g(\bullet)$	function of a quantity
$\overline{g}(\bullet)$	mean value of performance function; Equation (2.6)
H	Henry's law constant
H_s	significant wave height
H'	dimensionless Henry's law constant

h	slick thickness, plume element thickness
h_S	sediment depth
h_W	depth of the water compartment
I	moment of inertia about neutral axis
$I(\bullet)$	indicator function
$I_2(t)$	emission rate into the water column
K	stress intensity factor, drag inertia parameter as defined in Equation (3.25)
K_{OC}	organic carbon-water coefficient
K_{OW}	octanol-water partition coefficient
K_1	constant with default value of 150 s^{-1}
K_2	mass transfer coefficient for evaporation
k	reaction rate constant
k_{bw}	bioconcentration factor
k_{sw}	sorbent partition coefficient
ΔK	range of stress intensity factor
L	length of riser
$LC50$	lethal concentration corresponding to 50% mortalilty
MW	molecular weight
m	material property, mass per unit length
m_b	bubble mass of the control volume
m_k	kth spectral moment
m_l	liquid mass of the control volume
m_A	added mass of seawater
N	number of trials, number of fatigue cycles, rate of a process
N_ξ	number of cycles to failure at a constant stress amplitude (ξ)
N_f	number of cycles of failure

n_ξ	number of cycles less than failure cycles at a constant stress amplitude (ξ)
PC	predicted exposure concentration
$PNEC_{5\%}$	the 5th percentile of predicted no effect concentration
P_f	probability of failure
$\overline{P}_f$	sample mean of the probability of failure
P^s	vapor pressure
Q_f	forced entrainment
Q_s	shear-induced entrainment Q_s
Q_{ent}	oil volumetric flow rate
Q_{gas}	gas release rate
Q_{oil}	oil release rate
R	structural strength/resistance, gas constant (8.314 Pa·m^3/mol·K), radius of the water compartment
R_e	reliability
RQ	risk quotient
S	resultant stress, sensitivity of a parameter , oil salinity
S_a	ambient salinity
S_m	standard deviation of the lognormally transformed data, obtained from the CHARM model
S_{St}	source strength
S_η	single sided power spectrum of surface elevation
s_t	oil-water interfacial tension
T	time period, absolute temperature
T_G	gradient of the boiling point, T_B, and fraction evaporation, F_E, line
T_m	mean period
T_{max}	time corresponds to the peak of hazard rate function

T_O	initial boiling point at zero evaporation
$T_r(z)$	effective riser tension
T_s	intended service life of a structure
T_z	mean zero crossing period
$\hat{T}$	time to fatigue failure
t	time
t_{res}	residence time
t_{Sp}	spill duration
Δt	small discrete time step
U_c	horizontal current velocity
U_r	radial velocity
U_{Bur}	sediment solids' burial rate
U_{DS}	suspended solid deposition rate
U_{RS}	sediment re-suspension rate
u	horizontal velocity component of the plume element
u_a	average current speed
$V(t)$	horizontal displacement of the floating structure
V_m	volume of spilled oil
V_O	initial volume of spilled oil (m^3)
$\vec{V}$	local centerline jet/plume velocity
$\vec{V}_C$	depth-averaged current velocity
$\vec{V}_W$	wind velocity at 10 m above the mean water surface level
v	lateral velocity component of the plume element
$w(z,t)$	horizontal displacement of water particles due to surface waves
w	vertical velocity component of the plume element

w_b	slip velocity
w_m	centerline velocity following the Gaussian distribution at the exit
X	original coordinate system
$X(t)$	random process
$X(z,t)$	horizontal deflection of the riser
X_i	random variables
X_m	average of the lognormally transformed data, obtained from the CHARM model
X_i^*	design points on the failure surface in original coordinate system; Equation (2.14)
$\bar{x}_i s$	mean values of random variables $X_i s$
Y	reduced/normalized coordinate system, fraction of water in oil
$Y(a)$	function of crack geometry
Y_i	reduced/normalized variables; Equation (2.11)
Y_i^*	design points in reduced coordinate system; Equation (2.17)
W	wind speed
Z	various fugacity capacities as explained in Table 4.3
z	vertical distance from riser base
$\sim$	represents median value of random variables
ρ	densities of a mixture, seawater
ρ_b	density of biota, local density of bubble
ρ_s	density of sorbent
σ^2 / Var	variance
σ	standard deviation
$\Phi(\bullet)$	standard normal distribution function; $N \sim (0,1)$
$\phi(\bullet)$	density functions for the standard normal variate
ϕ	various organic fractions of dispersed phases as described in Table 4.3, angle between jet trajectory and the water surface

θ	jet angle with respect to x-axis
$\Gamma(\bullet)$	Gamma function
$\alpha(x)$	parameter as defined in Equations (3.26) and (3.28)
α_C	current drift factor
α_W	wind drift factor
$\beta(x)$	parameter as defined in Equations (3.27) and (3.29)
β	reliability index, entrainment coefficient
β_o	target reliability index
Δ	fatigue damage parameter
Δ_S	diffusion path length in sediment
$\hat{\Delta}$	fatigue damage variable
Ω	parameter as defined by Equations (2.39) and (2.40)
λ	rainflow correction parameter
λ_i	half the wavelength of a lightly damped tensioned string
λ_d	half the wavelength of a highly damped tensioned string
δ	damping parameter
ε	spectral width parameter, bubble fraction
ω_z	mean zero-up crossing
$(\bar{x}_i^N, \sigma_X^N)$	parameters of the equivalent normal distribution; Equations (2.19) and (2.20)
$\gamma(a,z)$	incomplete Gamma function
$\Gamma(a,z)$	incomplete Gamma function
η	water surface elevation following normal distribution $N \sim (0, \sigma_\eta)$
$\dot{\eta}$	derivative of water surface elevation with $N \sim (0, \sigma_{\dot{\eta}})$
ω	angular frequency
ω_n	natural frequency
$\mu_{\ln(\bullet)}$	mean of the lognormal distribution

μ	viscosity
μ_O	parent oil viscosity
v	volume fractions of sub-compartments in a multimedia marine environment as defined in Table 4.3

[1] If the above illustration of any symbol conflicts with the illustration of that symbol given in the following text then preference should be given to the illustration, which is provided in the following chapters.

Chapter 1

Introduction

A marine riser is the critical component of offshore oil and gas production systems that links the floating unit (e.g. a vessel or a semi-submersible) to the seabed manifold. Due to large economical and environmental risks associated with riser's failure, its safe design/operation is of great importance for the offshore oil and gas (OOG) industry. The results of environmental risk analysis become vital to evaluate scenarios of oil and gas release in a case of breach of structural reliability of the riser.

This research has been conducted to integrate the structural reliability of a rigid marine riser with the associated environmental risk. The structural failure risk associated with the riser design life is assessed using the reliability-based method. The environmental risk is evaluated by simulating the behavior of an underwater oil and gas release from the riser using an ecological risk assessment framework.

1.1 Background

The increasing demand of energy recourses due to industrial development and rapid population growth has accelerated the search for new sources of oil and gas. With the advancement in technology, oil and gas explorations have gone into a deepwater: depth > 300 m (MMS, 1997). There are many active deepwater sites for oil and gas production, which include: the Gulf of Mexico, the North Sea, offshore West Africa, and offshore Brazil. In Newfoundland and Labrador, Orphan Basin site can be characterized

as the deepwater site, which is likely to be gas prone at the depth range of approximately 1000 to 3000 m.

Due to a rapid increase in the offshore oil and gas production activities, the potential for oil and gas release from marine risers has also increased significantly. In case of the North Sea risers, pipeline and riser loss of contaminant (PARLOC) study documented seven incidents of contaminant loss during a period 1975-1993 (Robertson *et al.*, 1995). The failure data are presented in Table 1.1. There is much practical significance to use the risk-based design methods that improve the safety and reliability of offshore structures. Further, the development of coastal oil spill contingency plans requires prediction of the fate/transport of oil in the marine environment in case of structural failure.

Subsequent sections present brief discussions on riser's configuration and its design, and fate and impact of released oil in a marine environment.

1.1.1 Riser Configuration and Design

There are three main categories of risers:

(i) drilling risers

(ii) workover/completion risers

(iii) export/production/injection risers

Drilling risers are rigid with vertical configuration. They contain a rigid internal drill pipe. Workover/completion risers are also rigid and commonly have vertical configurations. The external casing contains an internal pipe for transportation of system components and tools required for the various operations.

Table 1.1 Riser failure statistics (1975-1993)*

Location of Incident	Pipeline Diameter Range		
	2-8 inch	**10-16 inch**	**>16 inch**
Splash Zone	1 (0-20mm) 1 (Rupture)	1 (Rupture)	1 (Rupture)
Subsea		1 (0-20mm) 1 (20-80mm)	
Unknown		1 (Rupture)	

*Robertson *et al.* (1995)

Production/export/injection risers transport fluid (oil and gas) from the seabed to the surface and vice versa. The most severe consequences of failure are typically associated with these risers. A wide variety of different configurations exist under this riser category.

Vertical top-tensioned rigid risers are historically the most commonly employed for production. Tension force is applied to prevent the buckling of a long and slender riser to reduce deflections. These risers may also be non-rigid without any requirement of top tensioning. Leira (1998) provided details of configurations, operations and functional requirements for these riser categories.

There are two basic codes in practice to design a riser (Bai, 2001):

1) working stress design (WSD)

2) limit state design (LSD)

The LSD is the most popular design method and accounts for the following:

i) serviceability limit state (SLS)

ii) ultimate limit state (ULS)

iii) fatigue limit state (FLS)

iv) progress collapse limit state (PLS)

The SLS design criterion ensures the serviceability requirements of the riser system. The ULS accounts for the structure safety under a static response. The static behavior modelling always employed deterministic calculations in the design (Hughes, 1983). Safety factors are applied to service loads and the structure is safely designed for yielding, bursting, buckling, etc. For example, API RP1111 (1998) provides the guidelines for the safe burst pressure design. The provision of the static behavior in the ULS is employed on structural synthesis process in establishing the basic dimension (wall thickness) of the riser. The FLS meets the safety criterion for a dynamic response under a dynamic loading, such as: wave loading, floater motion and vortex induced vibrations (VIV) due to currents.

Accidental events (corrosion, dropped objects, loss of pre-tension etc.) are taken into account using PLS design criteria. In general, the limit state includes safety of the structure against collapse, limitations on damage or other safety criteria. A structural failure not only causes production and economic loses but also causes environmental damage. The fate of released fluid, in the case of riser failure, and its impact is discussed in a later section.

1.1.2 Fate of Released Oil/Gas and Associated Impacts

Evaluation of the risk associated with accidental oil/gas release is vital for an offshore facility. It helps in identifying the potential hazard to aquatic entities. Various studies have been reported on simulating spill of a mixture of oil and gas from underwater accidents such as, McDougall (1978), Fannelop and Sjoen (1980), Fannelop

et al. (1991), Yapa and Zheng (1997), Johansen (2000), and Zheng *et al.* (2002). These researchers addressed the complexity of the spill problem to the different extent.

One of the governing parameters in modelling the spill behavior is the depth of oil and gas release. In shallow to moderate depths an oil and gas plume reaches the sea surface within a few minutes (Yapa and Zehng, 1997). On reaching the surface the released oil makes a thin slick and a sizeable quantity of the gas enters the atmosphere from a turbulent bubble area that forms above the plume. A wide variety of physicochemical and biological processes transform an oil slick. The transformation process is called *weathering*, which influences the composition, routes of exposure and toxicity of discharged oil. Due to the weathering, the oil components start mixing with the water column and the sediment pore water (MMS, 1997). FOCS (2002) reported the effects of the weathered oil on aquatic life. According to this report, the spilled oil may have lethal or sub-lethal effects on aquatic life and their supporting ecosystems. Once the fate of contaminants in the water column and the sediment pore water is determined, the results can be used in the ecological risk assessment.

1.2 Risk Terminology

Covello and Merkhofer (1992) define *risk* as follows:

"Risk is, at minimum, a two-dimensional concept involving (1) the possibility of an adverse outcome, and (2) uncertainty over the occurrence, timing, or magnitude of that adverse outcome. If either attribute is absent, then there is no risk."

Another definition of *risk* as documented in CMPT (1999) is:

"Risk is the combination of the likelihood and consequence of accidents."

Accidents are the actual realization of a hazard. *Hazard* is commonly defined as: *the potential to cause harm.*

A systematic process in which the *risk* posed by hazardous substances, processes, and events are estimated either quantitatively or qualitatively is known as "Risk Assessment". Generally, risk assessment involves the definition of the system and its boundaries, identification of an adverse event, assessment of likelihoods, and consequences. Qualitative/subjective risk assessment uses judgment and expert opinion to evaluate the probability and consequence values. However, quantitative/objective risk method relies on probabilistic and statistical methods and risk is quantified in terms of the numerical probability values. Quantitative risk assessment (QRA) accounts for uncertainties in the parameters defining a complex engineering system. QRA has long been a part of risk-based offshore structural design and assesses time-dependent failure probabilities for corrosion, fatigue, buckling, and permanent deformations. CMPT (1999) provides a comprehensive guideline for QRA of offshore installations. U.S. EPA (1998) has also established a framework for the quantification of ecological risk assessment.

The benefits of QRA include safe and more cost-effective engineering designs, operations, and maintenance planning. The outcomes of risk assessment provide help for informed decision making, and it is an integral part of *Risk Management.* This is a process of weighting alternatives (options), selecting the most appropriate action, and integrating the results of risk assessment with engineering data, social, economic, and political concerns to make an acceptable decision. Generally the risk assessment process involves objectivity, whereas risk management involves preferences and attitudes, which

have objective and subjective elements (Asante-Duah, 1993). Economic models can be employed to perform tradeoffs among risk mitigation options to keep the risk at an acceptable level. In this connection, QRA helps in keeping the balance between economics and safety of oil and gas production (CMPT, 1999). The four primary risk mitigation methods are (Ayyub, 2003): 1) risk reduction, 2) risk transfer (e.g., to a contractor or an insurance company), 3) risk avoidance, 4) risk pooling (e.g., joint ventures and partnerships). Risk acceptance constitutes a definition of "safety"; therefore the level of risk acceptance is often subject to much debate.

1.3 Fatigue Reliability

Fatigue is commonly used in engineering to describe repeated load phenomena and their effects on the strength of a structure (Assakkaf and Ayyub, 2000). It is estimated that 50–90% of structural failure is due to fatigue (Hancq et al., 2000); therefore structural engineers should consider this vital phenomenon in their designs, especially for those structures and their structural components that are exposed to cyclic loading.

For offshore structures, potential cyclic loading that can cause fatigue damage includes: wave induced hydrodynamic forces, platform motion, vortex-induced-vibrations (VIV), and thermal expansion loads. There are two major approaches for fatigue life prediction: 1) the S-N curve approach, and (2) the fracture mechanics approach. The fatigue life of an offshore structure is subjected to large uncertainties, due to highly uncertain environmental forces and structural response of the marine structure in terms of fatigue strength and damage accumulation. In the past, it was common to determine an average performance by cycling a component under supposed service

conditions. The average life was then divided by a safety factor to obtain the service life. The typical values of the safety factor used to be 2 to 20. However, the committee on fatigue and fracture reliability (ASCE, 1982) and Nilsen and Hanson (1995) pointed out that a structure design using safety factors *a priori* does not ensure a uniform level of safety for all design situations. For example, if the level of uncertainty varies among designs, the application of the same safety factor to all of them will by no means provide consistent reliability levels. Contrary, for the different target reliability levels for portions of the structure (depending on the consequence of failure or ease of repair, or both) the allowable stress approach cannot be used to accomplish these goals consistently without considering uncertainties. Consistent safety levels in structures can be achieved using reliability-based design criteria.

Reliability-based methods are the tools for optimal structural designs at the acceptable level of risks. These methods also provide the basis for the code calibration of partial safety factors. Assakkaf and Ayyub (2000) used reliability theory in developing a load and resistance factor design (LRFD) methodology for fatigue design of surface ships.

1.4 Objectives

This research is aimed at providing an integrated approach for structural failure of a marine riser and the associated ecological risk. A layout of the current research is presented in Figure 1.1. The research has following main objectives:

1. to develop a reliability-based technique for estimating the design life of a rigid riser using fatigue criterion in a simple and time efficient but effective framework;

2. to model the fate/transport of contaminants in the case of riser damage;

3. to quantify ecological risk.

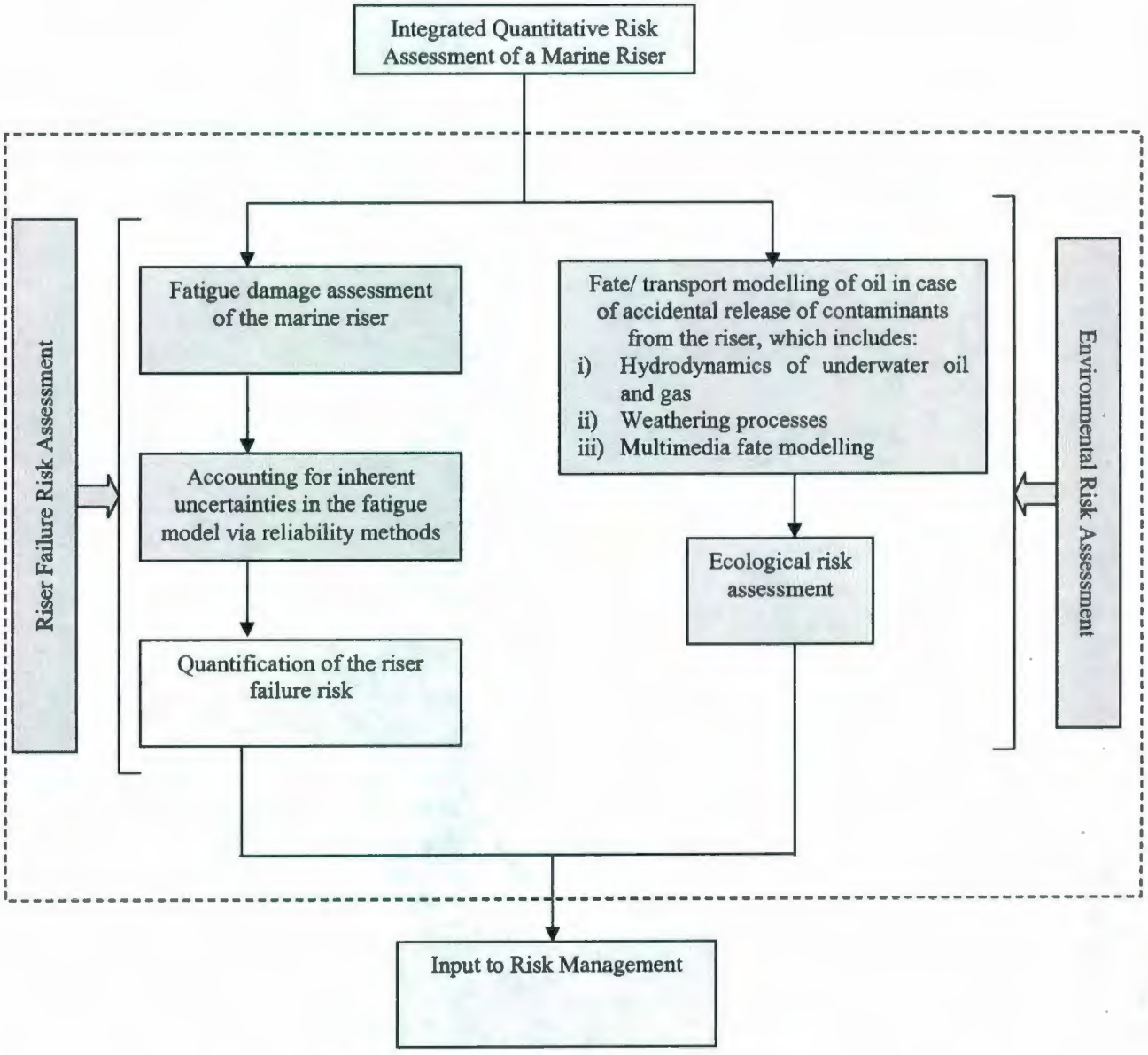

Figure 1.1 Layout of the proposed research

The main objective of the research is the quantification of structural and environmental risks of a marine riser, which will help in improved design and operation of the riser.

1.5 Organization of the Thesis

The thesis is organized into six chapters. Chapter 1 introduces the riser problem and the scope of the research. Chapter 2 reviews methods for risk-based structural design. A brief discussion about the fatigue assessment methods is also presented. Chapter 3 develops a methodology for reliability-based riser fatigue design. This chapter also demonstrates an application with reference to the calculation of riser fatigue life.

In Chapter 4, an integrated modelling approach is presented to predict the multimedia fate of oil spills in a marine environment. In this context, a case study of surface oil release is conducted to show the practical application of fate modelling methodology. The chapter also deals with the identification of significant transport processes in a marine environment. In Chapter 5, ecological risk assessment (ERA), due to accidental oil release from the riser is carried out based on U.S. EPA (1998) ecological risk assessment framework. Two case studies are used to demonstrate the ERA framework for assessing and characterizing ecological risks.

Chapter 6 provides the conclusions of the present research. Recommendations are also made for the future research work related to the risk-based riser design. Finally, it summarizes the novelty and contribution of the present work. Figure 1.2 illustrates sequence of the thesis to achieve the objectives outlined above.

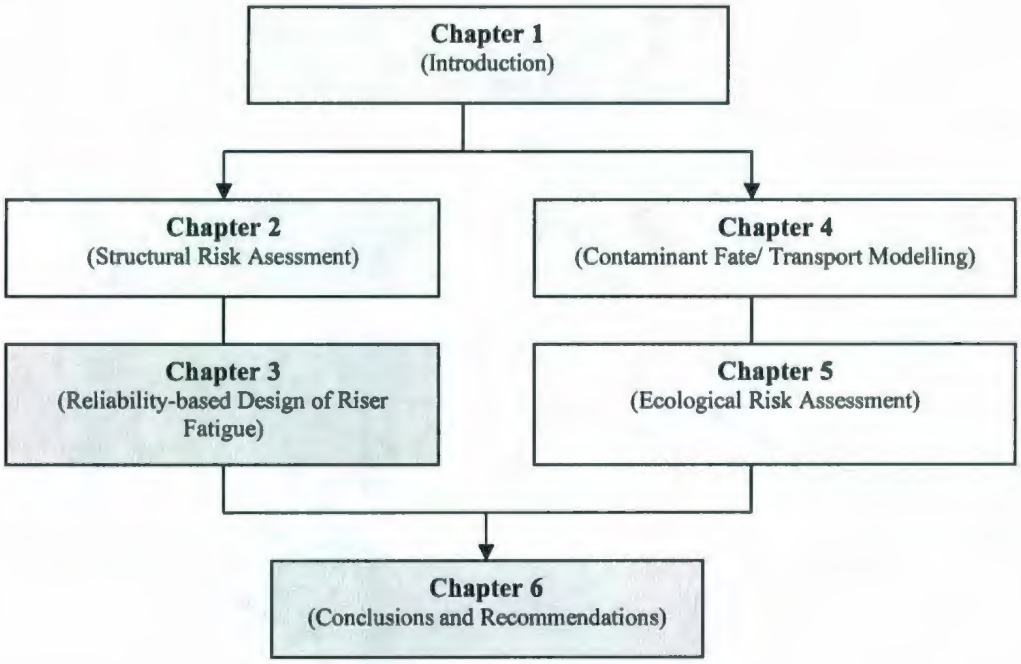

Figure 1.2 Organization of the thesis

Chapter 2
Structural Risk Assessment

Reliability-based design methods provide the basis for structural risk assessment of a marine riser. This chapter provides a review of the reliability methods used for structural risk assessment. Because fatigue is the most common degradation mechanism in material strength and stiffness, the structural risk is quantified in fatigue units.

2.1 Structural Risk Quantification

Risk is defined here as a probability of failure P_f of the riser structure during its intended design life. A structural element is considered failed if its resistance, R, is less than the resultant stress, S, acting on it during its design life. The P_f can be presented mathematically as:

$$P_f = p(R \le S) \tag{2.1}$$

or

$$P_f = p(R - S \le 0) \tag{2.2}$$

Risk (probability of failure) of an element can be determined on a performance function that can be expressed in terms of independent and/or dependent variables (X_i) for relevant stresses and structural strength. Mathematically it is described as:

$$G = g(X_1, X_2, ..., X_n) = R - S \tag{2.3}$$

where G is the performance/limit state function.

The failure surface (the limit state) can be defined as $G = 0$. At $G < 0$ the element would be in the failure domain. If the joint probability density function for the basic random variables (X_i) is $f_{X_1, X_2 \ldots, X_n}(x_1, x_2, \ldots, x_n)$, then the P_f of the element can be given by the integral (Ayyub, 2003):

$$P_f = \int \ldots \int f_{X_1, X_2 \ldots, X_n}(x_1, x_2, \ldots, x_n) dx_1 dx_2 \ldots . dx_n \tag{2.4}$$

where the integration is performed over the region of $G < 0$. In general, the joint probability density function is unknown and the integral in Equation (2.4) becomes a formidable task.

Reliability of a structure, R_e, is defined as the probability that it performs its intended functions over its intended design life. It may be considered as the probability of success. Reliability is the complement of risk (probability of limit state violation). Limit state includes safety of the structure against collapse, limitations on damage or other safety criteria. Reliability can be expressed as:

$$R_e = 1 - P_f \tag{2.5}$$

2.2 Reliability-Based Methods

Numerous methods are available in the literature for reliability assessment. These methods are based on resistance-and-stress performance function. This section provides a brief review of two reliability assessment methods: (1) the first–order second–moment method, and (2) the Monte Carlo simulation method using 'direct' and 'conditional expectation'.

2.2.1 First–Order Second–Moment Reliability Method

To avoid the computational difficulties of Equation (2.4), the first order second moment (FOSM) reliability method is commonly used in structural reliability analysis. Consider a general case in which G is a function of several random variables as given in Equation (2.3). The approximate first order mean and variance of G may be calculated by expanding the function $g(X_1, X_2, ...X_n)$ through Taylor series about the mean values of X_is and truncating the series at the linear terms, that is:

$$\bar{g} = g(\bar{x}_1, \bar{x}_2, ...\bar{x}_n) \tag{2.6}$$

and

$$\sigma_G^2 \approx \sum_{i=1}^{N}\left(\frac{\partial g}{\partial X_i}\right)^2 \sigma_{x_i}^2 + \sum_{i\neq}^{N}\sum_{j}^{N}\left(\frac{\partial g}{\partial X_i}\right)\left(\frac{\partial g}{\partial X_j}\right) COV(X_i, X_j) \tag{2.7}$$

where $\bar{g}$ is the mean value of G, σ_G^2 and σ_G are variance and standard deviation of G respectively, $\bar{x}_i s$ are the mean values of random variables $X_i s$, and $COV(x_i, x_j)$ represents the covariance.

The partial derivatives of $g(X_1, X_2, ...X_n)$ are evaluated at the mean values of all random variables. The approximate mean may be improved considering the square term in the Taylor series and known as second order approximation of mean of G:

$$\bar{g} \approx g(\bar{x}_1, \bar{x}_2, ...\bar{x}_n) + \frac{1}{2}\sum_{i=1}^{n}\sum_{j=1}^{n}\left(\frac{\partial^2 g}{\partial X_i \partial X_j}\right) COV(X_i, X_j) \tag{2.8}$$

However, the estimation of the second order variance is much more involved and the use of the second order mean and the first order variance are adequate for most engineering applications (Ayyub and Haldar, 1984).

If G is assumed to follow a normal distribution then the probability of failure can be given by the following expression:

$$P_f = 1 - \Phi(\beta) \tag{2.9}$$

where

$\Phi(\bullet)$ is the standard normal distribution function, $N \sim (0,1)$;

β is known as *reliability index* and conventionally prescribed as:

$$\beta = \frac{\bar{g}}{\sigma_G} \tag{2.10}$$

If σ_G remains constant then increasing β will cause the mean of the performance function to increase and will reduce the probability of failure. The concept of reliability index is shown graphically in Figure 2.1.

This approximate method has a few shortcomings. It linearizes the function at the mean values of the variables and the selection of the appropriate linearizing point is critical (Hasofer and Lind, 1974; ASCE, 1982; Ayyub and Haldar, 1984; PERD, 1993; Ayyub, 2003). A significant error may be introduced by neglecting the higher order terms in the Taylor series expansion of the function. It is an approximate method and ignores the information on distribution type of the random variables. It is valid only when the $X_i s$ variables are assumed normally distributed and the function $\mathbf{g(X)}$ is linear.

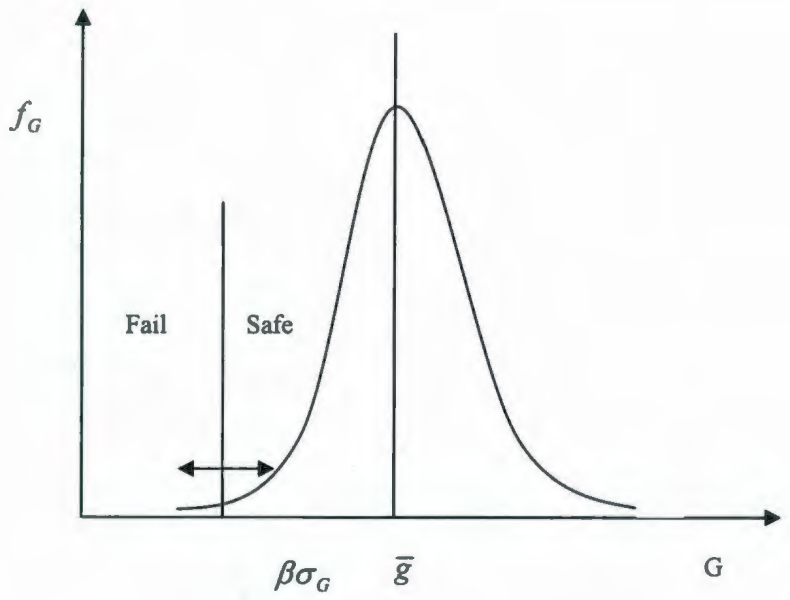

Figure 2.1 Concept of reliability index (β)

To overcome the aforementioned shortcomings, the Taylor series expansion of G is linearized at some point on the failure surface g(**X**) = 0: referred to as the design point, say $\left(X_1^*, X_2^*, ..., X_n^*\right)$. Conventionally all random variables $X_i s$ are first transformed to their standardized form N ~ (0,1) using the well known transformation:

$$Y_i = \frac{X_i - \bar{x}_i}{\sigma_{X_i}} \tag{2.11}$$

This transformation results in a reduced/normalized coordinate system. In the Y space, the joint density function is the standardized multivariate normal and many well-known properties of multivariate normal distribution can be easily applied (Hasfor and Lind, 1974). The reliability index, β, is the shortest distance to the failure surface from the origin in the reduced/normalized Y coordinate system (Figure 2.2).

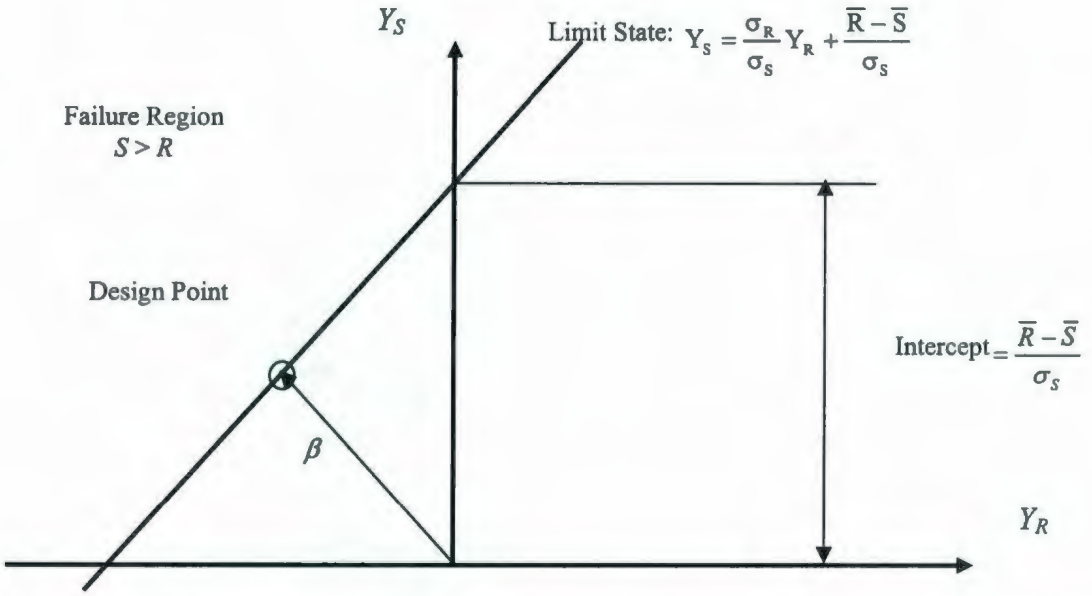

Figure 2.2 Performance function for a linear, two-random variable case in reduced coordinates (modified from Ayyub, 2003)

The limit state ($G = 0$) from Equation (2.3) implies $S = R$, which in the reduced/normalized coordinate becomes:

$$Y_S = \frac{\sigma_R}{\sigma_S} Y_R + \frac{\overline{R} - \overline{S}}{\sigma_S} \tag{2.12}$$

The concept of the shortest distance from the origin to the line of Equation (2.12) is shown in Figure 2.2.

The reliability index β can be calculated in both the reduced coordinate system (i.e., Y coordinate) or the original coordinate system (i.e., X coordinate). Using the original X coordinate system, the design point $\left(X_1^*, X_2^*, ..., X_n^*\right)$ and the reliability index β can be determined by solving the following system of non-linear equations iteratively for β (Ayyub and Haldar, 1984):

$$\alpha_i = \frac{\left(\frac{\partial G}{\partial X_i}\right)\sigma_{X_i}}{\left[\sum_{i=1}^{n}\left(\frac{\partial G}{\partial X_i}\sigma_{X_i}^2\right)^2\right]^{\frac{1}{2}}} \tag{2.13}$$

$$X_i^* = \bar{x}_i - \alpha_i \beta \sigma_{X_i} \tag{2.14}$$

$$g\left(X_1^*, X_2^*, ..., X_n^*\right) = 0 \tag{2.15}$$

The partial derivatives in the above set of equations are evaluated at the design point and the values α_i are the directional cosines of random variables. In the reduced Y coordinate system the following expressions are used (Melchers, 1987):

$$\alpha_i = \frac{\left(\frac{\partial G}{\partial Y_i}\right)}{\left[\sum_{i=1}^{n}\left(\frac{\partial G}{\partial Y_i}\right)^2\right]^{\frac{1}{2}}} \tag{2.16}$$

$$Y_i^* = -\alpha_i \beta \tag{2.17}$$

$$g\left(Y_1^*, Y_2^*, ..., Y_n^*\right) = 0 \tag{2.18}$$

When all the basic random variables are normally distributed, the relationship between the probability of failure and β can be given by Equation (2.9). However, in many applied structural engineering problems, the design variables are non-normal (Ayyub and Halder, 1984). The non-normal probability distributions can be incorporated in the above stated reliability analysis by transforming the non-normal variables into equivalent normal variables. Considering the cumulative distribution functions and the probability density functions of the actual variables and the approximate normal variables

equal at the design point on the failure surface, would give the parameters $(\bar{x}_i^N, \sigma_X^N)$ of the equivalent normal distribution. Mathematically (Rackwitz and Fiessler, 1978):

$$\sigma_{X_i}^N = \frac{\phi\left(\Phi^{-1}\left[F_i(X_i^*)\right]\right)}{f_i(X_i^*)} \tag{2.19}$$

$$\bar{x}_i^N = X_i^* - \Phi^{-1}\left[F_i(X_i^*)\right]\sigma_{xi}^N \tag{2.20}$$

where F_i and f_i are the non-normal cumulative distribution and density functions of X_i, and $\Phi(.)$ and $\phi(.)$ are the cumulative distribution and density functions for the standard normal variate, respectively. After calculating $\bar{x}_i^N$ and $\sigma_{X_i}^N$ for each random variable, the system of equations (2.13-2.15) can be solved to obtain the value of β. The algorithm of this method is summarized in Figure 2.3.

The aforementioned method is applicable only to uncorrelated variables. If $X_i s$ are correlated, then they must be transformed to uncorrelated random variables. The procedures are quite involved and details are given in textbooks including Melchers (1987), and Ayyub (2003). Moreover, in reliability analysis of fatigue for offshore structures, the random variables are generally considered uncorrelated (ASCE, 1982; Wirsching 1984; Wirsching and Chen, 1988; PERD, 1993; Souza and Goncalves, 1997; Ayyub et al. 2002; and Ayyub, 2003). The discussion on correlated variables is, therefore, beyond the scope of this thesis.

In the first order reliability method the failure surface is approximated by a tangent hyperplane at the design point.

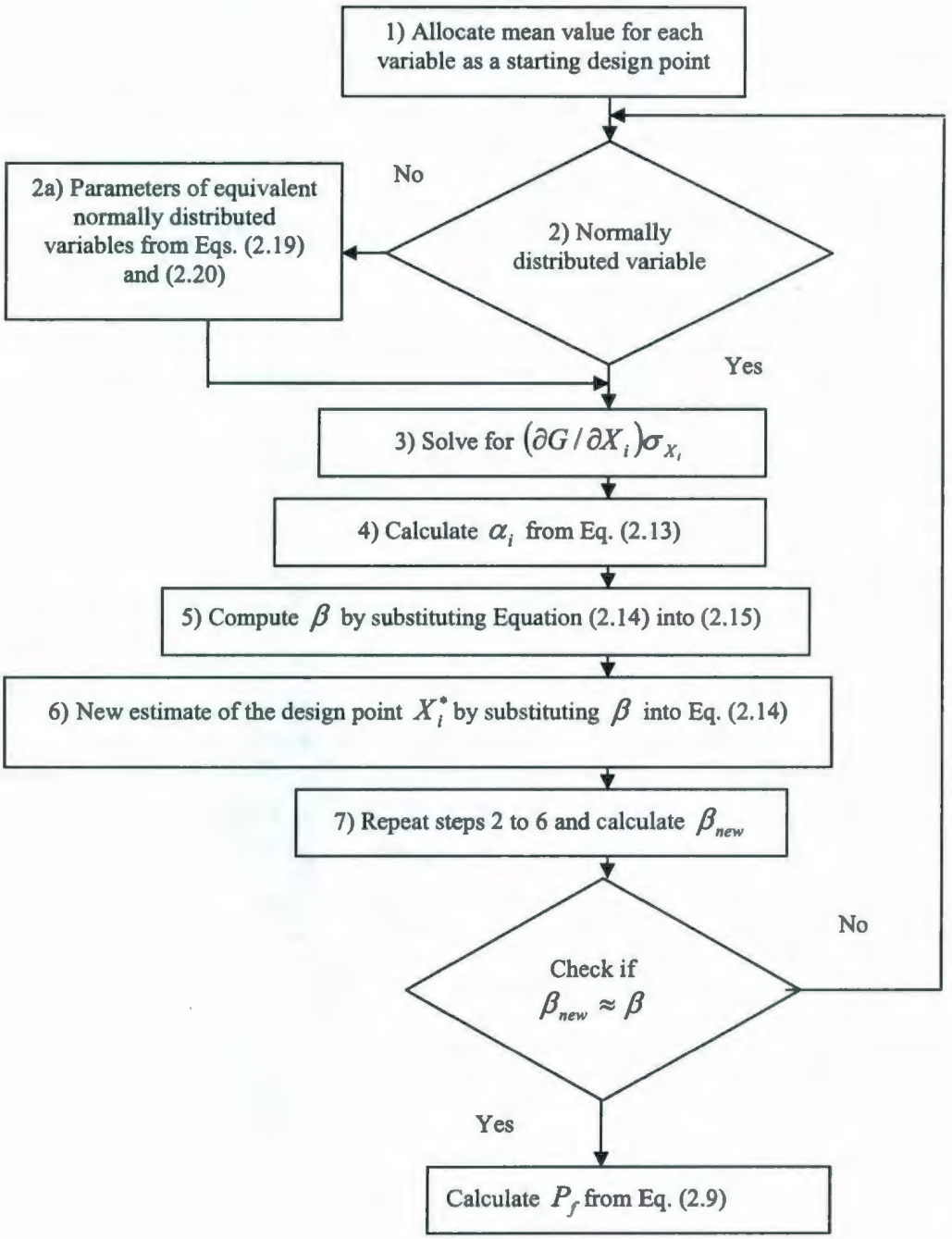

Figure 2.3 Algorithm for FOSM method for uncorrelated variables in original coordinate

The method is capable of dealing with non-linear normal functions and non-normal probability distribution. However, the accuracy of the solution and convergence of the procedure depend on the non-linearity of the performance function in the vicinity of the design point and the origin. Second-order reliability methods (SORM) utilize quadratic approximations instead. The accuracy of a non-linear limit state solution can be improved by employing the SORM method. Breitung (1984) gave a simple closed-form solution for the probability computation using a second-order approximation. Breitung's SORM method uses a parabolic approximation and it ignores the mixed terms and their derivatives in the Taylor series approximation. The Breitung method is based on the theory of asymptotic approximation and is suitable only for large values of β, which is the case for practical high-reliability problems.

Tvedt's SORM method uses a parabolic and a general second-order approximation to the limit state, and it is not based on asymptotic approximations. The main disadvantage of the general curvature-based scheme is that it requires high computation efforts in solving the matrix of second-order derivatives, known as the Hessian (PERD, 1993). For further details, reference is made to Tvedt (1990).

If a limit state function is expressed as the product of k independent lognormal variables for relevant stress and structural strength, then a closed form solution for the failure probability can be obtained (discussed in Chapter 3).

2.2.2 Simulation-Based Methods

The Monte Carlo simulation approach is often used to estimate the probabilistic characteristics of the limit state function given by Equation (2.3). In the 'Direct' Monte

Carlo technique, the independent variables are sampled at random. After feeding them in a performance function, sample points of G are obtained. Each point is checked to see whether it is inside or outside the failure domain. This is accomplished in the simulation by using the indicator function $I(X)$:

$$I(X)=\begin{cases}1, G(X)\le 0\\ 0, G(X)>0\end{cases} \tag{2.21}$$

where $G(X)$ is the performance function.

The indicator function is evaluated at each sampled point. The failure probability is estimated as the average number of hits in the failure domain during the N trials, which can be presented as:

$$P_f \approx \frac{1}{N}\sum_{i=1}^{N} I(X_i) \tag{2.22}$$

Obviously the number of trials (N) required is directly related to the desired accuracy for P_f. Broding et al. (1964) suggested that a first estimate of the N simulations for a given confidence level C in the failure probability P_f can be obtained from:

$$N > \frac{-\ln(1-C)}{P_f} \tag{2.23}$$

At a 95% confidence level with $P_f = 10^{-3}$, the required number of simulations is more than 3000. Error analysis using Shooman's (1968) recommendation of calculating N shows that for N = 10,000 samples with expected $P_f = 10^{-3}$, the error in P_f will be less than 20% at 95% confidence. Others have recommended the number of simulations

in the range of 10,000-20,000 (Melchers, 1987). The estimated failure probability should approach the true value when N approaches infinity (Ayyub, 2003). The variance of the estimated probability failure can be approximately measured using the variance expression for a binomial distribution as:

$$Var(P_f) \approx \frac{(1-P_f)P_f}{N} \tag{2.24}$$

The coefficient of variation (CV) would be:

$$CV(P_f) \approx \frac{1}{P_f}\sqrt{\frac{(1-P_f)P_f}{N}} \tag{2.25}$$

At the desired P_f value of 0.01 and N = 1000, the magnitude of CV from Equation (2.25) would be 0.315. To avoid higher level of uncertainty at $P_f = 0.001$, the N should be increased from 1,000 to 10,000.

The direct simulation can be computationally prohibitive for small failure probabilities. To control the high uncertainty associated with direct sampling approach, variance reduction techniques (VRT) may be used. This method uses the given information about the problem during simulations. In fact, if no statistical information about the problem is known, then it cannot be applied (Rubinstein, 1977). Sometimes, results from direct simulations can also be used to define variance reduction techniques that improve the efficiency of second simulation. There are various VRT techniques. Here, the conditional expectation technique is discussed, which will be used in the analysis in the next chapter.

The conditional expectation method requires conditioning of one or more basic variables of least variability in the performance function. The random variable with the highest variability is not generated and is used as a control variable. The control variable can also be selected on the basis of being able to reduce the performance function to an analytically acceptable form.

The probability of failure during each cycle P_{fi} is calculated using the probabilistic characteristics of the control variable. Therefore the sample mean of the probability of failure is given by (Ayyub, 2003):

$$\overline{P}_f = \frac{\sum_{i=1}^{N} P_{fi}}{N} \tag{2.26}$$

The uncertainty in terms of coefficient of variation (CV) associated with this estimation can be expressed as:

$$CV_{\overline{P}_f} = \frac{\sqrt{Var(\overline{P}_f)}}{\overline{P}_f} \tag{2.27}$$

where

$$Var(\overline{P}_f) = \frac{\sum_{i=1}^{N} (P_{fi} - \overline{P}_f)^2}{N(N-1)} \tag{2.28}$$

The discussion associated with fatigue damage, which is used in the performance function to quantify risk, is given in the following section.

2.3 Fatigue Damage Assessment

Fatigue is the most common degradation mechanism in material strength and stiffness due to cyclic stress-strain operation. Fatigue failures are attributed to dynamic response (either a deflection, a strain, or a stress), which is a random process $X(t)$, of a stable structure. These do not include failures under fixed or random static loads, failures due to static or dynamic instability, or failures caused by corrosion and abrasion (Lin, 1967). Fatigue failure occurs when the damage to the structure accumulates to a critical level (allowable fatigue strength); this is due to $X(t)$ fluctuations at small and moderate excursions which are not large enough to cause first-excursion failures.

Fatigue Reliability involves the measure of fatigue damage and resistance over fatigue lifetime. Expressions used for the fatigue damage assessment are described in Maddox and Wildenstein (1975), Maddox (1975), Nolte and Hansford (1976), ASCE (1982), Wirsching (1984); Wirsching and Chen (1988); PERD (1993); and Ayyub et al. (2002). There are two major approaches for evaluating fatigue life prediction (ASCE, 1982; and Assakkaf and Ayyub, 2000): (1) the fracture mechanics approach, and (2) the characteristic S-N approach.

2.3.1 The Fracture Mechanics Approach

The approach is based on crack growth data. It involves determining the number of load cycles that cause initial defects to grow into the cracks of critical sizes. The rate at which a crack grows can be expressed as the Paris-Erdogan (1963) power law:

$$\frac{da}{dN} = C\Delta K^m \tag{2.29}$$

where

C and m = empirical material parameters;

a = crack size;

N = number of fatigue cycles;

ΔK = range of stress intensity factor.

The stress intensity factor K accounts for the magnitude of the stress, current crack size, and weld and joint details.

$$\Delta K = SY(a)\sqrt{\pi a} \tag{2.30}$$

where $Y(a)$ is a function of crack geometry. Equation (2.29) always applied to variable stress range models that ignore sequence effects (Byers et al. 1997).

Rearrangement and integration of Equation (2.29) gives the relation of the number of cycles of failure, N_f, to the size of the initial flaw length, a_o, and the critical crack length, a_c. Mathematically:

$$N_f = \frac{1}{CS^m}\int_{a_o}^{a_c}\frac{da}{\left[Y(a)\sqrt{\pi a}\right]^m} \tag{2.31}$$

Since the stress process is a random process, each stress range is a random variable and the interest lies in the calculation of expected/mean value of S^m. Assuming narrow band stress, the Rayleigh distribution can be used to calculate the expected value of S^m, which can be given as (PERD, 1993):

$$E\left[S^m\right] = \left(2\sqrt{2}\sigma_S\right)^m \Gamma\left(1+\frac{m}{2}\right) \tag{2.32}$$

where

$\Gamma(\bullet)$ = Gamma function;

σ_S = root mean square stress.

The material properties, such as C and m, and the value of critical crack size have inherent uncertainties (PERD, 1993). These uncertainties can be accounted for via reliability-based methods in fatigue design.

2.3.2 The Characteristic S-N Approach

The classical approach to describe fatigue life is based on the S-N curve approach. The S-N curve is based on experimental data obtained from deterministic loading conditions and is represented mathematically as (PERD, 1993):

$$NS_a^b = c \tag{2.33}$$

where S_a is stress amplitude, N is number of cycles to failure and b and c are positive empirical material constants. Equation (2.33) holds for all values of $S_a > 0$ for models in which an endurance limit does not exist.

The problem in calculating fatigue life using the S-N curve is to establish a rational means of combining test data based on cyclic stresses of fixed amplitude and frequency to predict the real structural failure under the range of amplitudes and frequencies of concern. Miner (1945) gave the solution of this problem in the form of a linear cumulative damage or Miner's rule. It is based on the S-N curve, which gives the number of cycles to failure, N_ξ, at a constant stress amplitude ξ. The basic assumption behind Miner's rule is that if a certain stress level is applied for only $n_\xi < N_\xi$ cycles, then the fraction of total fatigue life consumed is $n_\xi / N_\xi = \Delta_\xi$, at stress amplitude of ξ.

The quantity Δ_ξ is known as the damage fraction. Failure is assumed to occur when the sum of all the applicable damage fractions reaches unity. The total damage Δ is expressed mathematically as (Lin, 1967):

$$\Delta = \sum \frac{n_\xi}{N_\xi} \tag{2.34}$$

Total damage Δ at failure may be expressed by combining Equations (2.33) and (2.34) as:

$$\Delta = \frac{1}{c} \sum n_\xi \xi^b \tag{2.35}$$

Due to the random nature of the stress $X(t)$, the accumulated damage in the structure is considered as a random variable in time (stochastic process), denoted by $D(t)$. The objective is to find the mathematical expression for the expectation of this damage, $E[D(t)]$. Equation (2.35) provides the basis for deriving the expression for $E[D(t)]$. The expression for the expected damage under stationary condition using the spectral approach is extensively documented in the literature as:

$$E[D_T] = T \frac{1}{c} E[M_T] \left(2\sqrt{2}\right)^b (\sigma_X)^b \Gamma\left(\frac{b}{2}+1\right) \tag{2.36}$$

where

$E[M_T]$ = expected total number of peaks per unit time;

$\Gamma(\bullet)$ = Gamma function;

σ_X = root mean square stress.

Wave loadings may be considered stationary for a 3-hour period, during which they cause stationary stresses in an offshore structure. Therefore, the assumption of being

stationary is not applicable for calculating the long-term expected total damage of the structure as described in Equation (2.36).

However, the long-term non-stationary response process can be measured as the sum of a large number of short-term stationary processes (Chakrabarti, 1990). Accounting for the non-stationary process, Equation (2.36) can be presented as:

$$E[D_T] = \left(2\sqrt{2}\right)^b Tc^{-1}\Gamma\left(\frac{b}{2}+1\right)\sum_{i=1}^{k}\left[p_i.E[M_T]_i.\left(\sigma_X^b\right)_i\right] \tag{2.37}$$

or

$$E[D_T] = \frac{T\Omega}{c} \tag{2.38}$$

where

p_i is the probability of occurrence of an environmental loading in terms of wave statistics during the structure life (site specific), and

$$\Omega = \left(2\sqrt{2}\right)^b \Gamma\left(\frac{b}{2}+1\right)\sum_{i=1}^{k}\left[p_i.E[M_T]_i.\left(\sigma_X^b\right)_i\right] \tag{2.39}$$

The rainflow correction parameter λ can be introduced in Equation (2.39) to calculate the damage under a wide band stationary process:

$$\Omega = \lambda\left(2\sqrt{2}\right)^b \Gamma\left(\frac{b}{2}+1\right)\sum_{i=1}^{k}\left[p_i.E[M_T]_i.\left(\sigma_X^b\right)_i\right] \tag{2.40}$$

Wirsching and Light (1980) prescribed the following empirical solution for λ:

$$\lambda(\varepsilon, b) = a + (1-a)(1-\varepsilon)^d \tag{2.41}$$

where

ε is the spectral width parameter;

$a = 0.926 - 0.033b$;

$d = 1.587b - 2.323$.

Wirsching and Light (1980) documented $\varepsilon > 0.5$ for typical ocean structure problems and showed that $\lambda \approx 0.79$ for $b = 4.38$ and $\lambda \approx 0.86$ for $b = 3$. Lutes et al. (1984) also attempted to reduce the conservatism associated with narrow-banded assumption by giving an empirical fit for λ.

The above stated empirical equations are based on the rainflow counting method. This method determines the number and magnitudes of stress ranges from a stress history. However, the rainflow counting method is valid only for the specific stress history and may not be generally representative. So the use of empirical equations which are independent of the stress history is common (ASCE, 1982). Besides the spectral method, there are several methods available which calculate the stress parameter Ω for the long-term response of the offshore structure. These methods include: deterministic method (based on wave exceedance diagram), Weibull model for stress ranges, and Nolte-Hansford model (extension of the Weibull model).

A distribution of peaks for a narrow-band Gaussian stationary process is a Rayleigh distribution. For design purposes the random stress is commonly assumed as a narrow-band Gaussian stationary process, hence the application of spectral method for fatigue analysis is widely favorable by analysts (Wirching, 1984; and PERD, 1993).

Another damage model assumes an evolutionary probabilistic structure utilizing the Markovian process from the start (Bogdanoff, 1978). Unlike Miner's rule, the order and severity of the loading must be known. Furthermore, damage states are not uniquely

related to measurable physical quantities. Due to these reasons the method is not attractive to the offshore industry and Miner's rule is preferred because of its ease in dealing with a probabilistic structure.

Chapter 3*

Reliability-Based Design of Riser Fatigue

A methodology is proposed that constitutes the basis for fatigue reliability design due to Morison-type wave loading. The fatigue damage response is modeled using the spectral method as discussed in Chapter 2. For the riser dynamic response modelling, the analytical formulae given by Verbeek and Brouwers (1986) are utilized in the methodology. A discussion on the dynamic response is presented in section (3.1.2).

Uncertainties associated with strength and stress in the limit state function, are quantified by the lognormal distributions. A closed form reliability analysis is carried out, which is based on the limit state function formulated in terms of Miner's cumulative damage rule. The Monte Carlo method is also used for reliability assessment. A worked example is provided to demonstrate riser design problem based on the proposed methodology.

3.1 Proposed Fatigue Reliability Methodology

The proposed methodology for riser fatigue modelling is illustrated in Figure 3.1; detailed discussion of each step is presented in subsequent sections.

3.1.1 Definition

Expressing the limit state in terms of fatigue strength and damage caused by Morison-type wave loading defines the fatigue reliability problem. The riser strength is related to

---

* A part of this chapter is published and cited as:
Nazir, M., Khan, F., and Amyotte, P. 2007. Fatigue Reliability Analysis of Deep Water Rigid Marine Risers with Morison-Type Wave Loading. *Stochastic Environmental Research and Risk Assessment*, DOI: 10.1007/s00477-007-0125-2.

fatigue damage model. Uncertainty associated with each component, i.e., load and strength, is also accounted for in the present analysis.

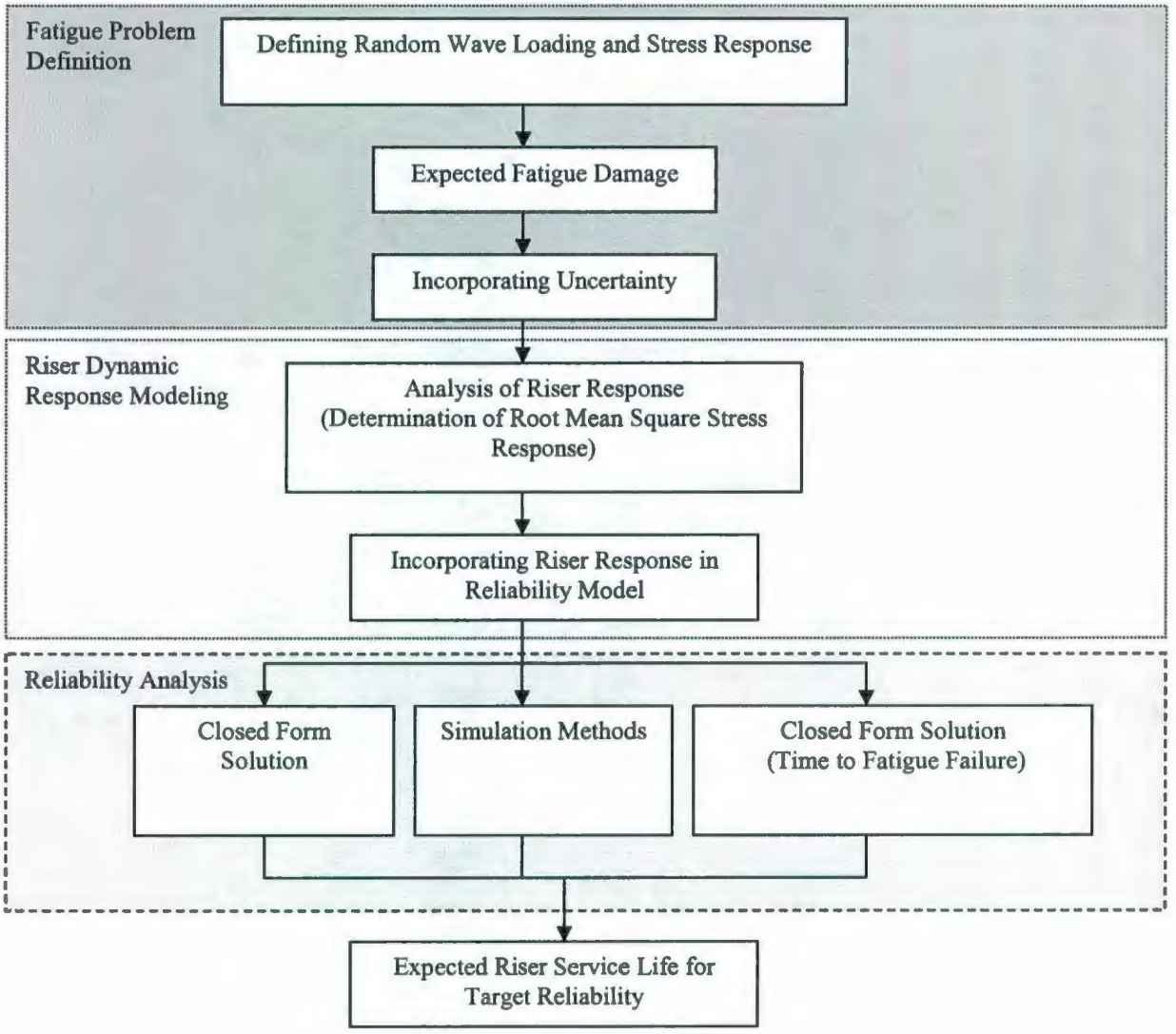

Figure 3.1 Riser fatigue reliability modelling methodology

Fatigue Reliability–Limit State

The fatigue process can be categorized into two regimes: 1) crack initiation, and 2) crack propagation or sub-critical crack growth. The importance of these regimes depends upon the nature of the structure and service loads applied to it. For example, under high cyclic fatigue with low stress fluctuations, the crack initiation period consumes a substantial percentage of the usable fatigue life. When stress fluctuations are high or cracks and notches are present, fatigue cracks initiate quite early and a significant portion of the service life may be spent in propagating the crack to critical size. In low cycle fatigue (total life less than 100,000 cycles), the two regimes are of equal importance. For those structures where defects are practically unavoidable due to fabrication, crack propagation may virtually begin with the first load application (ASCE, 1982).

For reliability assessment, the riser is considered free of initial cracks and other defects and is expected to have high cycles during its service life. Therefore the S-N diagram and Miner's rule are used to relate stress to total fatigue life. The variable Δ as given by Equation (2.34) defines the resistance of the structure element for fatigue reliability. Failure is assumed to occur when the sum of all the applicable damage fractions reaches unity. However, Miner (1945) reported the failure in the range of $0.61 \leq \Delta \leq 1.45$. The large uncertainty in Δ arises from the empirical nature of Equation (2.34) and can be defined as a random variable denoted as $\hat{\Delta}$. The lognormal distribution with unit median and a coefficient of variation of 0.3 is assumed for $\hat{\Delta}$ and is used for modelling error associated with Miner's rule, after Wirsching (1984). Replacing the

parameter Δ with the variable $\hat{\Delta}$, the nature of the cumulative damage rule becomes probabilistic.

Considering the expected damage $E[D]$ in the structure associated with the stresses, the limit state function in fatigue reliability can be prescribed as:

$$G(X) = \Delta - E[D(t)] \tag{3.1}$$

The mathematical expression for probability of fatigue failure can be given as:

$$P_f = p[\Delta - E[D(t)] \leq 0] \tag{3.2}$$

Subtracting this probability of failure from unity gives the fatigue reliability of the element. The discussion on expected damage is presented in the following section.

Expected Fatigue Damage

Equation (2.37) is used to model the expected fatigue damage due to the long-term non-stationary wave loading. For linear systems subject to Gaussain excitation, the response is also a Gaussian (Bendat, 1958). However, non-linearity in the riser system arises because of the drag force term of the wave loading. The discussion on accounting for the system non-linearity in Equation (2.37) is given in section (3.1.2).

Incorporating Uncertainty

For a narrow band process, the variance of the total damage is small near the time of failure (Lin, 1967). So the uncertainty in the expected damage at failure seems negligible. However, in the analysis there are other sources of uncertainty. These sources are inherent to scatter in laboratory test data, the effects of fabrication and workmanship, stress analysis and fatigue strength of the structure during service life.

In the past, significant efforts have been made to quantify uncertainty in the factors of fatigue damage expression, e.g., ASCE (1982), Wirsching(1984), and Wirsching and Chen (1988). Therefore the true nature of $E[D_T]$ may be predicted as:

$$\hat{E}[D_T] = \frac{T\hat{B}^b\Omega}{\hat{c}} \tag{3.3}$$

where $\hat{B}$ is a ratio of actual stress to estimated stress and is used to quantify modelling errors in the estimation of fatigue stress. Wirsching (1984) considered uncertainty in $\hat{B}$ stemming from five sources: 1) fabrication and assembly operations, 2) sea state description, 3) wave load predictions, 4) nominal member loads, and 5) estimation of hot spot stress concentration factors. Contrary to the previously used parameter c, here $\hat{c}$ is considered as a random variable. It accounts for the uncertainty associated with the scatter in S-N data, considering the constant slope b. The related probabilistic characteristics of random variables used in this work are drawn upon from Wirsching (1984) and the data are reported in Table 3.1.

In the fatigue assessment, the expected damage also becomes a random variable, $\hat{E}[D_T]$, due to the random nature of variables $\hat{B}$ and $\hat{c}$. Furthermore, the uncertainty in each random variable will influence the uncertainty in $\hat{E}[D_T]$ to a different extent.

Table 3.1 Statistical properties of random variables

Random Variable	Median	Coefficient of Variation	Probability Distribution
$\hat{\Delta}$	1	0.3	Lognormal
$\hat{B}$	0.8	0.17	Lognormal
$\hat{c}$ (MPa) with b = 4.38	2.16E16	0.73	Lognormal

3.1.2 Riser Dynamic Response Modelling:

The basic equation of riser response is generally derived by assuming a straight vertical and tensioned beam, which is subjected to an axially distributed force $F(z,t)$. The governing partial differential equation for a marine riser is (Brouwers, 1982):

$$\frac{\partial^2}{\partial z^2}\left(EI\frac{\partial^2 X}{\partial z^2}\right)-\frac{\partial}{\partial z}\left(T_r\frac{\partial X}{\partial z}\right)+m\frac{\partial^2 X}{\partial t^2}=F(z,t) \tag{3.4}$$

where

$X(z,t)$ = horizontal deflection of the riser;

z = vertical distance from riser base;

t = time;

E = Young's modulus of elasticity;

I = moment of inertia about neutral axis;

EI = bending stiffness of riser;

$T_r(z)$ = riser tension (usually greater than the submerged weight of the riser system);

m = mass per unit length;

$F(z,t)$ = external fluid force per unit length.

The bottom end is considered fixed to the base and the top end is assumed connected by a hinge to a floating structure. The boundary conditions at bottom end are:

$$X=0 \text{ at } z=0 \tag{3.5}$$

$$EI\frac{\partial^2 X}{\partial z^2}=C_b\frac{\partial X}{\partial z} \tag{3.6}$$

where C_b is the rotational stiffness of the riser base. The boundary conditions at the top can be prescribed as:

$$X = V \text{ at } z = L \tag{3.7}$$

$$EI\frac{\partial^2 X}{\partial z^2} = 0 \text{ at } z = L \tag{3.8}$$

where $V(t)$ is the horizontal displacement of the floating structure and L is the length of the riser. The configuration of the riser system is shown in Figure 3.2.

The first term on the left-hand side of Equation (3.4) represents bending forces, the second term represents tension forces, and the third term accounts for inertial forces. These forces are balanced by Morison-type fluid force $F(z,t)$ on the right side of Equation (3.4). The fluid force can be presented as a modified form of Morison equation to account for the riser motion. This hydrodynamic force can be presented as:

$$F(z,t) = F_I + F_D . \tag{3.9}$$

The term F_I in the above expression is the inertia force per unit length and can be shown as:

$$F_I = \frac{1}{4}\pi d^2 C_M \rho \frac{\partial^2 w}{\partial t^2} - \frac{1}{4}\pi d^2 C_A \rho \frac{\partial^2 X}{\partial t^2} \tag{3.10}$$

and the drag force per unit length F_D can be given by:

$$F_D = \frac{1}{2}\rho d C_D \left(\frac{\partial w}{\partial t} + U_c - \frac{\partial X}{\partial t}\right)\left|\frac{\partial w}{\partial t} + U_c - \frac{\partial X}{\partial t}\right| \tag{3.11}$$

where

ρ = density of seawater;

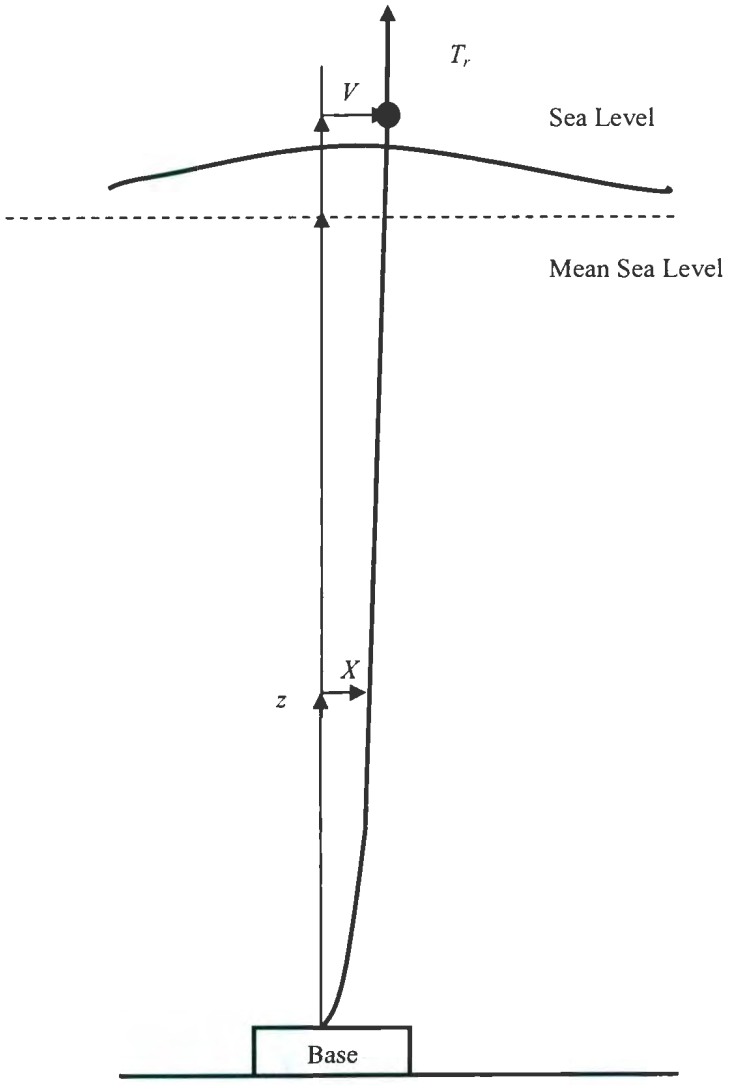

Figure 3.2 Riser configuration

C_M = hydrodynamic inertia coefficient ≈ 2 (Brouwers, 1982);

C_A = added mass coefficient that accounts for the entrained water during riser motion ≈ 1 (Brouwers, 1982);

C_D = drag coefficient ≈ 1 (Brouwers, 1982);

d = diameter of riser;

$w(z,t)$ = horizontal displacement of water particles due to surface waves;

U_c = horizontal current velocity.

The use of the absolute value sign on one of the velocity terms assures that F_D will oppose the direction of the net fluid velocity. For further details on the Morison Equation and hydrodynamic coefficient, reference is made to Sarpkaya (1981), Faltinsen (1990), and Baltrop and Adams (1991).

Equation (3.4) defines the motion of a riser and can be solved to obtain the dynamic riser response. The dynamic response is a random process and is commonly analyzed either in the frequency domain (Tucker and Murtha, 1973; Kirk et al., 1979) or the time domain (Harper, 1979). The analysis of dynamic response in the frequency domain is valid for linear systems with Gaussian excitation that leads to a Gaussian response. Non-linearity in a riser system arises due to Morison-type hydrodynamic forces. Commonly used spectral analysis techniques are unable to predict deviations from a Gaussian form due to non-linearity (Brouwers and Verbeek, 1983).

Morooka *et al.* (2006) featured the dynamic response in both time and frequency domains for a top tensioned vertical riser. The frequency domain solution can be obtained by linearizing the quadratic velocity term of the wave loading. The time domain simulation method is able to account for system non-linearity. However, the solution routine is time consuming (Morooka *et al.*, 2006). The method is not suitable for fatigue reliability analysis, which depends on a large number of sea states over a long duration of time. It also does not help in identifying general trends in riser response. Due to these

shortcomings, the time-domain method becomes less attractive in determining uncertainty propagation of riser response.

Brouwers (1982), and Verbeek and Brouwers (1986) have investigated the riser response analytically and validated the solution results with the time-domain simulation results. The accuracy of the approximate formulae is comparable with the time-domain numerical simulations and they are easy to implement. The proposed methodology utilizes the analytical formulae in modelling the dynamic rise response.

For a slender riser in deep water, Brouwers (1982) proposed three different regions along the length of a slender riser (risers about 0.5 m or less in diameter in water depths of approximately 150 m or more): a wave active zone at the top, a boundary layer at the bottom, and a riser main section in between (Figure 3.3). The wave-active zone lies near the mean sea level and is exposed to direct wave loading due to wave-induced motions. The wave-induced motions decay exponentially in magnitude from mean sea level over a length λ_w (magnitude of 10-40 m in practice). This length can be calculated by the following expression (Verbeek and Brouwers, 1986):

$$\lambda_w = \frac{g}{\omega_z^2} \tag{3.12}$$

where g is gravitational acceleration and ω_z is the characteristic (mean zero-up crossing) frequency of the sea surface elevation. Generally, the height of the riser above mean sea level is of the same order of magnitude as that of λ_w. The wave-active zone is the region that extends from the riser top to a distance of the order λ_w below mean sea level. Below this region, wave induced particle displacements and associated forces can be

disregarded. Boundary layers appear at discontinuities in the riser due to top and bottom connections. The boundary layer length, λ_b, can be given as (Verbeek and Brouwers, 1986):

$$\lambda_b = \sqrt{\frac{EI}{T_r}} \tag{3.13}$$

where

EI is bending stiffness of riser;

T_r is effective riser tension.

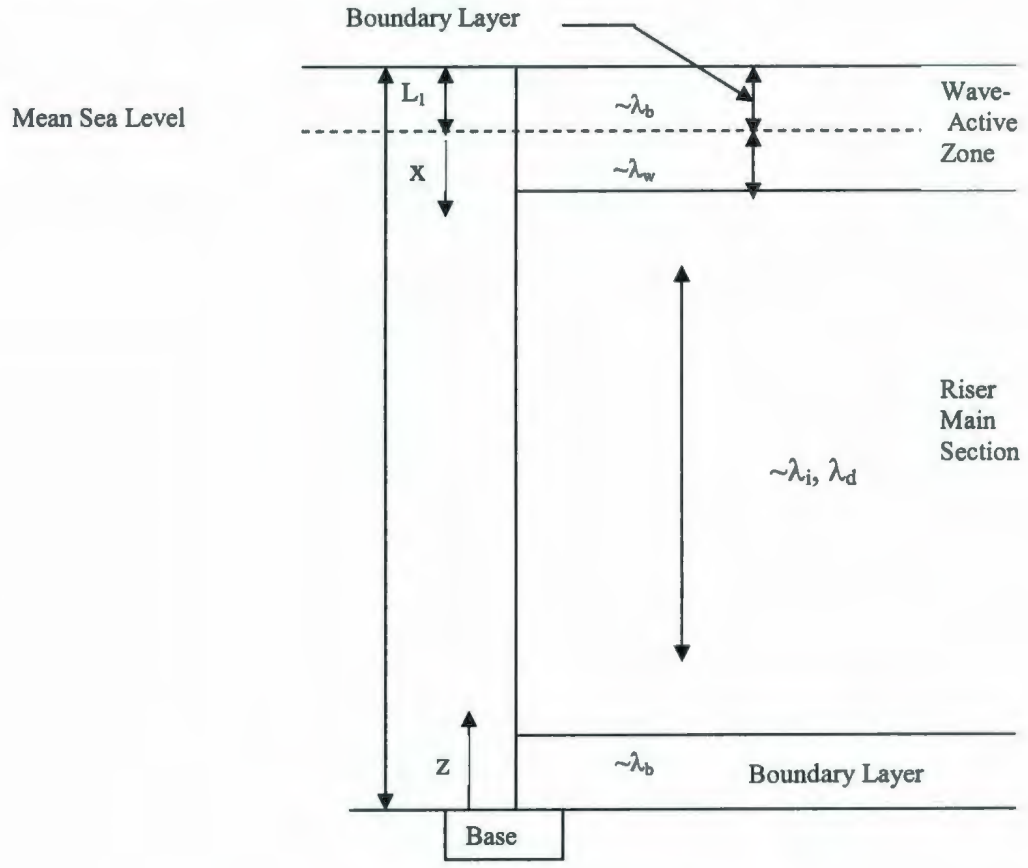

Figure 3.3 Regions of riser response

The characteristic length over which the response in the riser main section varies is presented here as λ_m. This length may be defined as the minimum of the dynamic lengths λ_i, and λ_d, and riser length L (Verbeek and Brouwers, 1986):

$$\lambda_m = \min[\lambda_i, \lambda_d, L] \tag{3.14}$$

where

$$\lambda_i = \pi T_r^{1/2} (m + m_A)^{-1/2} \omega_z^{-1} \tag{3.15}$$

$$\lambda_d = \lambda_i \delta^{-1/2} \tag{3.16}$$

$$\delta = \frac{0.5 \rho d C_D \sigma_v}{m + m_A} \tag{3.17}$$

where

λ_i = half the wavelength of a lightly damped $(\delta << 1)$ tensioned string;

λ_d = half the wavelength of a highly damped $(\delta = O(1))$ tensioned string;

δ = damping parameter;

σ_v = standard deviation of FPSO vessel displacement;

ρ = density of seawater;

C_D = drag coefficient ≈ 1;

m = riser mass per unit length;

m_A = added mass of sea water.

As long as λ_i or λ_d are approximately equal to or less than the riser length L, the response in the main section will be dynamic. Otherwise, the riser response would be quasi-static. The lengths of the boundary layer and wave-active zone are much shorter

than the half wavelength of the riser so the response will be quasi-static in these regions (inertia and damping forces may be disregarded and the response is governed by a balance between tension and bending forces).

The response of the riser in the wave-active zone is linearly related to force and is quasi-static in nature. Probability distributions of response, normalized with respect to standard deviation, are the same as those of the force (Brouwers, 1982). The non-linearity in the system arises because of the water-particle velocity term in the drag force of Morison-type wave loading. Brouwers and Verbeek (1983) have derived the probability distribution of peak forces based on Borgman's narrow-band model. The probability distribution of force reduces to a narrow band Gaussian process with Rayleigh distribution only in the inertia-dominated regime, as does the response. In the inertia regime, the loading remains linear. However, in the drag-dominated regime where non-linearity arises in the system, the response deviates from Rayleigh distribution and the use of Equation (2.37) will give a small magnitude of expected total damage. To overcome this problem, Brouwers and Verbeek (1983) have defined expected fatigue damage based on non-linear distribution and the expected fatigue damage from Rayleigh distribution using the following relation:

$$f(b,K)=\frac{E[D]_{non-lin}}{E[D]_{lin}}=(3K^2+1)^{-(b/2)}\frac{1}{\Gamma\left(\frac{b}{2}\right)}\left[\gamma\left(\frac{b}{2},\frac{1}{8K^2}\right)+2^{1+(b/2)}K^b\exp\left(\frac{1}{8K^2}\right)\Gamma\left(b,\frac{1}{4K^2}\right)\right] \tag{3.18}$$

where $\Gamma(a)$ is the Gamma function and $\gamma(a,z)$ and $\Gamma(a,z)$ are incomplete Gamma functions as defined by Abramowitz and Stegun (1970). Factor $f(b,K)$ is the ratio of non-linear to linear expected fatigue damages and is a function of the slope of the S-N curve (b) and drag inertia parameter (K).

The problem due to deviation of the peak response magnitude from the Rayleigh distribution in calculating $E[D_T]$ is addressed by introducing the factor $f(b,K)$ in Equation (2.37) and the proposed $E[D_T]$ expression takes the form:

$$E[D_T] = \left(2\sqrt{2}\right)^b Tc^{-1}\Gamma\left(\frac{b}{2}+1\right)\sum_{i=1}^{k}\left[p_i f_i(b,K)E[M_T]_i.\left(\sigma_X^b\right)_i\right] \tag{3.19}$$

The variation of $f(b,K)$with K and for three different slopes is shown in Figure 3.4. It is evident that $f(b,K)$ is approximately equal to unity in the limit of $K \to 0$ (inertial force dominant regime) and reaches a maximum value when $K \to \infty$ (drag force dominant regime). The variation of this factor is significant in the region $0.3 < K < 10$ for the three different slopes.

The comparison of narrow-band, non-linear distributions in the drag and inertia dominated limits with those obtained from a wide band model (spectral width = 0.7) was made by Brouwers and Verbeek (1983). The narrow-band model yielded results similar to the results obtained from the wide-band model. This justifies the use of a narrow-band assumption in the current study.

Since the riser response is quasi-static in nature (response frequencies are lower than the resonance frequency) and the response is linearly related to wave force, the number of response peaks can be considered equal to the number of force peaks. For deep

waters, the probability density function of sea elevation is commonly considered Gaussian with zero mean (Hughes, 1983). For a stationary narrow-band Gaussian process, the number of force peaks per unit time may be approximated from the expected frequency of the surface elevation process (Moe and Crandall, 1978). The expected total number of peaks per unit time is given by the following expression (Melchers, 1987):

$$E[M_T] = \frac{1}{2\pi}\frac{\sigma_{\dot{\eta}}}{\sigma_{\eta}} \tag{3.20}$$

where

η = water surface elevation following normal distribution $N \sim (0, \sigma_{\eta})$;

$\dot{\eta}$ = derivative of water surface elevation with $N \sim (0, \sigma_{\dot{\eta}})$.

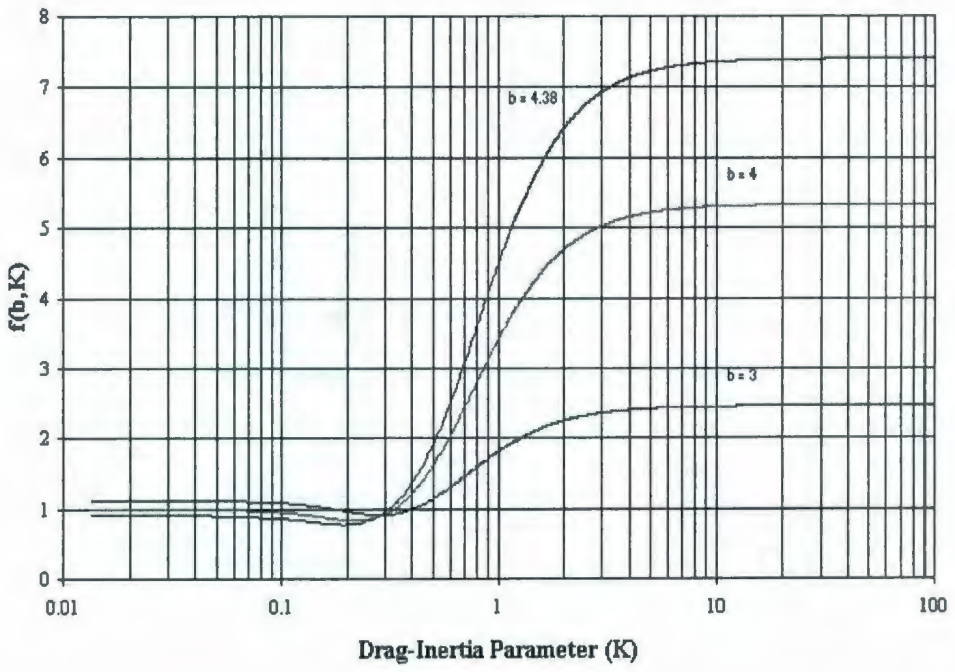

Figure 3.4 Variation of factor f(b,K) with parameter K for three different slopes of the S-N curve (after Brouwers and Verbeek, 1983)

In terms of spectral moments:

$$E[M_T] = \frac{1}{2\pi}\sqrt{\frac{m_2(\omega)}{m_0(\omega)}} \tag{3.21}$$

The *k*th spectral moment can be defined as (Barltrop and Adams, 1991):

$$m_k = \int_0^\infty \omega^k S_\eta(\omega) d\omega \tag{3.22}$$

where ω is an angular frequency and S_η is a single sided power spectrum of surface elevation.

The right-hand side of Equation (3.21) is equal to the number of expected equivalent cycles per unit time between two consecutive zero crossings with positive slope. Spectral moments can be based on either angular frequency, ω, or cyclic frequency, *f*, and the relationship between these two is given as (Barltrop and Adams, 1991):

$$m_k(\omega) = (2\pi)^k m_k(f) \tag{3.23}$$

The analytical expression for the standard deviation of bending moment (σ_M) for this zone is (Verbeek and brouwers, 1986):

$$\sigma_M = 0.21\rho C_M d^2 \omega_z^2 \lambda_b^2 H_s \alpha(x)\sqrt{\left(1+3K^2(x)\right)} \tag{3.24}$$

where

H_s = significant wave height;

$\omega_z = \sqrt{\frac{m_2(\omega)}{m_0(\omega)}}$ is mean wave zero-crossing frequency;

C_M = hydrodynamic inertia coefficient ≈ 2;

d = diameter of a riser.

The drag-inertia parameter, *K(x)*, can be defined as:

$$K(x) = 0.125 \frac{\beta(x)}{\alpha(x)} \frac{C_D d}{C_M d^2} H_s \tag{3.25}$$

The x-dependent constants $\alpha(x)$ and $\beta(x)$ are defined as following (for the orientation of x see Figure 3.3):

- for $x \le 0$ (below mean sea level)

$$\alpha(x) = \frac{1}{2}(1 + \lambda_b / \lambda_w)^{-1}\{\exp(x/\lambda_w) - \exp((x - 2L_1)/\lambda_b)\}$$
$$+ \frac{1}{2}(1 - \lambda_b / \lambda_w)^{-1}\{\exp(x/\lambda_w) - \exp(x/\lambda_b)\} \tag{3.26}$$

$$\beta(x) = \frac{1}{2}(1 + 2\lambda_b / \lambda_w)^{-1}\{\exp(2x/\lambda_w) - \exp((x - 2L_1)/\lambda_b)\}$$
$$+ \frac{1}{2}(1 - 2\lambda_b / \lambda_w)^{-1}\{\exp(2x/\lambda_w) - \exp(x/\lambda_b)\}; \text{ where } \lambda_b, \lambda_w \neq 0 \tag{3.27}$$

- for $x > 0$ (above mean sea level)

$$\alpha(x) = \frac{1}{2}(1 + \lambda_b / \lambda_w)^{-1}\{\exp(-x/\lambda_b) - \exp((x - 2L_1)/\lambda_b)\} \tag{3.28}$$

$$\beta(x) = (1 + 2\lambda_b / \lambda_w)^{-1}(1 + \lambda_b / \lambda_w)\alpha(x) \tag{3.29}$$

In the above expressions L_1 is the extension of the riser above mean sea level. The parameters $\alpha(x)$ and $\beta(x)$ are at most equal to unity and both reach a maximum value at some distance below mean sea level.

The parameter of σ_X in Equation (3.19) may be given as:

$$\sigma_X = \frac{\sigma_M d/2}{I} \tag{3.30}$$

In the solution for bending moment Verbeek and Brouwers (1986) assumed that the standard deviation of sea surface elevation was much smaller than the boundary layer length. The effects of free-surface fluctuations would then be small. Furthermore, they neglected the dynamic effects from the response of the main riser section.

The analytical formulation for the dynamic response in the riser main section can be represented as the vector sum of a 'quasi-static' component and a 'resonant' component (Verbeek and Brouwers, 1986). The quasi-static component describes the static deflection of the riser owing to FPSO displacement at the top and the resonant component represents the dynamic response in one of the natural modes of the riser. The natural frequency can be calculated as (Verbeek and Brouwers, 1986):

$$\omega_n = \frac{n\pi}{2L}\frac{T_t^{1/2} + T_b^{1/2}}{(m+m_A)^{1/2}} \tag{3.31}$$

For a lightly damped riser of length $L \sim \lambda_i$ the response will be predominantly in the first natural mode, in the second mode when $L \sim 2\lambda_i$ and in the nth mode when $L \sim n\lambda_i$. Maximum response occurs when one of the natural frequencies coincides with the frequency of excitation, i.e. when $L = \lambda_i, 2\lambda_i, ...n\lambda_i$.

The response in the lightly damped riser main section and the boundary layer at the bottom may be considered conservatively Rayleigh distributed. So for these two regions in the limit of $K \to 0$, the ratio factor $f(b,K)$ in Equation (3.19) approaches unity. For the dynamic analysis purposes of the main section, the period of response can be given by the natural period of the riser, and the expression for $E[M_T]$ takes the form:

$$E[M_T] = \frac{1}{2\pi}\omega_n \tag{3.32}$$

In the main section, currents cause additional damping and reduce the amplitude of the resonant response. However, a current may excite a dynamic response through vortex shedding, i.e. vortex-induced vibrations (VIVs). The discussion on expected damage due to VIVs is beyond the scope of this work.

A reliability assessment of a multi-bore riser in the wave-active region is undertaken as a representative example. The two main reasons for selecting this region are i) the response in the wave-active zone is the most sensitive to wave height parameter, and ii) the response deviates from a Rayleigh distribution.

3.1.3 Reliability Assessment

The stress response will be incorporated in the reliability analysis. The following solution approaches are employed in carrying out reliability analyses:

1. closed form format, and
2. simulation methods

The result of simulation methods provides a base to validate the result of the simple closed form format. The probability of failure can be calculated on a yearly basis of riser service life. Finally, fatigue design life can be estimated by setting the target reliability, which depends on the type of structure and ease of repair.

Closed Form Solution

Quantifying the uncertainties of variables $\hat{\Delta}$ and $\hat{E}[D_T]$, an expression for reliability can be derived using the lognormal distribution. Using the reproductive

property (details are given in Appendix I), the parameters of the lognormal distribution for $\hat{E}[D_T]$ would be:

$$\mu_{\ln \hat{E}[D_T]} = \ln \Omega + \ln T + (b\mu_{\ln \hat{B}} - \mu_{\ln \hat{C}}) \tag{3.33}$$

or alternatively,

$$\mu_{\ln \hat{E}[D_T]} = \ln \tilde{E}[D_T] \tag{3.34}$$

and

$$\tilde{E}[D_T] = \frac{T\tilde{B}^m \Omega}{\tilde{C}} \tag{3.35}$$

where $\tilde{E}[D_T]$ is the median value of the random variable $\hat{E}[D_T]$, and tildes (~) represent median values of random variables. T is time period in seconds. The variance in terms of the coefficient of variation (CV) can be given as:

$$\sigma^2_{\ln \hat{E}[D_T]} = \ln\left[\left(1 + CV^2_{\hat{C}}\right)\left(1 + CV^2_{\hat{B}}\right)^{b^2}\right] \tag{3.36}$$

Similarly, the parameters of the distribution for the strength variable $\hat{\Delta}$ are:

$$\mu_{\ln \hat{\Delta}} = \ln \tilde{\Delta} \tag{3.37}$$

and

$$\sigma^2_{\ln \hat{\Delta}} = \ln\left[\left(1 + CV^2_{\hat{\Delta}}\right)\right] \tag{3.38}$$

Furthermore, the performance function $\hat{G} = \hat{\Delta} / \hat{E}[D(t)]$ will also have a lognormal distribution with the following parameters:

$$\mu_{\ln \hat{G}} = \mu_{\ln \hat{\Delta}} - \mu_{\ln \hat{E}[D_T]} \tag{3.39}$$

$$\sigma^2_{\ln \hat{G}} = \sigma^2_{\ln \hat{\Delta}} + \sigma^2_{\ln \hat{E}[D_T]} \tag{3.40}$$

In terms of the coefficient of variation (CV) of random variables, Equation (3.40) takes the form:

$$\sigma^2_{\ln \hat{G}} = \ln\left[\left(1+CV^2(\hat{\Delta})\right)\left(1+CV^2(\hat{c})\right)\left(1+CV^2(\hat{B})\right)^{b^2}\right] \tag{3.41}$$

At any value of the lognormal distributed $\hat{G} < 1$, the performance function would be in the failure state. So the failure probability is:

$$P_f = \Phi\left(\frac{\ln 1 - \mu_{\ln \hat{G}}}{\sigma_{\ln \hat{G}}}\right) = \Phi\left(-\frac{\mu_{\ln \hat{G}}}{\sigma_{\ln \hat{G}}}\right) \tag{3.42}$$

or

$$P_f = \Phi\left(\frac{\ln \tilde{E}[D_T] - \mu_{\ln \hat{\Delta}}}{\sigma_{\ln \hat{G}}}\right) \tag{3.43}$$

where $\Phi(.)$ is the standard normal distribution function, N(0,1).

Expression (3.43) can be presented in the reliability index format, β, as:

$$P_f = \Phi(-\beta) \tag{3.44}$$

Equation (3.43) is different from the expression recommended by various structural codes:

$$P_f = \Phi\left(\frac{\ln D - \mu_{\ln \hat{\Delta}}}{\sigma_{\ln \hat{\Delta}}}\right) \tag{3.45}$$

In the above expression, the admissible damage factor D is not considered as a random variable and the uncertainty in the analysis is considered by the resistance ($\hat{\Delta}$) only (Souza and Goncalves, 1997). To characterize the probabilistic nature of fatigue analysis

and to utilize extensive data on the quantification of uncertainty of the stress part, Equation (3.43) should preferably be used instead of Equation (3.45).

Simulation Methods

To control the high uncertainty associated with a direct sampling approach (as discussed in section 2.2.2), the following procedure is adopted. Considering the fact that $\hat{\Delta}$ is lognormal, the probability of failure can be given as:

$$P_f = \Phi\left(\frac{\ln \hat{D} - \mu_{\ln \hat{\Delta}}}{\sigma_{\ln \hat{\Delta}}}\right) \tag{3.46}$$

The simulation algorithm becomes: (1) generate $\hat{\mathrm{E}}[\mathrm{D_T}]$, (2) calculate P_f as given by Equation (3.46) for the *ith* simulation(P_{fi}) and return. Therefore the sample mean and the associated uncertainty in terms of coefficient of variation of failure probability can be given by Equations (2.26) and (2.27).

Closed Form Solution (Based on Time to Fatigue Failure)

The limit state function for crack initiation can also be formulated in terms of time to fatigue failure $\hat{T}$ as (Wirsching, 1984):

$$\hat{G}(X) = \hat{T} - T_s \tag{3.47}$$

where the parameter T_s is the intended service life of the structure. The fatigue life $\hat{T}$ may be approximated by setting the expected damage equal to its critical failure value $\hat{\Delta}$ in Equation (3.3) (Lutes et al., 1984 and Souza and Goncalves, 1997).

$$\hat{T} = \frac{\hat{c}\hat{\Delta}}{\hat{B}^b \Omega} * \frac{1}{365*24*3600} \tag{3.48}$$

where the conversion factor $\frac{1}{365*24*3600}$ converts the unit of $\hat{T}$ from seconds to years. By virtue of the lognormal behavior of variables in Equation (3.48), $\hat{T}$ will also follow a lognormal distribution with the following parameters:

$$\mu_{\ln \hat{T}} = (\mu_{\ln \hat{c}} + \mu_{\ln \hat{\Delta}} - b\mu_{\ln \hat{B}}) + \ln\left(\frac{1}{\Omega}\right) - 17.267 \tag{3.49}$$

where $-17.267 = \ln\left(\frac{1}{365*24*3600}\right)$

alternatively,

$$\mu_{\ln \hat{T}} = \ln \widetilde{T} \tag{3.50}$$

where $\widetilde{T} = \frac{\widetilde{c}\widetilde{\Delta}}{\widetilde{B}^b \Omega} * \left(\frac{1}{365*24*3600}\right)$

Variance is given as:

$$\sigma^2_{\ln \hat{T}} = \ln\left[\left(1 + CV^2(\hat{\Delta})\right)\left(1 + CV^2(\hat{c})\right)\left(1 + CV^2(\hat{B})\right)^{b^2}\right] \tag{3.51}$$

Using the mathematical properties of lognormal distribution for $\hat{T}$ the expression of P_f will be:

$$P_f = \Phi\left(\frac{\ln T_s - \ln \widetilde{T}}{\sigma_{\ln \hat{T}}}\right) \tag{3.52}$$

Equation (3.44) can be used to give the probability of failure in terms of a reliability index β; however, now β will be given as (Wirsching, 1984):

$$\beta = \frac{\ln\left(\tilde{T} / T_s\right)}{\sigma_{\ln \hat{T}}} \tag{3.53}$$

Quantifying all the uncertainties in the fatigue expression as lognormal will give a closed form solution for P_f. However, it can be argued that the lognormal behavior should not be advocated as a fatigue life model because the shape of the hazard function (details are given in Appendix I) is difficult to rationalize (Bury, 1999). The reason is that the lognormal hazard rate function rises from the origin to a peak and then it slowly decreases (i.e. it is an initially increasing failure rate and later a decreasing failure rate). A fatigue phenomenon corresponds to a wear-out region of the bathtub curve and should be characterized by increasing failure rate. A discussion on the justification of using the lognormal format in fatigue reliability assessment is presented in the subsequent paragraphs of this section.

Sweet (1990) provides approximations for the location of the peak of the hazard rate function $T_{\max}$ of the lognormal distribution. For large values of $\sigma_{\ln \hat{T}}$ (approximately of the magnitude of 3), the expression for $T_{\max}$ is:

$$T_{\max} \approx \exp\left(\mu_{\ln \hat{T}} - \sigma^2_{\ln \hat{T}}\right) \tag{3.54}$$

For small values of $\sigma_{\ln \hat{T}}$ (approximately of the magnitude of 0.3), the expression for $T_{\max}$ becomes:

$$T_{\max} \approx \exp\left(\mu_{\ln \hat{T}} + 1 - \sigma^2_{\ln \hat{T}}\right) \tag{3.55}$$

The parameter $\sigma_{\ln \hat{T}}$ from Equation (3.51) and Table 3.1 can be calculated as 1.0295. Using this value and considering the large $\sigma_{\ln \hat{T}}$ approximation, Equation (3.54) prescribes T_{max} in terms of median time to failure ($\tilde{T}$) as:

$$T_{max} \approx 0.347\tilde{T} \tag{3.56}$$

and for the small $\sigma_{\ln \hat{T}}$ approximation, Equation (3.55) takes the form:

$$T_{max} \approx 0.942\tilde{T} \tag{3.57}$$

The intended lifetime T_s is based on the reliability index, β. For a riser, the typical value of β is 2 (Wirsching and Chen, 1988). So the service life in terms of $\tilde{T}$ from Equation (3.53) can be given as:

$$T_s \approx 0.128\tilde{T} \tag{3.58}$$

T_s is less than T_{max} given by Equations (3.56) and (3.57). This shows that during the intended design life the hazard rate remains an increasing function conforming to the shape of the bathtub curve in the wear out region (under the quantification of uncertainties as presented in Table 3.1 and the selective reliability index of 2).

3.2 Application

The methodology is applied to evaluate the fatigue reliability of a multi-bore riser (14 peripheral lines and a central riser). The properties of a multi-bore riser, such as EI, m etc. are calculated by the sum of values of these parameters for every individual flow line (Verbeek and Brouwers, 1986). The structural and loading parameters of a riser system, used in the analysis, are reported in Table 3.2.

Table 3.2 Riser parameters used in analysis

Parameter	Notation	Value	Unit
Extension above MSL	L_1	15.2	m
Riser length	L	115.2	m
Peripheral line – Outer diameter	$(D_o)_P$	88.9	mm
Peripheral line – Inner diameter	$(D_i)_P$	77.9	mm
Riser – Outer diameter	$(D_o)_R$	600	mm
Riser – Inner diameter	$(D_i)_R$	575	mm
Bending stiffness	$\sum_{i=1}^{n} E_i I_i$	214.2	MNm^2
Young's modulus	E	2.1×10^5	MPa
Mass	m	628	Kg/m
Added mass	m_a	165	Kg/m
Effective weight	W_e	4.1	KN/m
Top tension	T_t	1.78	MN
Bottom tension	T_b	1.31	MN
Drag force parameter	$\sum_{i=1}^{n} C_D d_i$	1.85	m
Inertial force parameter	$\sum_{i=1}^{n} C_M d_i^2$	0.94	m^2

The long-term sea state data in terms of the significant wave height are given in Table 3.3. The Pierson-Moskowitz (P-M) wave spectrum is used to calculate mean zero crossing period (T_z) and mean period (T_m) associated with the significant wave height. Figure 3.5 shows two spectra associated with significant heights of 1.75 and 4.75 m.

Table 3.3 Sea states used in analysis

Serial Number	Significant Wave Height (m)	Probability of Occurrence
1	1.75	0.005
2	2.75	0.03
3	3.25	0.09
4	3.75	0.13
5	4.25	0.185
6	4.75	0.25
7	5.25	0.18
8	5.75	0.09
9	6	0.04

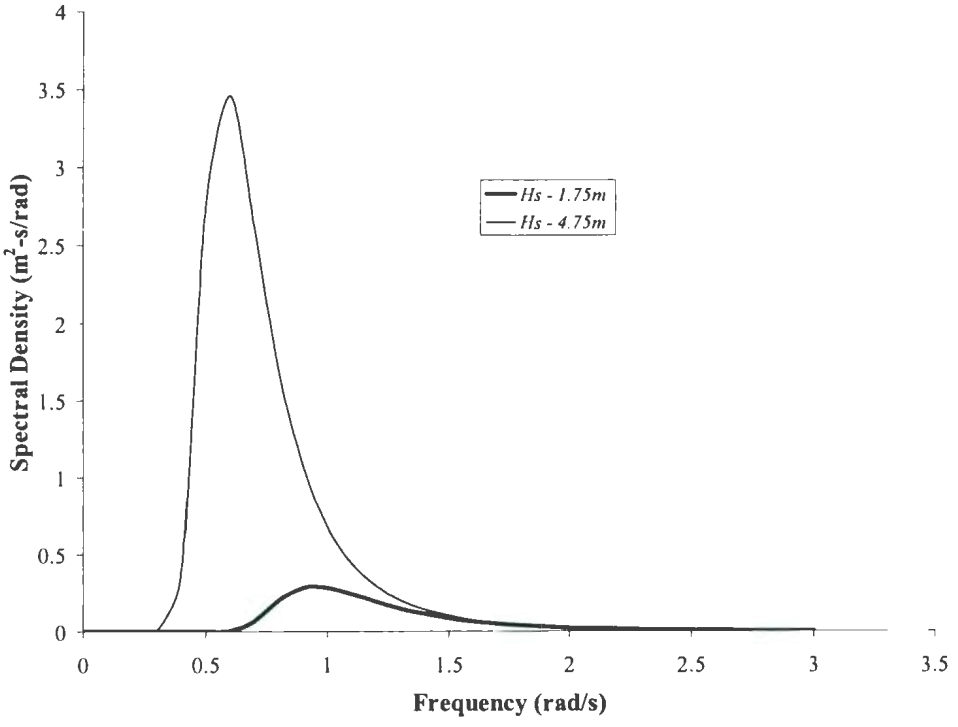

Figure 3.5 Pierson-Moskowitz wave height spectrum

The wave spectrum can be expressed as (Wilson, 2002):

$$S_\eta = 0.0081\frac{g2}{\omega^5}\exp\left(-B/\omega^4\right) \tag{3.59}$$

where

$B = \frac{3.11}{H_s^2}$;

H_s = Significant wave height (m);

ω = angular frequency (rad/s).

The expressions for T_z and T_m can be given as (Barltrop and Adams, 1991):

$$T_z = 2\pi\sqrt{\frac{m_0}{m_2}} \tag{3.60}$$

$$T_m = 2\pi\frac{m_0}{m_1} \tag{3.61}$$

The expressions for the kth moment (m_k) calculations are given in equations (3.22) and (3.23). The calculated values for T_z and T_m associated with two significant wave heights are listed in Table 3.4. The parameter T_z can be used to calculate ω_z in equation (3.24).

Table 3.4 Parameters zero crossing period (T_z) and mean period (T_m) calculated from Pierson-Moskowitz spectrum

Serial Number	Significant Wave Height (m)	Zero Crossing Period (s)	Mean Wave Period (s)
1	1.75	4.7	5.1
2	4.75	7.8	8.4

3.3 Results and Discussion

The simulations for fatigue reliability assessment were carried out using MATLAB 6.5. The implementation of special functions, such as Gamma function, is presented in Appendix II. The results are presented in Figure 3.6. Both closed form solutions give the same reliability index. The P_f values for two successive years are closely spaced. In the illustrative example 50,000 simulation cycles are used to estimate the probability of failure within an acceptable level of statistical error. Results obtained from the simulation method are comparable to the closed form solutions (see Figure 3.6). At the P_f value of 0.0011 and 50,000 simulation cycles, the magnitude of CV is calculated as 0.0932. At these desired P_f and CV values the number of simulation cycles should be increased from 50,000 to 104,544 in the direct sampling method (see Equation (2.25)). The illustrative example shows that the conditional expectation simulation method is more efficient in addressing the uncertainty than the direct sampling method.

The target reliability index (β_o) for the riser is defined as 2 by Wirsching and Chen (1988). This corresponds to a probability of failure of ≈ 0.023. Thus, a service life of approximately 39 years is recommended in the illustrative example. However, the choice of β_o is critical in the prediction of the riser service life. The selection of β_o is part of the decision making process and its selection is influenced by factors such as safety, and ease in the inspection and maintenance of the structure. The analysis is based only on Morison-type wave forces, for which the riser response is critical in the wave-active zone. Vortex induced vibrations (VIVs) due to current loading are critical in the

riser main section. The fatigue damage associated with VIVs can be combined with the wave force fatigue damage, in calculating the riser life (Serta *et al.*, 2000). However, the treatment of VIVs in calculating the service life is beyond the scope of the current work.

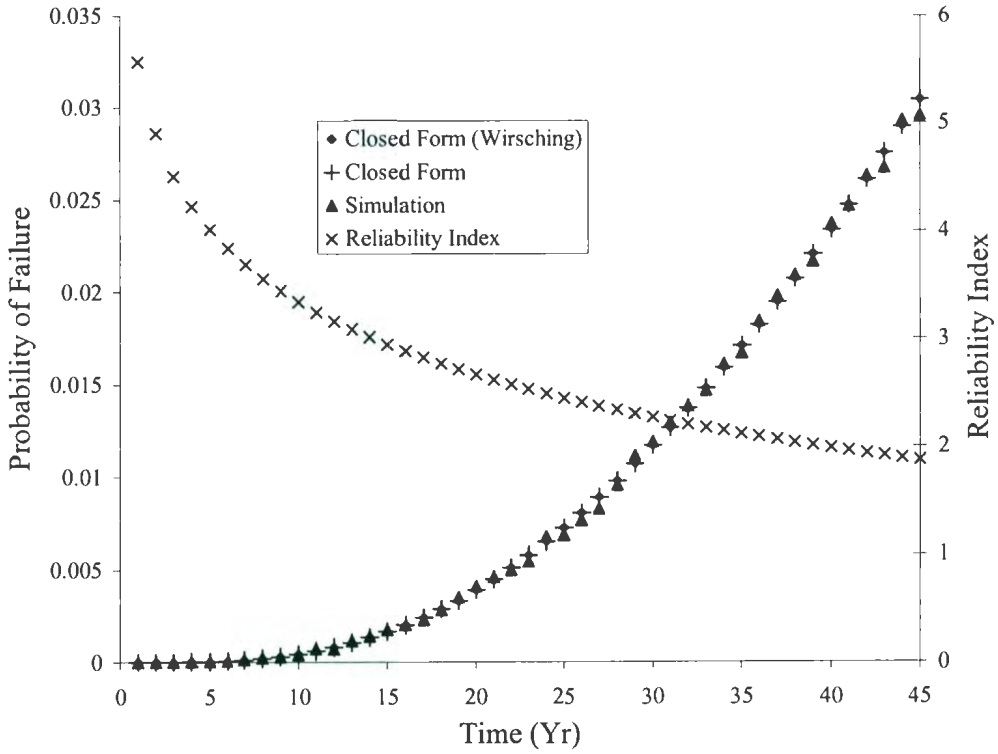

Figure 3.6 Fatigue reliability results

Chapter 4**

Contaminant Fate and Transport Modelling

The consequence of a production riser failure is the release of contaminants in a marine environment causing irreversible environmental damage. Therefore, prediction of the fate and transport of oil plays a vital role in the development and implementation of coastal oil spill contingency plans. A marine system is a complex multimedia environment that can be divided into two main (henceforth referred to as bulk) compartments, namely water, and sediments. These bulk compartments contain sub-compartments such as suspended solids and biota in the water column, and solids and pore water in the sediment compartment.

The transformation of oil, which is also known as weathering, is associated with a wide variety of physiochemical and microbiological processes. Mackay *et al.* (1980) developed semi-empirical equations to describe the weathering processes. These equations were subsequently incorporated into the sub-module of a *natural resource damage assessment modelling system* for marine and coastal areas (Reed, 1989). The sub-module was designed to estimate the distribution of a contaminant on the sea surface, and to predict concentration in the water column and sediment. Sebastiao and Soares (1995) transformed the time dependent weathering algorithms of Mackay *et al.* (1980) and Reed (1989) into a system of differential equations. They solved a system of model equations

** A part of this chapter is published and cited as:

Nazir, M., Khan, F. I., Amyotte, P. R., and Sadiq, R. 2007. Multimedia Fate of Oil Spills in a Marine Environment – An Integrated Modelling Approach. *Process Safety and Environmental Progress*, DOI: 10.1016/j.psep.2007.10.002.

numerically to describe spreading (area growth), evaporation, volume balance (accounts for the volume lost by evaporation and by natural dispersion into the water column), water incorporation, and viscosity increase with time. However, their work was limited to modelling the fate of surface oil, and did not include the dispersion of oil in the water column or sedimentation at the sea floor. Hudda *et al.* (1999) combined models for oil slick dynamics at the water surface, 3-D transport of the oil phase in the water column using the conventional advection-diffusion equation, and oil sedimentation at the seabed. Chen et al. (2007) synthetically considered oil weathering models (e.g. spreading, evaporation, emulsification, dissolution), and adopted the Monte Carlo method to establish the ocean dynamic and mathematical model of oil spill on the sea

During the last two decades, a fugacity-based approach in modelling the distribution of contaminants in a multimedia environment for complex ecological systems has been studied by various researchers (e.g. Mackay *et al.*, 1983; Mackay 1991; Mackay *et al.*, 1992; Sadiq, 2001; Sweetman *et al.*, 2002). Sadiq (2001) used fugacity- and aquivalence-based approaches for determining the fate of drilling waste discharges in the water column and pore water of sediments in the marine environment. Sweetman *et al.* (2002) determined the fate of PCBs in the multimedia, also using a fugacity-based approach.

Fugacity can be regarded as the tendency of a solute to escape from a phase. It is identical to partial pressure in ideal gases and is logarithmically related to chemical potential. When a solute achieves equilibrium between phases it seeks to establish an equal fugacity in all phases. A fugacity-based approach is an effective means to study the

behavior of organic chemicals in a multimedia environment because of its capability to handle an enormous amount of details on environmental transport processes and dispersed phases (sub-compartments) within a bulk compartment. However, the fugacity approach is applicable for low chemical concentrations in the media (Mackay, 1991). The fugacity-based approach is used to model the low-concentration oil fractions, which enter into the water column from surface oil slick due to one of the weathering processes—natural dispersion.

A methodology is proposed in this chapter, which can be employed in predicting the contaminant fate and transport for a batch spill scenario on the water surface. In the proposed methodology, oil weathering processes are coupled with a level IV (dynamic) fugacity-based model. In Chapter 5 the methodology is extended to account for the subsea oil release from a broken riser. The important transport processes are also identified. The practical application of the methodology is illustrated with the help of a case study.

4.1 Contaminant Fate and Transport Modelling: An Overview

The present study has drawn upon the work of Sebastiao and Soares (1995) in modelling the oil slick physiochemical weathering processes, namely spreading, evaporation, natural dispersion and emulsification. The multimedia oil fate modelling in a marine environment is performed using a level IV fugacity-based model.

A marine system consists of two bulk compartments — water and sediment. It is assumed that the water compartment contains homogenous dispersed phases (sub-compartments) of suspended solids and biota, and the sediment contains solids and pore

water. In a conventional fate modelling approach, the dimensions of the 'evaluative' environment are predefined (Mackay *et al.*, 1983; Sadiq, 2001; Sweetman *et al.*, 2002). The proposed methodology allows the growth of the water compartment to account for an oil spreading mechanism. The methodology integrates the weathering algorithms with the level IV model to predict the fate and transport of oil in a multimedia marine environment. The oil weathering processes and the level IV model are discussed in the subsequent sections.

4.1.1 Modelling for Oil Slick Weathering

API (1999) lists ten weathering processes for the fate and transport of a surface oil slick. These include: (1) spreading, (2) advection, (3) evaporation, (4) dissolution, (5) natural dispersion, (6) emulsification, (7) photo-oxidation, (8) sedimentation, (9) shoreline stranding, and (10) biodegradation. API (1999) also presents the concept of a generic timeline for the weathering processes. On the basis of the order of a few days and under calm sea conditions, four weathering processes, namely, spreading, evaporation, natural dispersion, and emulsification are of particular importance (Sebastiao and Soares, 1995). The algorithms adopted for these four weathering processes are presented in this section.

Surface spreading and advection

Fay (1969) distinguished three phases for the spreading of an oil slick. In each phase the spreading force is balanced by the retarding force. In the first phase, the spreading force of gravity is balanced by the retarding force of inertia. In the second phase the accelerating force of gravity is balanced by the viscous force. In the third and

final phase, the surface tension is balanced by the viscous force. Fay (1969), Hoult (1972), and Waldman *et al.* (1972) prescribed the spreading expressions for both one-dimensional and radial spreading for these three phases.

The first phase of *gravity-inertial* spreading lasts only for the order of a few minutes. The final phase of *tension-viscous* spreading is important for the dispersed or broken slicks, such as surface slicks formed due to an underwater oil release. For surface spills, therefore, it is common to employ the second phase of *gravity-viscous* spreading in simulations (Sebastiao and Soares, 1995).

Mackay *et al.* (1980) modified the Hoult (1972) oil spreading expression into a convenient form, since area change was calculated as a function of actual area, rather than time. Reed (1989), and Sebastiao and Soares (1995) used the modified expression of Mackay *et al.* (1980) in calculating the rate of spreading based on *gravity-viscous* formulation:

$$\frac{dA_S}{dt} = K_1 A_S^{1/3} \left[\frac{V_m}{A_S} \right]^{4/3} \tag{4.1}$$

where

A_S = area of slick (m^2);

V_m = volume of spilled oil (m^3);

K_1 = constant with default value of 150 s^{-1} (Mackay *et al.* 1980).

Allowance is usually made for loss of volume in the spreading rate expression as a result of evaporation, dissolution, and dispersion. A prerequisite for spreading of a crude oil is that its pour point should be lower than the ambient water temperature. The

spreading process is generally ceased at the terminal thickness of 0.01 cm for heavy crude oils, and 0.001 cm for less viscous substances such as gasoline, kerosene and light diesel fuel (Reed, 1989). The model assumes circular slicks of uniform thickness h, which can be calculated as:

$$h = \frac{V_m}{A_S} \tag{4.2}$$

Advection is the movement of the oil due to the influence of overlying winds and/or underlying currents (NRC, 1985). The advection or drift velocity $\vec{V}$ can be calculated from the following expression (Hoult, 1972):

$$\vec{V} = \alpha_W \vec{V}_W + \alpha_C \vec{V}_C \tag{4.3}$$

where

α_W = wind drift factor (~ 0.03);

$\vec{V}_W$ = wind velocity at 10 m above the mean water surface level;

α_C = current drift factor (~ 1.1);

$\vec{V}_C$ = depth-averaged current velocity.

In open seas the wind elongates the slick in the direction of prevailing winds and oil thickness varies within the slick. However, commonly the total slick area is approximated as a circular slick.

Evaporation

The preferential transfer of light-and medium-weight components of the oil from the liquid phase to the vapor phase is known as evaporation (Exxon, 1985). Evaporation

is considered to be the primary process resulting in a loss of mass during the first few hours of an oil spill (Buchanan and Hurford, 1988; Sebastiao and Soares, 1995). Two methods are typically used to compute evaporation rate: i) the pseudo-component approach (Yang and Wang, 1977; Sebastiao and Soares, 1998), and ii) the analytical approach (Mackay *et al.*, 1980; Stiver and Mackay, 1984).

In the pseudo-component approach, oil is characterized by a set of fractions grouped by molecular weight and boiling point; this results in different evaporation rates for different fractions. In the analytical approach, vapor pressure is expressed as a function of fraction evaporated. The oil's evaporation curve is predicted from its distillation curve. Sebastiao and Soares (1998) showed that the pseudo-component approach provides better results for a light crude oil. Another study carried out by ASCE (1996) recommended the use of the analytical approach for heavy and mixed oils. This suggests that the improvements obtained with either of the methods cannot be applicable to all situations. The current work utilizes the analytical method proposed by Stiver and Mackay (1984) in modelling the surface evaporation rates. The analytical method uses a simple algorithm and the required parameters are readily available from distillation data (Sebastiao and Soares, 1995). The expression for the volume fraction evaporated is (Stiver and Mackay, 1984):

$$F_E = \ln\left[1 + B\left(\frac{T_G}{T}\right)\theta \exp\left(A - B\frac{T_O}{T}\right)\right]\left[\frac{T}{BT_G}\right] \qquad (4.4)$$

where

$$\theta = \frac{K_2 A_S t}{V_O};$$

$K_2 = 0.0025\,W^{0.78}$ (Buchanan and Hurford, 1988);

F_E = volume fraction evaporated;

K_2 = oil mass transfer coefficient for evaporation (m/s);

W = wind speed (m/s);

V_O = initial volume of spilled oil (m^3);

T_O = initial boiling point at F_E of zero (K);

T_G = gradient of the boiling point, T_B, and F_E line (K);

T = environmental temperature (K);

A, B = constants derived from distillation data.

Stiver and Mackay (1984) calculated the magnitude of the constants A and B as 6.3 and 10.3, respectively, using linear regression of distillation data for five different types of crude oils.

Natural Dispersion

The natural dispersion process occurs due to mixing of oil into the water column, which is mainly attributed to breaking waves. Experimental studies (Mackay *et al.*, 1980) indicate that some of the energy of the breaking wave is imparted to the oil slick causing the formation of oil droplets (globulation). Another portion of the breaking energy is converted to turbulent eddies which transport the oil droplets into the water column. In general, oil-in-water emulsions are not stable and larger oil droplets (diameter > 0.1 mm) may coalesce and return to the surface under calm sea conditions.

The oil/water interfacial tension parameter affects globulation and coalescence. The viscosity of oil also affects the natural dispersion process. The more viscous the oil is, the lower its ability to form oil droplets.

Reed (1989) computed the dispersion rate per hour by employing the entrainment formulation of Mackay *et al.* (1980), which is given by the semi-empirical relation:

$$D = D_a \bullet D_b = \left[0.11(W+1)^2\right] \bullet \left[\left(1+50\mu^{1/2} h s_t\right)^{-1}\right] \tag{4.5}$$

where

D_a = the fraction of sea surface dispersed per hour;

D_b = the faction of the dispersed oil not returning to the slick;

W = wind speed (m/s);

μ = viscosity (cp);

h = slick thickness (m);

s_t = oil-water interfacial tension (dyne/m).

Natural dispersion is not a well-understood process (Mackay and McAuliffe, 1989). The viscosity of oil is allowed to increase due to the dispersion of water droplets into oil (emulsification), which is discussed in the following section.

Emulsification

The emulsification process involves the mixing of water droplets into the oil medium. According to CONCAWE (1983), a crude oil with relatively low asphaltene content is expected to be less likely to form a stable emulsion. The result of

emulsification is not only a large increase in volume but also a large increase in viscosity (Sebastiao and Soares, 1995).

Mackay *et al.* (1980) proposed the following expression for the rate of incorporation of water into an oil slick:

$$\frac{dY}{dt} = 2\times10^{-6}(W+1)^2\left(1-\frac{Y}{C_3}\right) \tag{4.6}$$

where

Y = fraction of water in oil;

C_3 = final fraction water content (0.7 for crude oils and heavy fuel oil, and 0.25 for home heating oil).

An increase in viscosity due to mousse formation is computed by the following equation (Mooney, 1951):

$$\mu = \mu_O \exp\left[\frac{2.5Y}{1-C_3Y}\right] \tag{4.7}$$

where μ_O = parent oil viscosity, which can be calculated with the percentage asphaltene content A_C as: $\mu_O = 224A_C^{1/2}$

Evaporation also causes a viscosity increase, which can be modelled as:

$$\mu = \mu_O \exp(C_4F_E) \tag{4.8}$$

where C_4 = a constant $\in$ [1, 10]; where 1 is for light substances such as gasoline, and 10 is for crude oils.

4.1.2 Fugacity-Based Multimedia Fate and Transport Models

This section presents an overview of fugacity-based multimedia models. Mackay (1991) has provided a comprehensive description of the fugacity-based modelling approach. Based on the level of complexity of the problem, Mackay (1991) recommended four systems: level I, level II, level III, and level IV.

In level I, all of the bulk compartments/phases are assumed to be at equilibrium. A chemical compound is considered as conserved; it is neither destroyed by reactions nor conveyed out of the evaluative environment by flows. The model is described in a fugacity format in which fugacity acts as a surrogate for concentration. Fugacities are related to concentrations by the following expression (Mackay, 1991):

$$C = Zf \tag{4.9}$$

where

Z = fugacity capacity (mol/m^3·Pa);

C = Concentration (mol/m^3);

f = fugacity (Pa).

The Z values (also known as fugacity capacities) establish equilibrium partitioning for a chemical in each phase. Using the basic fugacity equation for a chemical in the vapor state and the ideal gas law, Z for air can be determined as (Mackay, 1991):

$$Z = \frac{1}{RT} \tag{4.10}$$

where

R = gas constant (8.314 Pa·m^3/mol·K);

T = absolute temperature (K).

Z for water is then determined using the Z value for air and Henry's law. As the partition coefficients are ratios of solubility in one phase to that in water, Z for water is used to establish Z for other phases (such as biota, sediments etc.). Z for various media are defined in Table 4.1.

The level II scenario requires equilibrium among all phases (i.e. common fugacity). However, transformation and transport processes such as reaction and advection, respectively, are included in the model. D values are used to express the rate of a process as (Mackay, 1991):

$$N = Df \tag{4.11}$$

N = rate of a process (mol/h)

D = transport parameter (mol/h·Pa)

f = fugacity (Pa)

The D values for various processes in a medium are defined in Table 4.2.

At level III, equilibrium is assumed between dispersed phases/sub-compartments but not between bulk phases. The inter-media transport process between two bulk phases is accounted for by inter-media D values. The model presumes steady state conditions that can be obtained after prolonged exposure of the system to constant input conditions. Similar to the level II calculations, level III modelling allows reaction and advective transport of chemicals out of the bulk phase.

Table 4.1 Definition of fugacity capacities (modified from Mackay *et al.*, 1983)

Compartments	Definition of Z (mol/m^3·Pa)
Air	$Z_{air} = \frac{1}{RT}$, R = gas constant (8.314 Pa·m^3/mol·K), T = temperature (K)
Water	$Z_{water} = \frac{1}{H}$ or $\frac{C^s}{P^s}$, C^s = aqueous solubility (mol/m^3), P^s =vapor pressure, H = Henry's law constant (Pa·m^3/mol)
Solid Sorbent (sediment, soil, or particles)	$Z_{sorbent} = k_{sw}\rho_s / H$, k_{sw} = partition coefficient (L/kg), ρ_s = density (kg/L)
Biota	$Z_{biota} = k_{bw}\rho_b / H$, k_{bw} = bioconcentration factor, ρ_b = density (kg/L)

Table 4.2 Definition of transport parameter

Processes	Definition of D (mol/h·Pa)
Transformation	$D_{transf} = VZk$, V = volume (m^3), k = rate constant (h^{-1})
Diffusion	$D_{dif} = AKZ$, A = area (m^2), K = mass transfer coefficient (m/h)
Advection	$D_{adv} = GZ$, G = flow rate (m^3/h)

Mackay *et al.* (1983) developed the QWASI model using level III formulations. They applied the model to predict the fate of PCBs and heavy metals in a lake environment. Sadiq (2001) used the QWASI model in a probabilistic mode to simulate the fate of drilling waste discharges in a marine environment. The model presumes steady state conditions that can be obtained after prolonged exposure of the system to constant input conditions. Similar to the level II calculations, level III modelling allows reaction and advective transport of chemicals out of the bulk phase. Mackay *et al.* (1983)

developed the QWASI model using level III formulations. They applied the model to predict the fate of PCBs and heavy metals in a lake environment. Sadiq (2001) used the QWASI model in a probabilistic mode to simulate the fate of drilling waste discharges in a marine environment.

The level IV approach is an extension of level III, considering unsteady state conditions. Sweetman *et al.* (2002) implemented the level IV modelling to predict the fate of PCBs in multimedia over a 60-year period. The current study applies the level IV model in describing the fate of an oil spill in a marine environment.

4.2 The Proposed Methodology

In this section, the proposed methodology couples the weathering algorithms of spreading, evaporation, natural dispersion, and emulsification with a level IV fugacity-based model to predict the oil fate in case of a batch spill scenario on the water surface.

4.2.1 Governing equations of the weathering processes

The current work uses a set of differential equations that was proposed by Sebastiao and Soares (1995) to model the weathering processes. As the weathering processes occur simultaneously, the Sebastiao and Soares formulation of a system of differential equations allows the simultaneous variation of interdependent weathering variables. However, their formulation is limited to model the fate of surface oil. To account for the fate of oil also in the water and sediment compartments, the formulations of the weathering processes are coupled with an oil multimedia fate and transport model. The governing equations used to model the weathering processes are as follows (Sebastiao and Soares, 1995):

$$\frac{dF_E}{dt} = \frac{K_2 A_S}{V_O} \exp\left(A - \frac{B}{T}(T_O + T_G F_E) \right) \tag{4.12a}$$

$$\frac{dV}{dt} = -V_O \frac{dF_E}{dt} - DV \tag{4.12b}$$

$$\frac{dY}{dt} = 2 \times 10^{-6} (W+1)^2 \left(1 - \frac{Y}{C_3} \right) \tag{4.12c}$$

$$\frac{dA_S}{dt} = K_1 A_S^{-1} V^{4/3} \tag{4.12d}$$

$$\frac{d\mu}{dt} = C_4 \mu \frac{dF_E}{dt} + \frac{2.5\mu}{(1 - C_3 Y)^2} \frac{dY}{dt} \tag{4.12e}$$

The volume rate of oil entrained into the water column is calculated as:

$$\frac{dV_{ent}}{dt} = DV \tag{4.12f}$$

where V is the volume of oil at a given time and other parameters are defined elsewhere in this section.

4.2.2 Two-Compartment Level IV Modelling Approach

Two bulk compartments (i.e., water and sediment) are used for level IV modelling, where each bulk compartment consists of sub-compartments such as suspended solids and biota (fish) in the water column, and solids and pore water in the sediments. A system of differential mass balance equations for the two-compartment model is given as follows (Mackay, 1991):

For water

$$\frac{d}{dt}(V_{B2} Z_{B2} f_2) = I_2 + D_{42} f_4 - (D_{R2} + D_{A2} + D_{24}) f_2 \tag{4.13}$$

For sediment

$$\frac{d}{dt}(V_{B4}Z_{B4}f_4) = I_4 + D_{24}f_2 - (D_{R4} + D_{Bur} + D_{42})f_4 \quad (4.14)$$

The subscripts 2 and 4 represent water and sediment, respectively (adopted from Mackay, 1991), and B represents the bulk phase. The input rate of a chemical compound is denoted by I_i(mol/s). A description and the related equations for the parameters Z and D are presented in Table 4.3. The compartment volumes are a function of time so as to account for the growth of the oil slick due to spreading. However, the Z values are considered constant. This results in the following system of differential equations:

For water,

$$Z_{B2}V_{B2}\frac{df_2}{dt} = I_2 + D_{42}f_4 - (D_{R2} + D_{A2} + D_{24} + D_{G2})f_2 \quad (4.15)$$

For sediment,

$$Z_{B4}V_{B4}\frac{df_4}{dt} = I_4 + D_{24}f_2 - (D_{R4} + D_{Bur} + D_{42} + D_{G4})f_4 \quad (4.16)$$

where

$$D_{G2} = Z_{B2}\frac{dV_{B2}}{dt} \quad (4.17)$$

$$D_{G4} = Z_{B4}\frac{dV_{B4}}{dt} \quad (4.18)$$

Equations (4.15) and (4.16) are combined with a system of differential equations for the weathering processes and the solution can be obtained by employing the numerical integration methods.

Table 4.3 Description of parameters used in level IV model (Mackay, 1991)

Parameters and equations	Description
Z (mol/m^3·Pa), fugacity capacity calculations:	Z_{B2} is bulk fugacity capacity for water phase
• Water	Z_2, Z_5, and Z_6 are fugacity capacities for water, suspended solids, and biota, respectively
$Z_{B2} = \nu_2 Z_2 + \nu_5 Z_5 + \nu_6 Z_6$	ν_2, ν_5, and ν_6 are volume fractions of water, suspended solid, and biota in the water compartment, respectively. The magnitude of ν_2 is usually negligibly different from unity
$Z_2 = 1/H$	
$Z_5 = Z_2 \rho_5 \phi_5 K_{OC}$	ρ_5, and ρ_6 (kg/L) are densities of suspended solid, and biota in the water compartment, respectively
$Z_6 = Z_2 \rho_6 \phi_6 K_{OC}$	ϕ_5, and ϕ_6 are organic fractions of suspended solid and biota
• Sediment	Z_{B4} is bulk fugacity capacity for sediment
$Z_{B4} = \nu_8 Z_2 + \nu_7 Z_4$	ν_7, and ν_8 are volume fractions of solids, and pore water in the sediment compartment, respectively
$Z_4 = Z_2 \rho_4 \phi_4 K_{OC}$	ρ_4 is density of solids in the sediment compartment
	K_{OC} (L/kg) is organic carbon-water coefficient:
	$K_{OC} = 0.41 K_{OW}$
	K_{OW} is octanol-water partition coefficient
D-value (mol/h·Pa) calculations	D_{R2} and D_{A2} represent transport process due to reaction and advection within the water compartment
• Water	$V_2 \cong V_{B2}$
$D_{R2} = Z_{B2} V_2 k_2$	k_2 (h^{-1}) is a first order reaction (biodegradation) rate constant in water
$D_{A2} = Z_{B2} G_2$	G_2 (m^3/s) is volumetric flow rate, which can be calculated by current velocity (U) with the cross-sectional area perpendicular to the flow direction, i.e. $2Rh_W$
$D_{G2} = Z_{B2} \frac{dV_{B2}}{dt} = Z_{B2} h_W \frac{dA_2}{dt}$	R is radius and h_W is depth of the water compartment
$D_{24} = D_{Dif} + D_{DS}$	D_{G2} is a pseudo-D value, which accounts for the 'growth' within the water compartment.
Serial Configuration	$\frac{dA_2}{dt}$ is given by Equation (4.1)
$\frac{1}{D_{Dif}} = \frac{1}{k_{24} A_2 Z_2} + \frac{1}{\frac{B_{WX}}{\Delta_S} A_2 Z_2}$	D_{24} is an inter-media D value and represents the transport process from water to sediment. This is equal to an algebraic sum of two other transport processes occurring parallel, i.e. D_{Dif}, and D_{DS}.
$D_{DS} = A_2 U_{DS} Z_5$	
• Sediment	D_{Dif} denotes the diffusive process and its reciprocal is an

$D_{R4} = Z_{B4} V_4 k_4$ $D_{Bur} = A_2 U_{Bur} Z_4$ $D_{G4} = Z_{B4} \frac{dV_{B4}}{dt} = Z_{B4} h_S \frac{dA_2}{dt}$ $D_{42} = D_{Dif} + D_{RS}$ $D_{RS} = A_2 U_{RS} Z_4$	algebraic sum of the reciprocal D values on water side diffusion, and effective diffusivity within sediment. Usually, the error introduced by neglecting water side mass transfer coefficient (k_{24}) term is considered negligible D_{DS} is deposition process associated with the suspended solid U_{DS} (m/h) is suspended solid deposition rate k_{24} (m/h) is water side mass transfer coefficient B_{WX} (m^2/h) is effective diffusivity Δ_S (m) is diffusion path length in sediment h_S (m) is sediment depth D_{R4} and D_{Bur} represent transport process due to reaction and sediment burial k_4 (h^{-1}) is a first order reaction (biodegradation) rate constant in sediment U_{Bur} (m/yr) is sediment solids' burial rate D_{G4} is a pseudo-D value, which accounts for the 'growth dilution' within the sediment compartment D_{RS} is sediment re-suspension process U_{RS} (m/h) sediment re-suspension rate

4.3 Case Study

To demonstrate the application of the proposed methodology a case study is presented in which a surface spill of Statfjord crude oil of 100 tonne (~120 m^3) in a marine environment is simulated. Sebastiao and Soares (1995) also simulated the weathering processes for this spill and validated their results with previously published experimental data. The physical characteristics of the Statfjord crude oil used in the current simulation are presented in Table 4.4.

Table 4.4 Statfjord crude oil characteristics used in the modelling of weathering processes

Oil characteristics	Values
Density (kg/m^3)	832
Wind speed (m/s)	4.17
Viscosity @ 40 °C (cp)	3.03
T_O – initial boiling point at zero evaporation (K)	301
T_G – gradient of the boiling point and fraction evaporation line (K)	500
Oil-water interfacial tension (dyne/m)	2000
Water temperature (K)	288

The initial oil slick thickness of 0.02 m is fixed as recommended by Mackay *et al.* (1980). The subsequent area calculations are not sensitive to this initial thickness assumption. Use of Equation (4.2) leads to the initial area spread of 6000 m^2. The affected area of the water and the sediment phases is assumed equal to the area of the surface oil slick, and the area growth is a function of time. The volume of both compartments is determined by multiplying the average well-mixed depth with the surface area at a particular time.

The initial values for both the fraction evaporated and the fraction of water content in the slick are considered to be zero. Allowance is made for the loss of oil volume as a result of evaporation and natural dispersion. The oil volume entrained into

the water column due to the natural dispersion process is used to calculate the oil volumetric flow rate (Q_{ent}). Thus:

$$Q_{ent} = \frac{dV_{ent}}{dt} \tag{4.19}$$

The emission rate $I_2(t)$, is obtained by multiplying the oil volumetric flow rate with the molar concentration C_i (mol/m^3) of a compound constituting the oil, i.e.,

$$I_2(t) = Q_{ent} \cdot C_i \tag{4.20}$$

Oil is a complex mixture of thousands of various compounds (API, 1999); naphthalene is used as a representative compound in the present study, with the physicochemical properties given in Table 4.5. The particulate matter serves as a vehicle for the transport of naphthalene from the bulk of the water to the bottom sediments.

The environmental multimedia parameters used for the level IV fugacity-based model are provided in Table 4.6. These parameter values are taken as crisp estimates, and uncertainties that may be associated with the parameters are not considered in the analysis. To demonstrate the application of the proposed methodology, a deterministic analysis using point estimates is justified. However, the uncertainty in the fate and transport model is considered later in section 5.3.

Table 4.5 Physiochemical properties of naphthalene used in the simulation

Parameter	Notation	Value	Units
Molecular weight	MW	128.2	g/mol
Solubility @ 25°C	C^S	31.7	g/m^3
Vapor pressure @ 25°C	P^S	10.4	Pa
Logarithmic value - octanol-water partitioning coefficient	$\log K_{ow}$	3.35	-
Reaction (biodegradation) rate constant water	k_2	2.89×10^{-3}	h^{-1}
Reaction (biodegradation) rate constant sediment	k_4	1.93×10^{-4}	h^{-1}
Sediment-water phase effective diffusivity	B_{WX}	1.91×10^{-6}	m^2/h
Naphthalene concentration	C_1	8 (~1000)	mol/m^3 (ppm)

4.4 Results and Discussion

A system of differential equations as proposed in section 4.2 was solved using the Matlab ODE solver *ode 45*. The solver *ode 45* is a built-in Matlab function which uses a combination of fourth- and fifth-order Runge-Kutta methods in solving the differential equations numerically (Palm, 2001). The multimedia model output includes fugacity profiles for both bulk compartments (water and sediment), and concentration profiles for the water column and fish. Such profiles are conventionally used in calculating the exposure in ecological and human health risk analyses.

The surface oil slick area growth is shown in Figure 4.1(a). This area prescribes the dimensions of both evaluative compartments at a given time. The slick growth ceases as its thickness decreases to 0.01 cm, resulting in a final area of 1.52×10^5 m^2 at 225 h.

Table 4.6 Environmental multimedia parameters used in level IV fugacity-based model

Parameters	Notation	Value	Unit
Depth water	h_W	100	m
Volume fraction suspended solids in water	v_5	$5x10^{-6}$ [a]	-
Volume fraction biota in water	v_6	$1x10^{-6}$ [a]	-
Organic fraction suspended solid	ϕ_5	0.2 [b]	-
Organic fraction biota	ϕ_6	0.05 [c]	-
Density suspended solids	ρ_5	1500 [b]	kg/m^3
Density fish	ρ_6	1000 [a]	kg/m^3
Advection rate water	U_A	0.018 [d]	m/s
Deposition rate suspended solids	U_{DS}	$5x10^{-7}$ [b]	m/h
Depth sediment	h_S	0.05[e]	m
Diffusion path length in sediment	$\Delta_S = 0.5h_S$ [a]	0.025	m
Density sediment	ρ_4	2500 [d]	kg/m^3
Volume fraction sediment solids	v_7	0.37 [c]	-
Volume fraction pore water	v_8	0.63 [c]	-
Organic fraction sediment	ϕ_4	0.04 [b]	-
Re-suspension rate sediment	U_{RS}	$2x10^{-7}$ [b, d]	m/h
Burial rate sediment	U_{Bur}	$3.4x10^{-8}$ [c, d]	m/h

a: Sweetman *et al.* (2002)
b: Mackay *et al.* (1992)
c: Mackay (1991)
d: Sadiq (2001)
e: U.S. EPA (1999)

The oil volume curve is also shown in Figure 4.1(a), with volume decreasing by the processes of evaporation and dispersion. At an elapsed time of 24 h since the oil has released, approximately 62.5% of the total oil volume is lost from the surface slick.

Simulation results show that approximately 98% of the total oil volume is lost due to evaporation alone, with the remainder lost to the water column due to dispersion. The dispersion-emulsification formulation (as discussed in section 4.2) eventually drives the residual oil (oil not evaporated) into the water column, thus giving the surface slick a finite lifetime. In the current example, the calculated surface slick lifetime is 435 h (~ 18 d). Figures 4.1 (b), (c), and (d) present the dynamics of oil fraction evaporated, water content, and oil viscosity increase due to emulsification and evaporation, respectively. As expected, the results of the weathering simulations are similar to those obtained by Sebastiao and Soares (1995).

The emission rate of naphthalene into the water column is presented as a function of time along with the water fugacity curve in Figure 4.1(e). The chemical input to the water column becomes zero at 435 h, which corresponds to the surface slick lifetime. The shape of the emission rate curve depends on the natural dispersion rate and oil slick volume (see Equation 4.12f). Oil slick volume decreases with time due to the evaporation and natural dispersion weathering processes. Assuming constant wind speed and oil-water interfacial tension, the variation of the product term $\left(\mu^{1/2}h\right)^{-1}$ in Equation (4.5) governs an increase or decrease of dispersion rate with time in the current simulations. After reaching its peak at approximately 1 h (see Figure 1b), the emission curve begins to decrease. At an elapsed time of 16 h, a small increase in the emission rate curve is observed due to the higher dispersion rates.

The water and sediment fugacity curves are shown in Figure 4.1(f). A peak in the water fugacity curve occurs at 3 h (which is very close to the input curve peak), whereas

the sediment fugacity curve peaks at an elapsed time of 447 h. The water compartment shows a rapid decrease of its burden after the chemical input is stopped, but the sediment is slower to respond. Figure 4.1(f) thus indicates that the water compartment response is faster than that of the sediment compartment. This behavior stems from the fact that the water compartment has relatively fast transport and transformation processes.

The group $\frac{VZ}{D}$ provides valuable insight into the residence time associated with a transport process; the shorter the residence time, the more significant the process. The water-to-sediment transfer time for depletion of water through the D_{24} process can be calculated as:

$$t_{res24} = \frac{V_{B2} Z_2}{D_{24}} = \frac{h_W Z_2}{\left[\frac{B_{WX} Z_2}{\Delta_S} + U_{DS} Z_S \right]} = 53.3 \text{ yr} \tag{4.21}$$

The advection process residence time can be calculated as:

$$t_{resA2} = \frac{V_{B2} Z_{B2}}{D_{A2}} = \frac{\sqrt{\pi}}{2} \frac{\sqrt{A_2(t)}}{U_A} \tag{4.22}$$

The above expression shows that the advection residence time increases with the square root of area. The advection residence time, averaged over the analysis period of 500 h, is calculated as 5 h. The reaction process residence time $\left(t_{resR2} = \frac{1}{k_2} \right)$ is 346 h or ~ 14.4 days.

The last process associated with the water compartment is the growth process. The residence time for this pseudo transport process can be calculated as:

$$t_{resG2} = \frac{V_{B2} Z_{B2}}{D_{G2}} = A_2 \left[\frac{dA_2}{dt} \right]^{-1} \tag{4.23}$$

or alternatively, in terms of definition of the derivative term as given by Equation (4.1), the more convenient form is:

$$t_{resG2} = \frac{A_2^2}{K_1 V^{4/3}} \tag{4.24}$$

With respect to the time at which the slick growth ceases, i.e., $\left[\frac{dA_2}{dt} \right] \rightarrow 0$, Equation (4.23) shows that $t_{resG2} \rightarrow \infty$. This suggests that the growth transport process is only important during the area growth regime, and should not be included in model Equations (4.15) and (4.16) outside the growth regime. In the current example, at an elapsed time of 2 h, the growth residence time has the same value as that of the averaged advection residence time. Further, the growth process residence time increases and at an elapsed time of 106 h its magnitude becomes equal to the value of the reaction process residence time. Once the slick growth is ceased (at ~ 225 h), however, the growth process is no longer included in the fate modelling calculations.

Advection is seen to be the most important transport process, as the analysis suggests that the lowest residence time was for the advection process.

In the case of sediment-to-water inter-media processes, the residence time is:

$$t_{res42} = \frac{V_{B4} Z_4}{D_{42}} = \frac{h_S Z_4}{\left[\frac{B_{WX} Z_2}{\Delta_S} + U_{RS} Z_4 \right]} = 5.5 \text{ yr} \tag{4.26}$$

The reaction residence time $\left(t_{resR2} = \frac{1}{k_4}\right)$ is approximately 5200 h or ~ 7 months. The residence time for the sediment growth process is the same as that for the water compartment growth residence time. The last transport process is the sediment burial with an associated residence time of:

$$t_{resBur} = \frac{h_S}{U_{Bur}} = 168 \text{ yr} \tag{4.27}$$

The analysis shows that during the growth regime (up to 225 h), the growth process is the most important transport process in the sediment compartment.

Another important parameter is Z, which distributes the concentration between phases. A phase of high Z value (such as fish) absorbs a greater quantity of solute (organic chemical), resulting in higher concentrations while retaining a low fugacity. The converse is true for a phase having a low Z value. The Z value for fish (Z_6) is approximately 1.091 mol/m^3·Pa; for water, the value (Z_2) is 0.024 mol/m^3·Pa. This leads to fish concentrations which are $\frac{Z_6}{Z_2}$ times higher than the water column concentrations. Figure 4.1(g) provides a comparison of fish and water column concentration profiles for the case study.

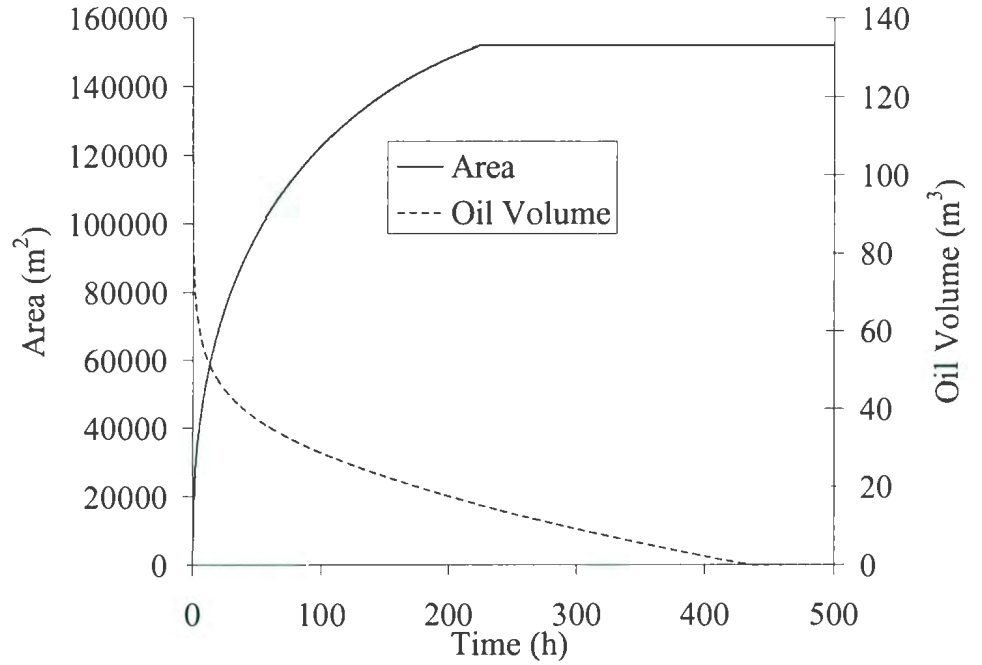

(a)

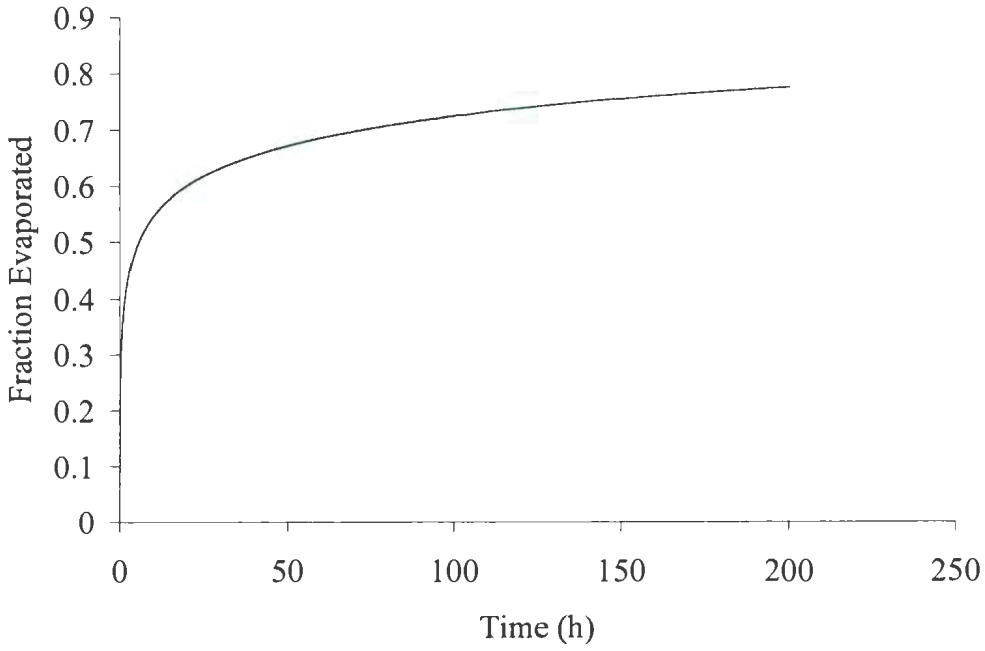

(b)

Figure 4.1 Multimedia fate of Statfjord crude oil in the marine environment

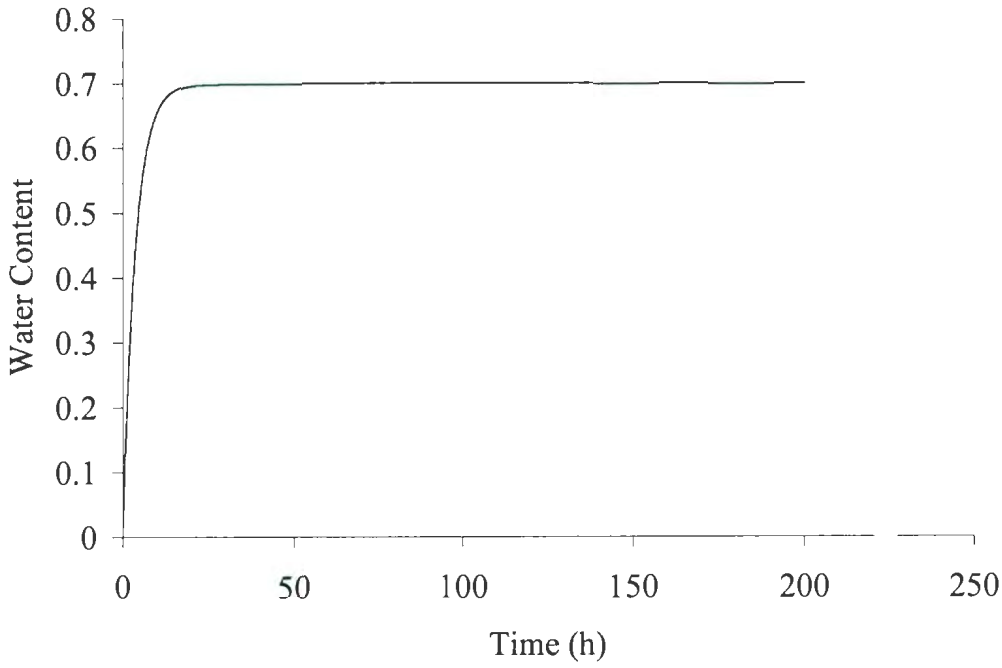

(c)

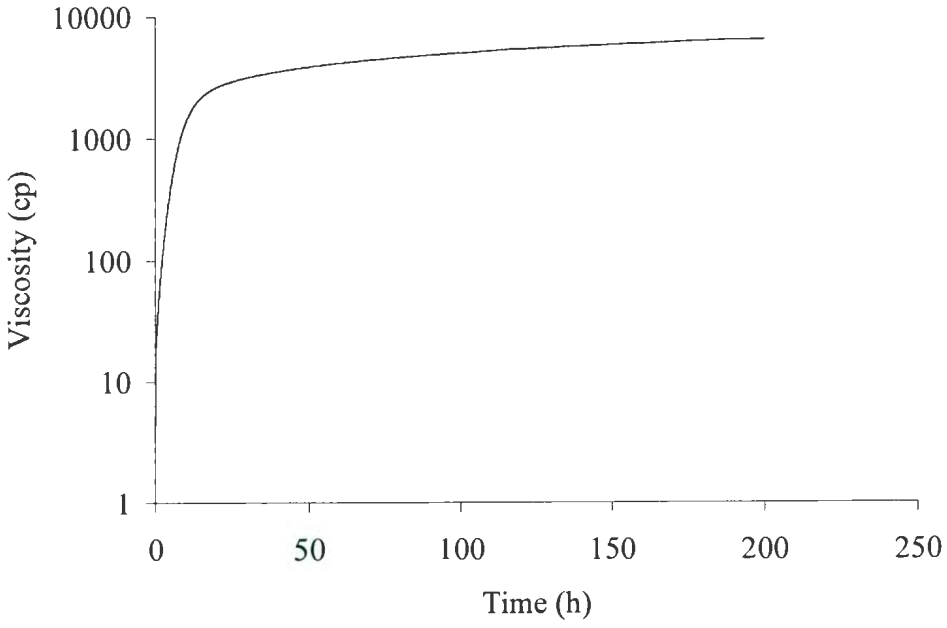

(d)

Figure 4.1 Multimedia fate of Statfjord crude oil in the marine environment

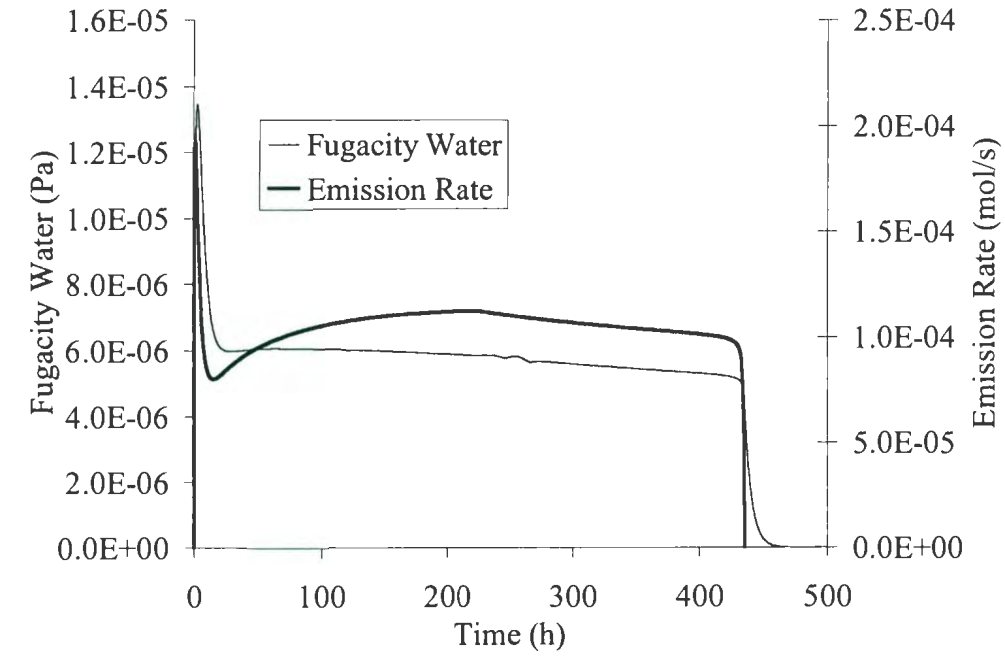

(e)

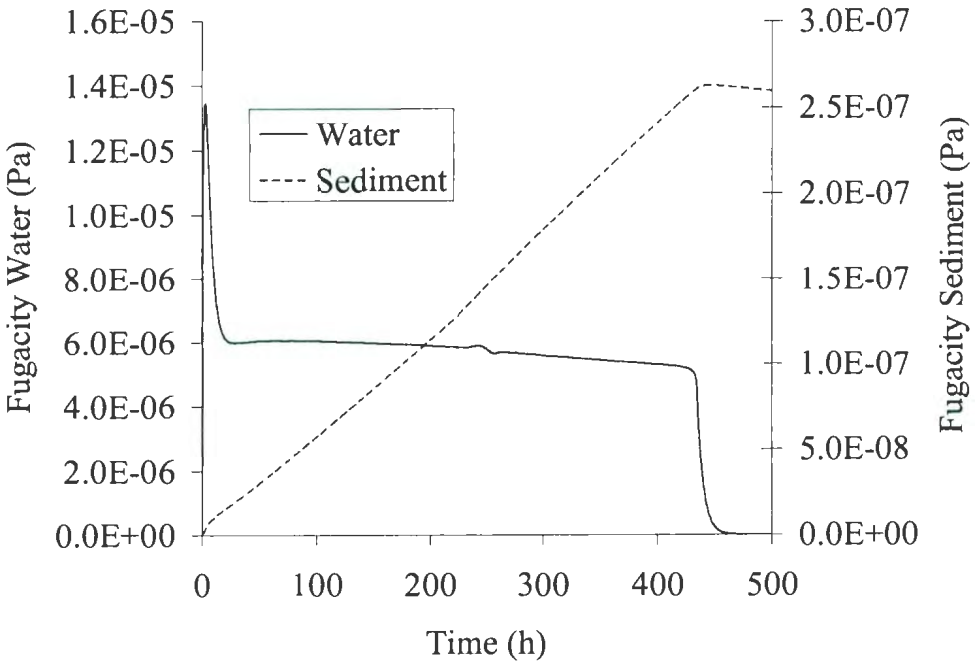

(f)

Figure 4.1 Multimedia fate of Statfjord crude oil in the marine environment

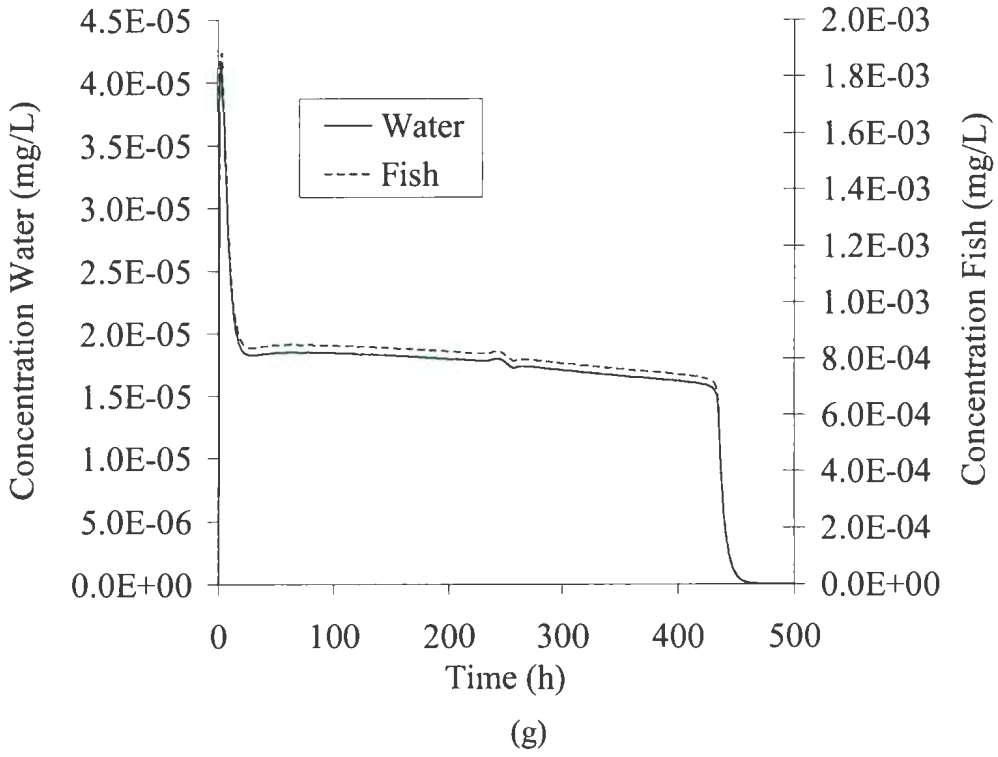

Figure 4.1 Multimedia fate of Statfjord crude oil in the marine environment.

Chapter 5

Ecological Risk Assessment

This chapter extends the previously developed surface release contaminant fate and transport methodology to account for an underwater release of contaminants (oil/gas mixtures) from a broken riser.

The underwater loss of oil and gas may result in a flash fire/explosion followed by a pool fire from an ignited oil release, and an oil slick due to an unignited oil release (Liera, 1998; CMPT, 1999). The thermal hazard posed by the fire/explosion consequences may have a severe impact on the offshore oil and gas platform. The thermal hazard is negligible for an unignited oil release; however, the toxic chemicals in the oil slick can have adverse effects on marine organisms. The scope of the current chapter is limited to the second potential consequence - ascribed as *ecological risk* - associated with an unignited oil release from a broken riser.

Ecological risk assessment (ERA) deals with a multitude of organisms, all with varying sensitivity to pollutants under various exposure scenarios (EEA, 1999). The diversity of marine life makes ERA more challenging than human health risk, where only one endpoint is involved—human. The U.S. EPA (1998) has established a systematic framework for ecological risk assessment. The ERA framework comprises three main steps: (1) problem formulation, (2) analyses of exposure and effects, and (3) risk characterization.

Various researchers, e.g. Karman *et al.* (1996), Karman and Reerink (1998), Sadiq *et al.* (2003), and Mukhtasor *et al.* (2004) carried out ERA studies from the

perspective of drilling waste discharges in a marine environment. In the case of underwater oil and gas releases, exposure analysis becomes very complex and demanding. Exposure analysis accounts for the hydrodynamics of the submerged oil/gas buoyant jet, and the oil fate and transport in a multimedia marine environment.

The proposed fate/transport methodology (Chapter 4) is used as a part of the ERA framework to conduct a probabilistic analysis. The current chapter presents a brief description of the ERA framework and provides an application of the proposed methodology using two case studies.

5.1 U.S. EPA Framework

The purpose of ecological risk assessment is to assess the nature and likelihood of adverse effects on an organism or on a collection of organisms due to environmental or anthropological changes. The U.S. EPA (1998) has developed a comprehensive framework for ERA (see Figure 5.1). Subsequent sections describe the basic components of the ERA framework in relation to an underwater oil and gas release from a broken riser.

5.2 Problem Formulation

Problem formulation is a process for generating and evaluating hypotheses about the ecological effects that have already occurred (retrospective risk approach) or may occur (prospective risk approach) from human activities.

An accidental discharge of an oil and gas mixture from a riser causes a release of toxic chemicals into the water column and sediment pore water.

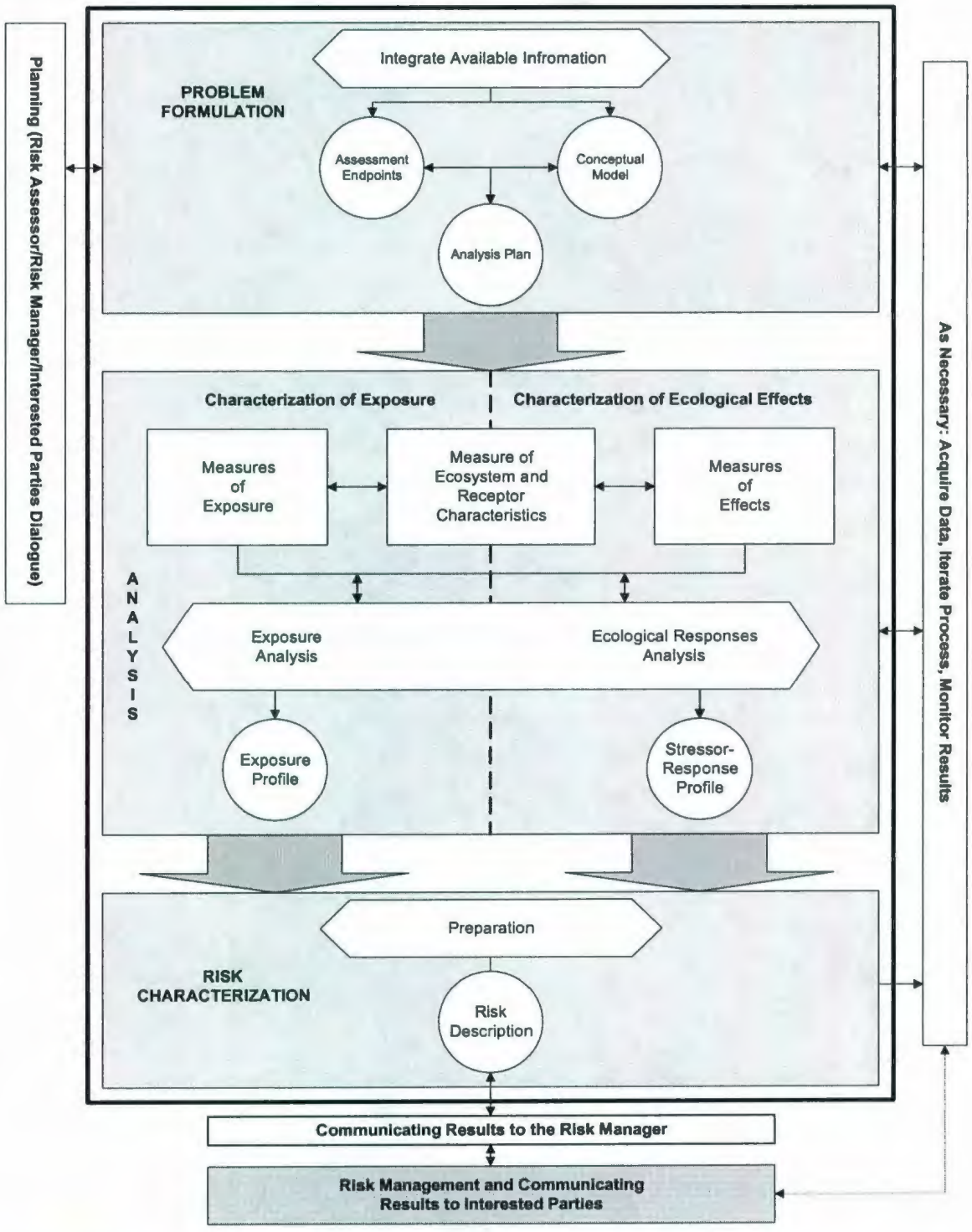

Figure 5.1 The ecological risk assessment framework (modified from U.S. EPA, 1998)

The potential primary effects associated with the toxic chemicals in oil include increased morbidity and mortality of marine life. The problem identified here is to quantify long-term (chronic) adverse effects on various species in a marine ecosystem due to an accidental underwater release of oil and gas.

The problem formulation process is further divided into three sub-steps: i) assessment endpoints, ii) conceptual models, and iii) analysis plan.

5.2.1 Assessment Endpoints

The U.S. EPA (1998) has listed three basic criteria to select ecological values that may be appropriate for assessment endpoints:

i) ecological relevance,

ii) susceptibility to known and potential stressors, and

iii) relevance to management goals.

An entity, which is currently or was historically a part of the ecosystem, is ecologically relevant. Marine organisms are susceptible to hydrocarbons and other pollutants in oil when subjected to excess concentrations above their threshold levels. The selection of the food web as an endpoint is more realistic than defining a single species or group as an endpoint (Husain *et al.*, 2001). This also seems the right choice from a management and scientific viewpoint. However, due to difficulty associated with obtaining toxicity data for all organisms in the ecosystem, traditionally selected representatives of major taxonomic groups are tested and used as the surrogate for the whole system (EEA, 1999). In the current study the endpoints are selected based on the availability of toxicity data for marine organisms in the literature.

5.2.2 Conceptual Model

A conceptual model involves a written description and a visual representation of predicted relationships between the ecological entities and the stressors. A flow diagram for such a conceptual model is presented in Figure 5.2.

Oil is a mixture of thousands of compounds; therefore, naphthalene is used as an indicator to carry out the risk assessment study. Reviews on the potential adverse effects of naphthalene on a marine ecosystem have been extensively published. The U.S. EPA AQUIRE database has compiled comprehensive data on the toxicity of naphthalene utilizing published work. Naphthalene is a polycyclic aromatic hydrocarbon (PAH) which has two benzene rings. In crude oils the naphthalene concentration is relatively high as compared to other higher molecular weight PAHs (three- through six-ring). Its acute toxicity is *high* to *moderate* to marine organisms (Bates *et al.*, 1997). Other toxicity effects include bioaccumulation, reproduction defects, and limited growth. These toxicity effects make naphthalene of considerable environmental interest. Furthermore, the bioavailability of naphthalene is 100% in the water column and its air-water partition coefficient is relatively low (13 times less than that of its parent compound - benzene). In general, the presented methodology is also applicable to other hydrocarbons.

The 'no observed effect concentration' (NOEC) is used to measure chronic effects. Due to limited availability of NOEC data, the predicted no effect concentration (PNEC) values are derived from the lethal concentrations at a mortality of 50% (LC_{50}) as suggested by Sadiq *et al.* (2003).

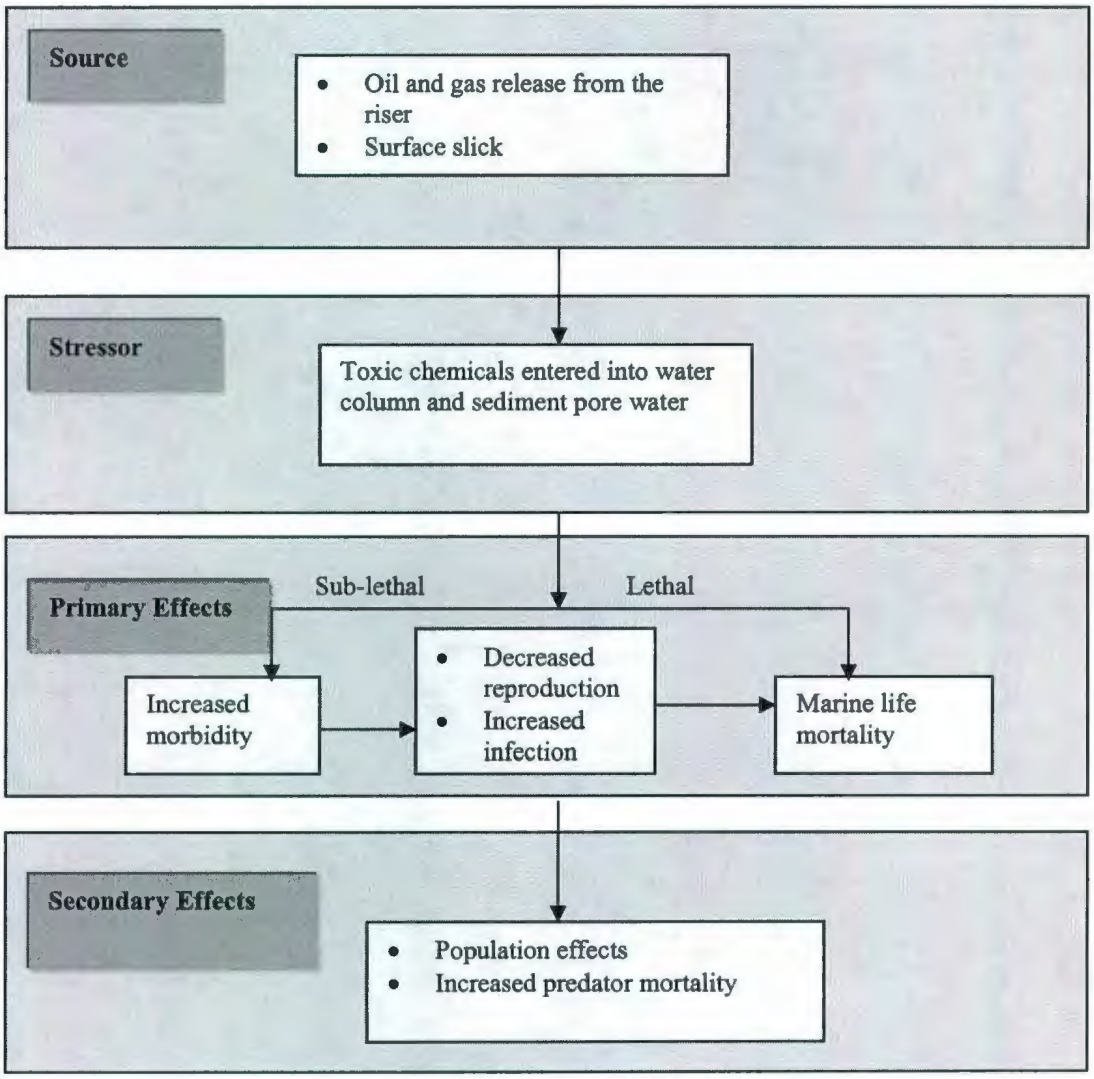

Figure 5.2 Proposed conceptual model for risk assessment

5.2.3 Analysis Plan

This is the final stage in the problem formulation. The stressor exposure to a marine organism could be through contaminated water and/or food. Physicochemical properties of the contaminant and physical parameters of the multimedia marine environment are

required to carry out exposure analysis. The acute and chronic toxicity effects of a stressor are used in the consequence analysis.

5.3 Analysis Phase

The analysis phase examines two components of risk - exposure and associated effects. Uncertainty analysis is an essential part of the analysis phase which enhances the credibility of the risk analysis (Mukhtasor *et al.*, 2001). A conceptual diagram of the analysis phase used in the present study is shown in Figure 5.3. The methods employed for the characterization of exposure and effects are described in the following subsections.

5.3.1 Characterization of Exposure

This section describes the methodology that is developed to characterize the exposure. An underwater release of an oil and gas mixture from shallow to moderate depths can reach the water surface within the order of a few minutes (Yapa and Zheng, 1997). Once production operations are stopped, oil releases from a broken riser are due to depressurization of the leftover gas. This suggests that the original source is effective only for a few minutes. Upon surfacing, the oil forms a slick and unignited gas escapes to the atmosphere. Weathering processes and environmental fate and transport models predict the oil concentrations in the multimedia marine environment. A flow diagram for the proposed exposure analysis is presented in Figure 5.4. Discussion on the development of the fate and transport modelling (part of the exposure analysis) and characterization of associated uncertainties is presented in the following sections.

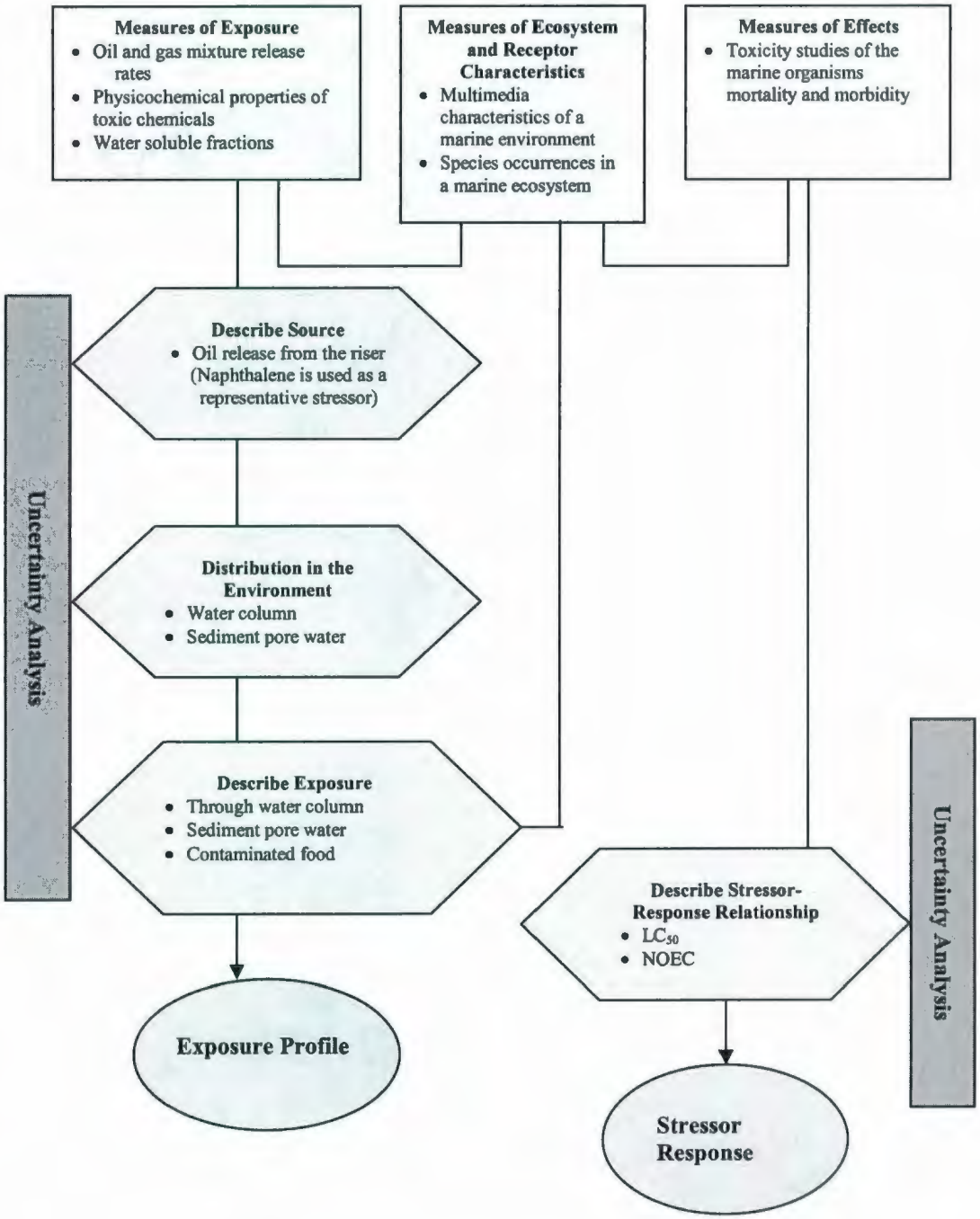

Figure 5.3 Analysis phase conceptual model

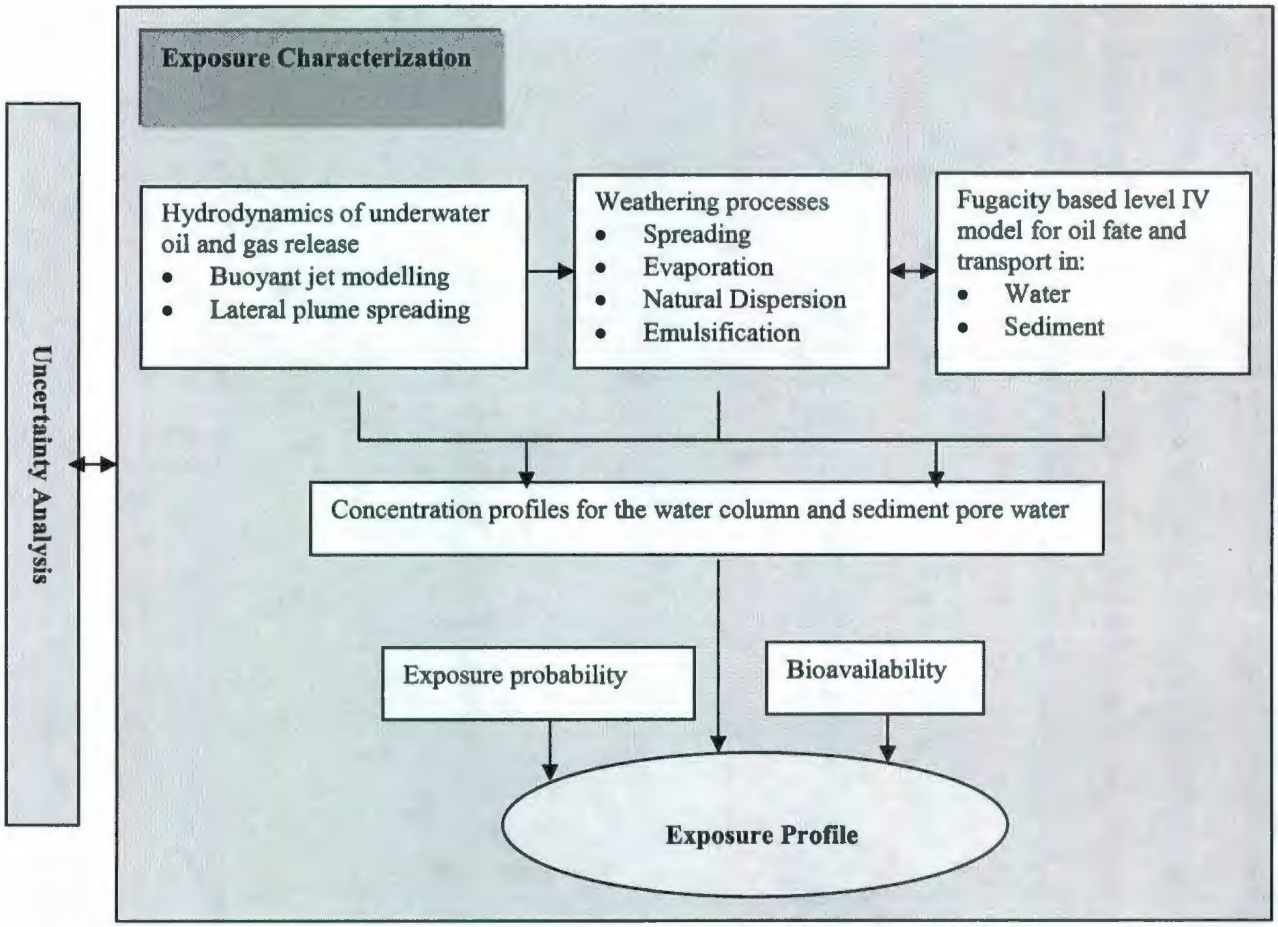

Figure 5.4 Proposed methodology for exposure analysis

a) Hydrodynamics of Underwater Oil and Gas Release

In underwater oil spills such as from a broken riser, oil usually behaves as a submerged buoyant jet. The fluid in a riser is considered either an oil and gas mixture or oil with no gaseous mixture. Submerged buoyant jets have been studied widely to observe the behavior of underwater sewage and thermal discharges and serve as a basis to simulate submerged buoyant jets of oil and gas mixtures (Yapa and Zheng, 1997). To simulate the behavior of submerged buoyant jets, two integral modelling approaches are in practice: (i) Eulerian, and (ii) Lagrangian integral approaches. The Eulerian integral

approach simulates buoyant jets based on a set of control volumes fixed in space. The Lagrangian integral approach considers buoyant jets as a series of non-interfering moving elements. These two types of approaches are essentially equivalent (Frick *et al.*, 1994).

Mc Dougall (1978), Fannelop and Sjoen (1980), Milgram (1983), and Fannelop *et al.* (1991) developed models to simulate underwater blowout, using an Eulerian integral approach. Yapa and Zheng (1997) were the first to extend Lee and Cheung's (1990) Lagrangian sewage discharge modelling to oil and gas submerged buoyant jets. The model was designed for releases from shallow to moderate depths ($\leq$ 300 m). Johansen (2000) developed a comprehensive gas plume model for subsea oil and gas mixture releases. The model is capable of simulating gas hydrate formation/decomposition, gas dissolution, and gas separation from the plume. However, the hydrate formation and decomposition modelling was based on thermodynamics only and no kinetics were taken into account.

Zheng *et al.* (2002) extended Yapa and Zheng's model to deep/ultra-deep water releases. They included gas hydrate formation/decomposition, gas dissolution, and gas separation modelling from the plume. The hydrate formation/decomposition module was based on the kinetics and the thermodynamics of hydrates. The Zheng *et al.* (2002) deepwater release modelling work was subsequently incorporated in the Clarkson Deepwater Oil and Gas Blowout (CDOG) model. To carry out an environmental impact assessment study, Ji *et al.* (2004) used the CDOG model to simulate the behavior of oil and gas accidentally released in deepwater areas.

The following assumptions are made in the current work in simulating oil and gas mixture releases:

i) The release of the mixture is limited to shallow to moderate depths (~ 300 m) and no gas converts into a solid hydrate.

ii) Gas dissolution into water is negligible because of the short residence time of the gas bubbles.

iii) Gas occupies the inner core of the jet/plume and no gas escapes from the plume during its journey to the surface.

iv) The oil/gas mixture reaches the surface and the plume does not become trapped at intermediate depths between the sea surface and the sea bed.

v) The gas obeys the ideal gas law.

These assumptions allow the use of the Yapa and Zehng (1997) model for the submerged jet/plume modelling. For simplicity, a one-dimensional ambient flow field is considered; the x-axis is oriented in the flow direction. A Lagrangian element is a control volume, which moves along the centerline of the buoyant jet/plume. As the element moves with the local centerline velocity, the element thickness, h, is given by (Yapa and Zheng, 1997):

$$h = \left|\vec{V}\right| \Delta t \tag{5.1}$$

where

$\vec{V}$ = local centerline jet/plume velocity;

Δt = small discrete time step.

The governing equations applied to the control volume (i.e. Equations T5.1 to T5.9) and their sources are presented in Table 5.1.

The momentum equations are modified from Yapa and Zheng (1997) for unidirectional ambient flow in the present study. The first term on the right-hand side of Equation (T5.6c) represents the vertical force acting on the liquid part. Scorer (1978) has shown that beyond several jet diameters, the pressure drag imposed by the current is negligible as compared to the contribution due to turbulent entrainment of the cross flow. The drag force is neglected in Equation (T5.6) and the last term on the right-hand side of Equation (T5.6c) represents the vertical force acting on the gas. The gas mass is very small compared to the liquid mass so its contribution to the momentum of the jet/plume is insignificant. This suggests that the second term in the square brackets of the left-hand side of Equation (T5.6c) can be neglected without affecting the simulation results.

The heat, salinity, and concentration diffusivities in Equation (5.7) are not considered in the simulations. This assumption does not affect the fate of oil calculations, as discussed by Yapa *et al.* (1999). A buoyant jet of oil and gas mixture is modeled as a two-phase flow (gas/liquid).

An oil/water mixture in the jet can be treated as a mixture of non-miscible fluids. For density calculations of the liquid part, water and hydrocarbon liquid are treated as a combined liquid with average properties. The UNESCO formula (Milero and Poisson, 1981) is used to calculate the seawater density in the mixture. Bobra and Chung (1986) gave the functional form of density variation for many oils. The state equation for the gas bubbles is the ideal gas law. The gas is assumed to follow isothermal expansion.

During the migration of a buoyant jet through the water column, the ambient fluid enters the jet through the exterior surface. Lee and Cheung (1990) separated entrainment into distinct processes identified as shear-induced entrainment (Q_s), and forced entrainment (Q_f).Shear-induced entrainment is present even when no ambient current exists.

Table 5.1 Governing equations for the jet/plume control volume—definition of the parameters and sources

Governing equations	Source	Parameters
Conservation of mass for liquid portion $\frac{dm_l}{dt} = \rho_a Q_e$ (T5.1) $m_l = \rho_l \pi b^2 (1-\beta^2 \varepsilon) h$ (T5.2) $\varepsilon = \frac{\rho_l - \rho}{\rho_l - \rho_b}$ (T5.3) **Conservation of mass for bubble portion** $\frac{dm_b}{dt} = 0$ (T5.4) $m_b = \rho_b \pi b^2 \beta^2 h \varepsilon$ (T5.5)	Yapa and Zheng (1997)	m_l = liquid mass of the control volume ρ_a = density of ambient fluid Q_e = volume flux entrained due to shear-induced entertainment (Q_s) and forced entrainment (Q_f) m_b = bubble mass of the control volume ρ_b, ρ_l, and ρ = local densities of bubble, liquid, and the mixture of bubble and liquid, respectively β = ratio between the bubble core width and the buoyant jet diameter (~0.7) b = local radius of the buoyant jet/plume ε = bubble fraction
Conservation of Momentum $\frac{d}{dt}\left[(m_l + m_b)u\right] = u_a \frac{dm_l}{dt}$ (T5.6a) $\frac{d}{dt}\left[(m_l + m_b)v\right] = 0$ (T5.6b) $\frac{d}{dt}\begin{bmatrix} m_l w + \\ m_b(w+w_b) \end{bmatrix} = \begin{bmatrix} \frac{(\rho_a - \rho_l)}{\rho_l} m_l g \\ + \frac{(\rho_a - \rho_b)}{\rho_b} m_b g \end{bmatrix}$ (T5.6c)	Modified from Yapa and Zheng (1997)	u = horizontal velocity component of the plume element v = lateral velocity component of the plume element w = vertical velocity component of the plume element w_b = slip velocity (vertical velocity difference between the bubbles and the liquid part of the buoyant jet, ~ 0.3 m/s) g = acceleration due to gravity

Table 5.1 Governing equations for the jet/plume control volume – definition of the parameters and sources

Conservation of heat, salinity, and oil mass $\frac{d(m_l I)}{dt} = \begin{bmatrix} I_a \frac{dm_l}{dt} \\ -\rho_a K 2\pi b h \cdot \frac{I - I_a}{b} \end{bmatrix}$ (T5.7)	Yapa and Zheng (1997)	Subscript "a" refers to the ambient fluid I = symbol for scalar parameter of the buoyant jet (for heat $I = C_p T$, for salinity $I = S$, and oil concentration by mass $I = C$) C_p = specific heat (assumed to be constant) T = temperature K = diffusivitie (e.g., heat diffusivity K_T, salinity diffusivity K_S, and oil concentration diffusivity K_c)
Entrainment $Q_s = 2\pi b h \alpha \lvert V - u_a \cos\phi \cos\theta \rvert$ (T5.8) $Q_f = \lvert u_a \rvert \begin{bmatrix} \pi b \Delta b \lvert \cos\phi \cos\theta \rvert \\ + 2b\Delta s \sqrt{1 - \cos^2\theta \cos^2\phi} \\ + \frac{\pi b^2}{2} \lvert \Delta(\cos\phi \cos\theta) \rvert \end{bmatrix}$ (T5.9)	Lee and Cheung (1990), and Yapa and Zheng (1997)	$\alpha = \sqrt{2} \frac{0.057 + \frac{0.554 \sin\phi}{F^2}}{1 + 5 \frac{u_a \cos\phi \cos\theta}{\lvert V - u_a \cos\phi \cos\theta \rvert}}$ $F = E \frac{\lvert V - u_a \cos\phi \cos\theta \rvert}{(g \frac{\Delta\rho}{\rho_a} b)^{1/2}}$ ϕ = angle between the jet trajectory and the horizontal plane θ = jet angle with respect to x-axis E = proportionality constant (~ 2) $V = \sqrt{u^2 + v^2 + w^2}$ $\Delta s = \sqrt{\Delta x^2 + \Delta y^2 + \Delta z^2}$ Δx, Δy, and Δz are displacements of a control volume during one time step in x, y and z respectively

Forced entrainment is present due to the advection of the ambient current into the buoyant jet.

According to Frick (1984), forced entrainment consists of three terms: (i) the projected buoyant jet area normal to the ambient flow (cylinder term), (ii) the growth of the buoyant jet radius (growth term), and (iii) the curvature of the trajectory (curvature term). Frick (1984) derived an expression of forced entrainment for a two-dimensional jet trajectory in unidirectional ambient flow. Lee and Cheung (1990) extended Frick's idea to a three-dimensional jet trajectory in unidirectional ambient flow. Utilizing a similar approach, Yapa and Zheng (1997) derived an expression for forced entrainment that deals with a three-dimensional trajectory in a three-dimensional ambient flow field. However, in the current study, the x-axis is aligned with the flow direction; this results in a three-dimensional jet trajectory in unidirectional ambient flow. Therefore, the Lee and Cheung (1990) formulation is used in the jet/plume modelling.

The expressions for Q_s and Q_f are given in Table 5.1. The maximum entrainment hypothesis is used to calculate the increase of mass, that is:

$$Q_e = \mathrm{Max}[Q_s, Q_f] \tag{5.2}$$

Lateral Plume Spreading

Once the plume reaches the surface, spreading of the surface oil will be governed by the radial outflow of entrained water within the surface interaction zone (Figure 5.5). A hydrodynamic analysis plays a vital role in predicting the extent and thickness of the resulting oil slick. Mathematical models have been previously developed to capture the essential physics of lateral plume spread, such as those by Fannelop and Sjoen (1980) and Akar and Jirka (1994).

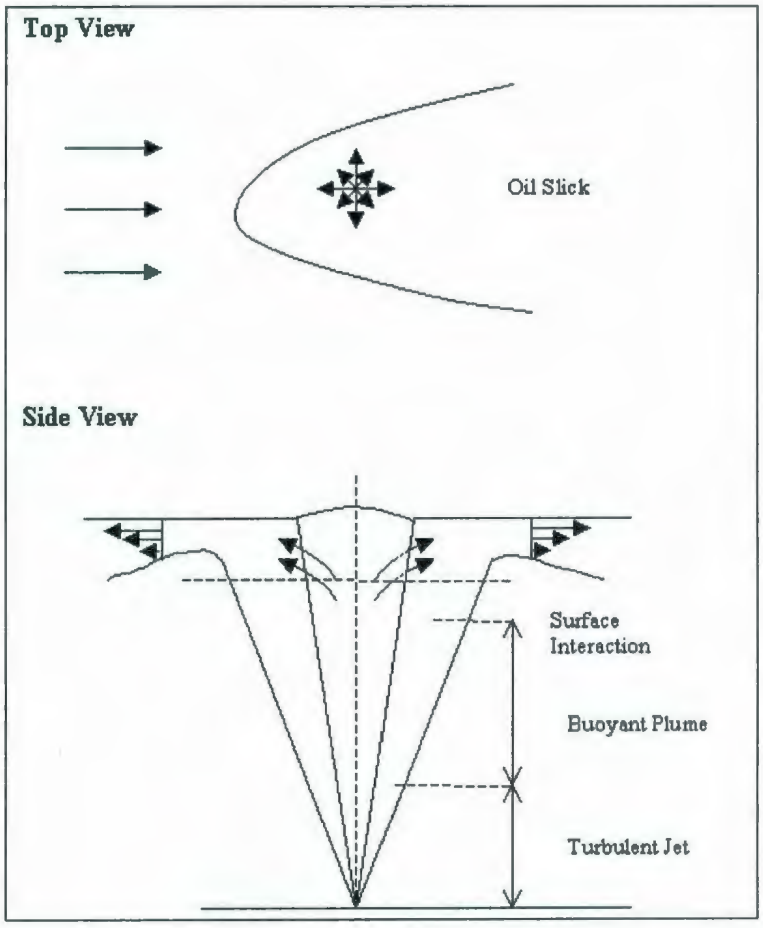

Figure 5.5 Schematic diagram for subsea blowout (modified from MMS, 1997)

The source strength, S_{St}, associated with radial flow can be determined from the plume radius and rise velocity as (Fannelop and Sjoen, 1980):

$$S_{St} = \pi\left(\frac{2}{\beta}\right)^{\frac{1}{2}} b_G w_m \tag{5.3}$$

where

b_G = plume radius following the Gaussian distribution at the exit;

w_m = centerline velocity following the Gaussian distribution at the exit;

β = entrainment coefficient, measured experimentally in the range of 0.07-0.08.

The radius and velocity from the present top-hat profile are multiplied by $\frac{1}{\sqrt{2}}$ and 2, respectively, to convert the values corresponding to the radius and velocity of the Gaussian profile.

Reed *et al.* (2006) suggested that if the submerged buoyant jet impinges at an angle different from 90°, its velocity w can be replaced by $w_m = \sqrt{U_m w_m}$, in which U_m is the magnitude of the axial velocity. For consistent formulation with the Gaussian profile, U_m is given by $U_m = 2 * \sqrt{u^2 + v^2 + w^2}$ (where u, v, and w are top-hat longitudinal, lateral, and vertical velocity components, respectively).

The source strength measures the radial velocity, U_r, in the surface flow at a radial distance, r, from the point where the plume emerges to the surface by the following expression (Fannelop and Sjoen, 1980; Reed *et al.* 2006):

$$U_r = \frac{S_{St}}{2\pi r} \tag{5.4}$$

Akar and Jirka (1994) proposed a system of ordinary differential equations for modelling lateral spreading of the buoyant plume, which was solved by a fifth order Runga-Kutta method. Yapa *et al.* (1999) used the Akar and Jirka (1994) algorithms in modelling the surface plume. Yapa *et al.* (1999) further assumed the impingement of the buoyant jet to be near horizontal if the angle between the submerged buoyant jet trajectory and the water surface (ϕ) is less than 45°, and near vertical otherwise.

The current study uses the work of Fannelop and Sjoen (1980) in integrating the submerged buoyant jet model with the model for lateral surface spreading. The algorithm

for non-vertical impingement is also implemented as prescribed by Reed *et al.* (2006). Considering, $U_r = \frac{dr}{dt}$, the present work uses Equation (5.4) to determine the plume spread associated with the source strength. This results in:

$$\frac{dr}{dt} = \frac{S_{St}}{2\pi r} \tag{5.5}$$

After solving this differential equation with the initial condition of $r(0) = 2b_G$, the extent of the radial spread associated with the source strength can be given as:

$$r = \frac{1}{\sqrt{\pi}}\left[\sqrt{S_{St} t_{Sp} + 4b_G^2 \pi}\right] \tag{5.6}$$

where

t_{Sp} = spill duration (s).

The previous chapter has presented a methodology to model the fate and transport of an oil slick in a multimedia marine environment for a batch spill release scenario on the water surface. The current chapter adopts that methodology with minor changes to account for the fate and transport of an oil slick for an underwater oil and gas release scenario. A brief illustration of the methodology with proposed minor changes is presented below.

b) Multimedia Oil Slick Modelling

As compared to a surface spill, an underwater release causes a slick that will be wider and more dispersed. Once the radial spread source vanishes, the spreading of oil is governed by the surface tension-viscous regime. In the present work, the Fay (1969), Hoult (1972), and Waldman *et al.* (1972) spreading expression is revised in terms of the

change in area as a function of actual area. The other weathering algorithms (i.e., evaporation, emulsification, and natural dispersion) are the same as discussed in Chapter 4. The governing equation of the area growth for the *surface tension-viscous* regime is revised as (see Appendix III):

$$\frac{dA_S}{dt} = 0.256 A_S^{1/3} \tag{5.7}$$

Fugacity level IV modelling (see Equations (4.12) and (4.13)) is employed to predict the fate and transport of oil in two bulk compartments (i.e. water and sediment). The water column concentration, C_W, is calculated using:

$$C_W(t) = Z_2 * f_2(t) * MW \tag{5.8}$$

where Z_2 is the fugacity capacity for water as defined in Table 4.2, and f_2 is fugacity of the water column.

The temporal average concentration is used for the predicted exposure concentration (PC), that is:

$$PC = \frac{1}{T}\int_0^T C_W(t)dt \tag{5.9}$$

Finally, the exposure concentration (EC) is given as (Sadiq *et al.*, 2003):

$$EC = p * PC * BF \tag{5.10}$$

where

p = probability of exposure, which is calculated by dividing the volume of the plume by the total volume in which fish are expected, and

BF = bio-available fraction (approximately 1 for chemicals having log of octanol-water partition coefficient less than five; i.e., $\log K_{OW}$ <5). Further details on the calculations of BF can be found in Clark *et al.* (1990).

c) Sensitivity and Uncertainty Analysis

A mathematical model is an approximation of the actual process, and thus epistemic uncertainty is inherent in such a model. Uncertainty in input parameters (epistemic) and its temporal and spatial variability in the environment (aleatory), also propagate uncertainty in the model results. In general, model uncertainties are not very significant in a well-tested physical model (CCME, 1997).

Only the uncertainties associated with sensitive multimedia model input parameters are accounted for in the present analysis. The methodology of MacLeod *et al.* (2002) is employed to identify the sensitive variables. In this context, an input variable is randomly sampled (while the other input parameters are fixed at their mean values) from the lognormal distribution characterized by the standard deviation (σ_I). Uncertainty in the input variable is propagated to model output by using 500 Monte Carlo simulations. The resulting output lognormal distribution with the standard deviation (σ_O) measures the sensitivity (S) of the input variable by the following expression (MacLeod *et al.*, 2002):

$$S = \frac{\sigma_O}{\sigma_I} \tag{5.11}$$

Generally, the standard deviation (σ) of a lognormal distribution can be expressed in terms of a confidence factor (CF) by the following relationship (MacLeod *et al.*, 2002):

$$\sigma = 0.5\ln(CF) \tag{5.12}$$

The MacLeod *et al.* (2002) method assumes that the input and output distributions are lognormally distributed and the input variables are independent. The assumption of lognormal distribution is justified by reference to the central limit theorem. However, the presence of systematic errors may violate this assumption of the central limit theorem (Haimes *et al.*, 1994). Sweetman *et al.* (2002) also used the MacLeod *et al.* (2002) approach in the sensitivity analysis of the level IV model parameters.

Uncertainties in input variables are propagated in the weathering and level IV model using Monte Carlo simulations. Conventionally, the 95th percentile of exposure concentration ($EC_{95\%}$) is used in the risk estimation (Sadiq *et al.*, 2003).

The present work uses a bootstrapping technique to calculate the 95th percentile response and the associated uncertainty. This involves sampling with replacement from 999 data for k iterations. During iteration, the data points are sorted in ascending order and for the k th iteration, the $EC_{95\%}$ value will be:

$$\left(EC_{95\%}\right)_k = EC_{(n+1)*0.95} \tag{5.13}$$

where

n = total number of data points;

subscript (n+1)*0.95 = number of the sorted data representing $EC_{95\%}$ value.

The mean $EC_{95\%}$ and its standard deviation are calculated from 10,000 bootstrap runs as recommended by Booth and Sarkar (1998). A macro written in Minitab software is used to carry out the bootstrapping procedure.

5.3.2 Characterization of Ecological Effects

A marine aquatic life is considered as an assessment endpoint subject to the availability of the data. To characterize long-term (chronic) response, a predicted no effect concentration (PNEC) is used as a criterion. A PNEC value is calculated using the methodology prescribed in section 5.2.2. Naphthalene LC_{50} data were obtained for 19 species of 5 groups from the Pesticide Action Network (PAN) ecotoxicity website. The website includes aquatic toxicity results from the U.S. EPA AQUIRE database, which are presented in Table 5.2. The lowest 5^{th} percentile on the response empirical distribution function is considered as a PNEC, which represents the whole community. The lowest 5^{th} percentile ($PNEC_{5\%}$) and the associated uncertainty are calculated using a bootstrapping procedure similar to that employed for $EC_{95\%}$. Sampling with replacement is done from 19 PNEC data points for 10,000 iterations. Each time the data points are sorted in ascending order. The $PNEC_{5\%}$ value will be:

$$PNEC_{5\%} = PNEC_{(n+1)*0.05} \tag{5.14}$$

where

n = total number of data points;

$(n+1)*0.05$ = number of the sorted data representing the 5^{th} percentile of PNEC.

The mean $PNEC_{5\%}$ and standard deviation are calculated from 10,000 bootstrap iterations.

Table 5.2 Toxicity data for naphthalene

Group	Time (h)	$(LC_{50})_t$(µg/L)*	$(LC_{50})_4$ (µg/L)**	PNEC+ (µg/L)
Annelida				
Polychaete worm	96	3800	3800	38
Crustaceans				
Blue crab	24	1980-3120	800.25	8
Dungeness or edible crab	96	2000	2000	20
Shortscale eualid	96	13900	13900	139
Shrimp	48-96	2000-4000	2131	21.31
Opossum shrimp	96	850-2000	1303.8	13.04
Humpy shrimp	24-96	971-1290	635.06	6.35
Brown shrimp	96	2500	2500	25
Fish				
Pink salmon	24-96	890-1840	726.13	7.26
Coho salmon, silver-salmon	96	2100-11800	4978	49.78
Rainbow trout, Donaldson trout	96	1600-6100	3124.1	31.24
Sheepshead minnow	24	2400	772.7	7.73
Molluscs				
Pacific oyster	48	110000	62416.7	624.17
Marine bivalve	24-96	57000-74000	36852	368.52
Pouch snail	48	5020	2848.5	28.49
Zooplankton				
Brine shrimp	24-48	83-12500	435.4	4.354
Water flea	24-96	1000-17000	2339.5	23.395
Calanoid copepod	24	3798	1222.23	12.22
Protozoa	24-48	40117-43706	17900	179

* LC_{50} at time t (source: PAN ecotoxicity website)
** LC_{50} at 96 h exposure time (calculation details: Sadiq *et al.*, 2003)
+PNEC= $(LC_{50})_4/100$

5.4 Risk Characterization

The risk quotient (RQ) is used to characterize ecological risk. The expression for RQ is given as:

$$RQ = \frac{EC_{95\%}}{PNEC_{5\%}} \tag{5.15}$$

The RQ critical value of unity means that 95% of the ecological community is protected 95% of the time. Quantifying the uncertainties of variables $EC_{95\%}$ and $PNEC_{5\%}$ (assuming lognormal variables), a probabilistic risk assessment is carried out in the current study. Using the reproductive property of the lognormal distribution it can be shown that RQ will also be lognormally distributed with the following parameters:

$$\mu_{\ln RQ} = \mu_{\ln EC95\%} - \mu_{\ln PNEC5\%} \tag{5.16}$$

$$\sigma^2_{\ln RQ} = \sigma^2_{\ln EC95\%} + \sigma^2_{\ln PNEC5\%} \tag{5.17}$$

Using the above parameters for the RQ distribution, 10,000 random lognormal samples are generated. Thus, for the i th iteration the risk is calculated as:

$$R_{(i)} = \Phi\left(\frac{1}{S_m}\left(\ln(RQ_{(i)}) - X_m\right)\right) \tag{5.18}$$

where

$\Phi(\bullet)$ = standard normal distribution function, N ~ (0,1);

X_m = average of the lognormally transformed data (2.85);

S_m = standard deviation of the lognormally transformed data (1.74);

$i = i^{th}$ iteration (1-10,000).

The values of X_m and S_m are obtained from the CHARM model user's manual (CIN, 2004). These values are calibrated to give an RQ value of unity at an acceptable risk level of 5%. The statistical rule for combining probabilities can be used to combine the risk estimates for a mixture of two stressors (Karman and Reerink, 1998).

5.5 Case Studies

To demonstrate the application of the proposed methodology, two different oil release scenarios are simulated. The first case includes a jet of liquid and gas mixture, and the second case simulates an oil jet with no gaseous mixture. The release depth for both cases is considered to be ~ 40 m (i.e. the release depth is within the wave-active zone) and the release duration is 30 min. The oil simulated is assumed to have the physicochemical characteristics of Hibernia oil (see Table 5.3). The values of parameters ρ_{oil}, T_O, and T_G for Hibernia oil are adopted from Bobra and Chung (1986). The oil dynamic viscosity value is taken from Environment Canada (1999). The gas is simulated using the physical properties of methane. The physical parameters used in the simulations of submerged buoyant jet modelling are presented in Table 5.4.

For the oil and gas mixture release, the initial conditions are set using the power series solution suggested by McDougall (1978). These equations appear in Appendix IV. Yapa and Zeng (1997) also used the power series solutions in calculating the plume initial radius, velocity, and bubble fraction.

Table 5.3 Hibernia oil characteristics used in the weathering algorithms

Oil characteristic	Notation	Value	Unit
Density at 15 °C and zero evaporation	ρ_{oil}	865.22	kg/m^3
Dynamic viscosity at 15 °C	μ	13	cp
Initial boiling point at zero evaporation	T_O	420	K
Gradient of the boiling point and fraction evaporation line	T_G	596.4	K
Oil-water interfacial tension	s_t	2000	dyne/m
Oil temperature	T	288 (15)	K (°C)

Table 5.4 Parameters used in the submerged buoyant jet simulation

Parameter	Notation		Value	Unit
Oil release rate	Q_{oil}	Case 1 Case 2	0.067 0.556	m^3/s
Initial radius	b_o	Case1 Case2	Power series solution 0.25	
Gas release rate	Q_{gas}		0.33	Nm^3/s
Gas to oil ratio	GOR		5	
Angle between jet trajectory and horizontal plane	ϕ		1.57	rad
Jet angle with respect to x-axis	θ		0	rad
Ambient oil concentration	C_a		0	ppm
Ambient water temperature	T_a		15	°C
Initial plume temperature	T		60	°C
Ambient salinity	S_a		35	ppt
Initial oil concentration	C		1000	ppm
Wind speed	W		4.17	m/s
Average current speed	u_a		0.018	m/s
Depth of release	d_r		40	M
Spill duration	t_{Sp}		30	min

For the oil jet with no gas, the jet diameter is set equal to the rupture size and the release velocity is calculated using the continuity equation for steady state flow. The numerical scheme for the governing equations is presented in Appendix V.

In modeling the weathering processes, the initial values for both the fraction evaporated and the fraction of water content in the slick are considered to be zero. Allowance is made for the loss of oil volume as a result of evaporation and natural dispersion. The oil volume entrained into the water column due to natural dispersion is used to calculate the oil volumetric flow rate. The emission rate $I_2(t)$ is calculated using Equation (4.20). The source strength lifetime for radial spread is approximated by a leak duration of 30 min. This radial spread as measured by the lateral spread plume modelling is used to calculate the initial slick area for the simulations of weathering processes. The initial oil volume over this slick area is calculated by multiplying the oil volumetric flow rate with the release duration.

Naphthalene is used as a representative stressor. It is assumed that the oil droplets remain in the water column and deposit to the sediment only after attaching to suspended solids within the water phase.

Alaee *et al.* (1996) reported Henry's law constant (H) values for naphthalene at various temperatures (ranging from 9.2 to 34.8 °C), corresponding to the average ocean salinity of 35 parts per thousand (ppt). The current study uses their data in developing the following dimensionless Henry's law constant (H') expression using the linear regression ($R^2 = 0.99$):

$$\ln(H') = 10.972 - \frac{4365.6}{T} \tag{5.28}$$

where

T = ambient temperature (K).

The above expression is used to calculate the Henry's law constant at 15 °C (288 K), which is later used as a point estimate in the simulations. The other physicochemical data and the associated sensitivity are provided in Table 5.5. The data for the environmental multimedia variables used in the level IV fugacity-based model are provided in Table 5.6. The sensitive parameters that significantly contribute to uncertainty in the water column concentration are used as variables. The sensitive values are also reported in Tables 5.5 and 5.6.

Table 5.5 Physicochemical properties of naphthalene used in the simulation

Parameter (Unit)	Notation	Value	CF	Sensitivity (S)	Input Type
Molecular weight (g/mol)	MW	128.2		-	PE*
Henry's law constant @ 15°C - water salinity 35 ppt ($Pa \cdot m^3 \cdot mol^{-1}$)	H	36.4	-	-	PE
Logarithmic value - octanol-water partitioning coefficient	$\log K_{ow}$	3.35	-	-	PE
Reaction rate constant water (h^{-1})	k_2	2.89×10^{-3}	3	0.01	PE
Reaction rate constant sediment (h^{-1})	k_4	1.93×10^{-4}	3	0	PE
Sediment-water phase effective diffusivity (m^2/h)	B_{WX}	1.91×10^{-6}	3	0	PE

* Point estimate

Table 5.6 Environmental multimedia parameters used in level IV fugacity-based model

Parameter (Unit)	Notation	Value	CF	Sensitivity	Input Type
Depth water (m)	h_W	100	-	-	PE*
Volume fraction suspended solids in water	v_5	$5x10^{-6}$	3	0.5	V**
Volume fraction biota in water	v_6	$1x10^{-6}$	3	0.018	PE
Organic fraction suspended solid	ϕ_5	0.2	1.5	0.6	V
Organic fraction biota	ϕ_6	0.05	1.5	0.02	PE
Density suspended solids (kg/m^3)	ρ_5	1500	1.5	0.6	V
Density fish (kg/m^3)	ρ_6	1000	1.05	0.02	PE
Advection rate water (m/s)	U_A	0.018	1.5	0.95	V
Deposition rate suspended solids (m/h)	U_{DS}	$5x10^{-7}$	1.5	0.002	PE
Depth sediment (m)	h_S	0.05	1.5	0	PE
Diffusion path length in sediment (m)	$\Delta_S = 0.5h_S$	0.025	1.5	0	PE
Density sediment (kg/m^3)	ρ_4	2500	1.5	0	PE
Volume fraction sediment solids	v_7	0.37	1.1	0	PE
Volume fraction pore water	v_8	0.63	1.1	0	PE
Organic fraction sediment	ϕ_4	0.04	1.5	0	PE
Re-suspension rate sediment (m/h)	U_{RS}	$2x10^{-7}$	3	0	PE
Burial rate sediment (m/h)	U_{Bur}	$3.4x10^{-8}$	3	0	PE

*Point Estimate
**Variable

5.6 Results and Discussion

It is assumed that a near vertical buoyant jet releases from the riser. The bubbles occupy the inner core of the plume. The simulated plumes take less than 1 min. to reach the surface from the release depth of 40 m. Therefore, a quasi-steady state assumption of

ambient flow is reasonable in the present study. The results of the underwater steady-state release of an oil and gas mixture simulations are presented in Table 5.7.

The change of the plume element velocity at the exit with respect to the initial velocity is approximately 64% for the oil and gas mixture. This change is 76% for the oil jet with no gaseous mixture. The presence of gas makes the plume element move faster in the vertical direction as expansion of the gas increases the buoyancy. Thus, the velocity deficit is lower for the oil and gas mixture release.

The velocity, radius, and concentration profiles obtained from the top-hat model are shown in Figure 5.6 for the bubble plume and in Figure 5.7 for the oil plume. In Figure 5.6(a) a small increase in the velocity is observed at a height of ~ 37 m (i.e. near the water surface). This velocity increase is a characteristic of a bubble buoyant jet and is due to the buoyancy increase because of the expansion of bubbles caused by the decrease in pressure (Fannelop and Sjoen, 1980; Yapa and Zheng, 1997a). No such velocity increase can be seen for an oil jet (see Figure 5.7a). In Figures 5.6(b) and 5.7(b) the radius of the buoyant jet element increases while rising to the surface. During the journey of the buoyant jet through the water column ambient fluid entrains into the jet element resulting in a decrease in oil concentration, with the minimum concentration at the surface; see Figures 5.6(c) and 5.7(c). The oil slick radius and exit surface velocity of the top-hat profile are converted to the corresponding radius and velocity of the Gaussian profile to calculate the source strength for the lateral plume spreading for both cases.

Table 5.7 Output of the submerged buoyant jet simulation

Parameter	Notation	Value		Unit
		Case 1*	Case 2**	
Centerline velocity following the Gaussian distribution at the exit	w_m	1.2	1.3	m/s
Plume radius following the Gaussian distribution at the exit	b_G	5.2	4.2	m
Ratio of surfacing concentration to initial concentration	$\frac{C}{C_o}$	$9.2\text{x}10^{-4}$	$6.2\text{x}10^{-3}$	-
Source strength	S_{St}	112.6	100.7	m^2/s
Area of spill due to source strength	A_{Sp}	$2.031\text{x}10^5$	$1.814\text{ x}10^5$	m^2

*Oil and gas mixture release scenario
**Oil release scenario with no gas

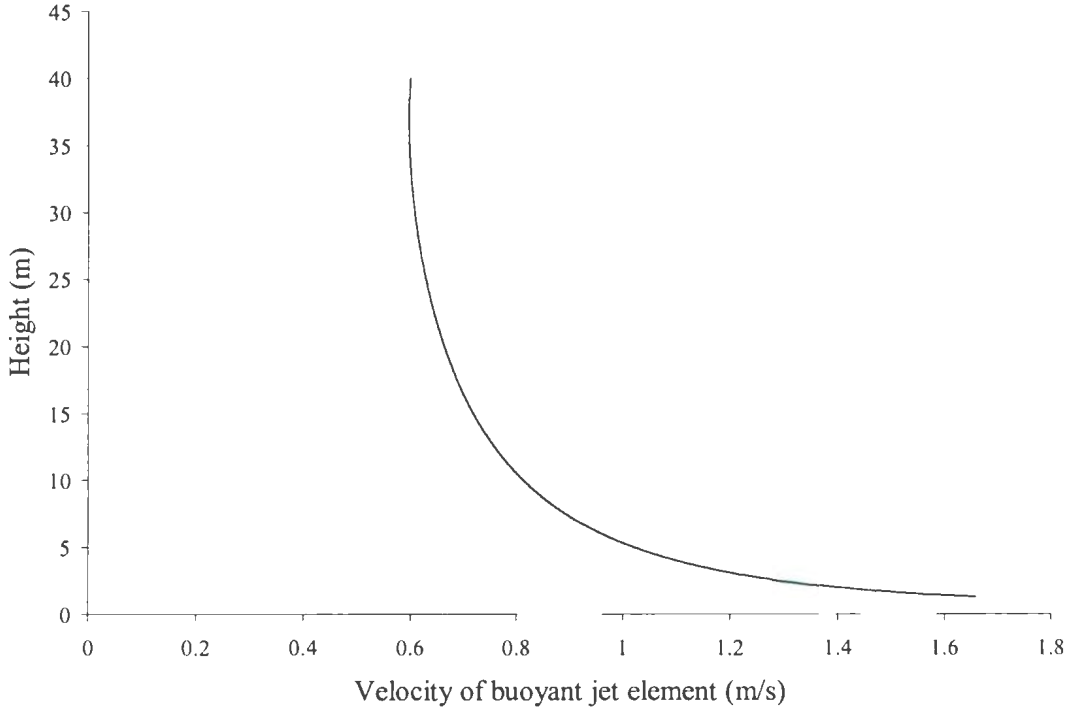

(a)

Figure 5.6 Simulation results of the submerged oil and gas mixture buoyant jet modelling

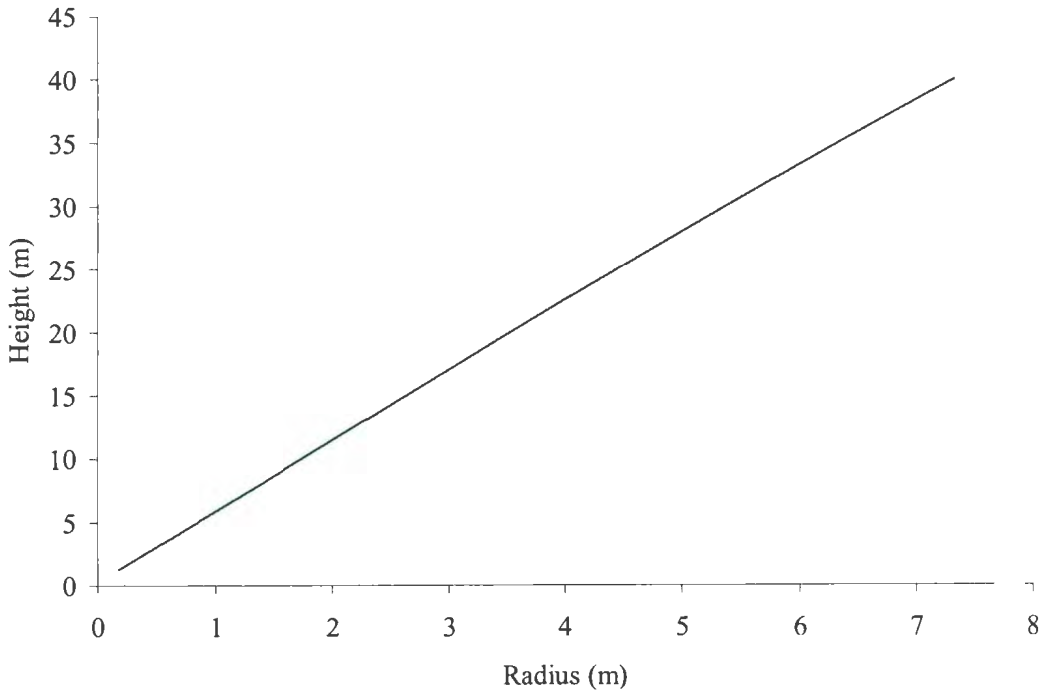

(b)

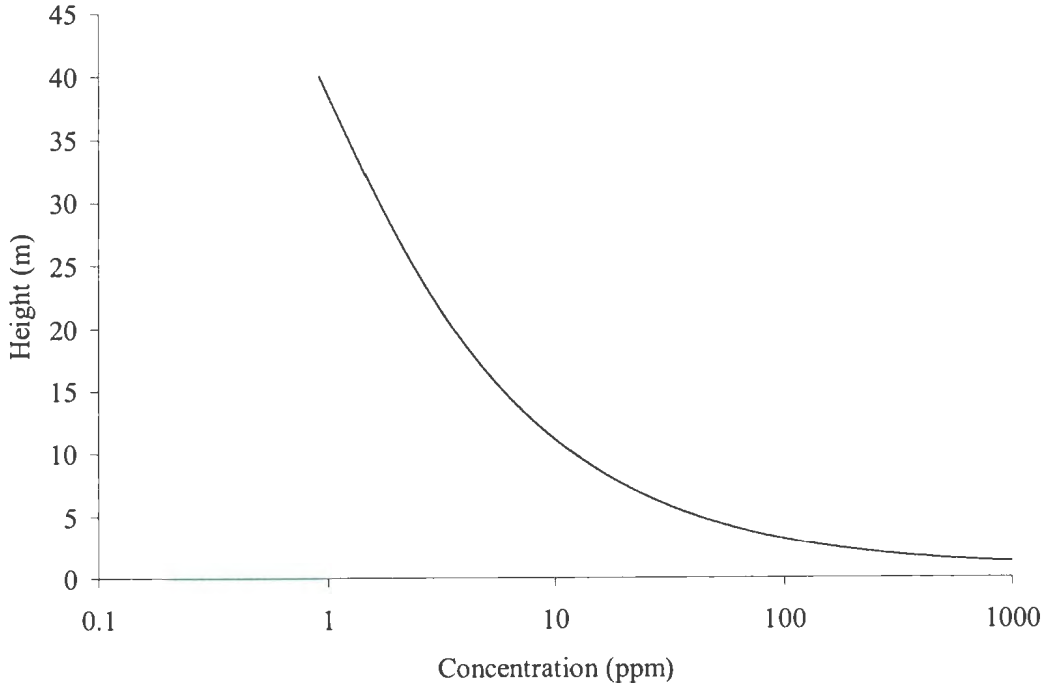

(c)

Figure 5.6 Simulation results of the submerged oil and gas mixture buoyant jet modelling

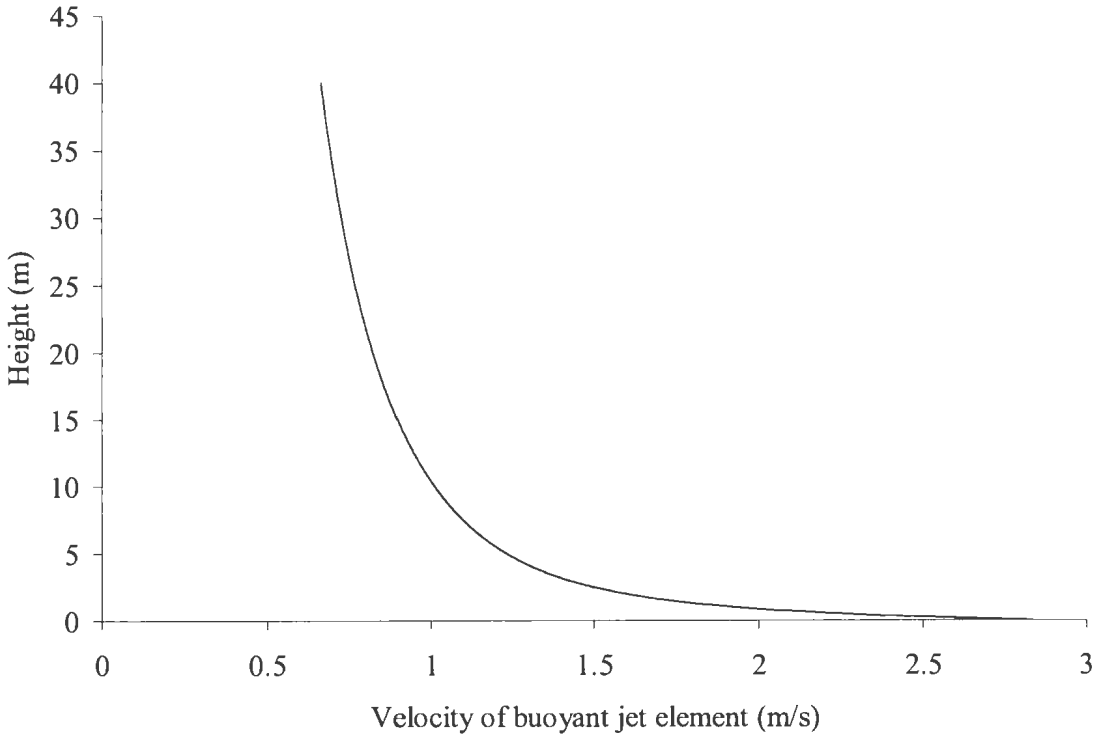

(a)

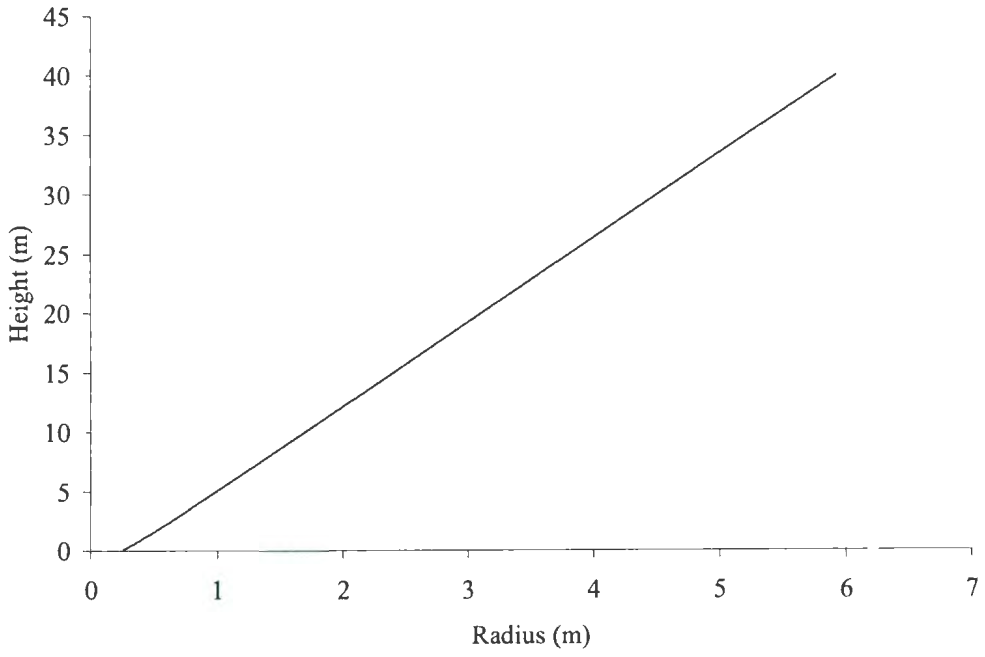

(b)

Figure 5.7 Simulation results of the submerged oil buoyant jet modelling with no gas

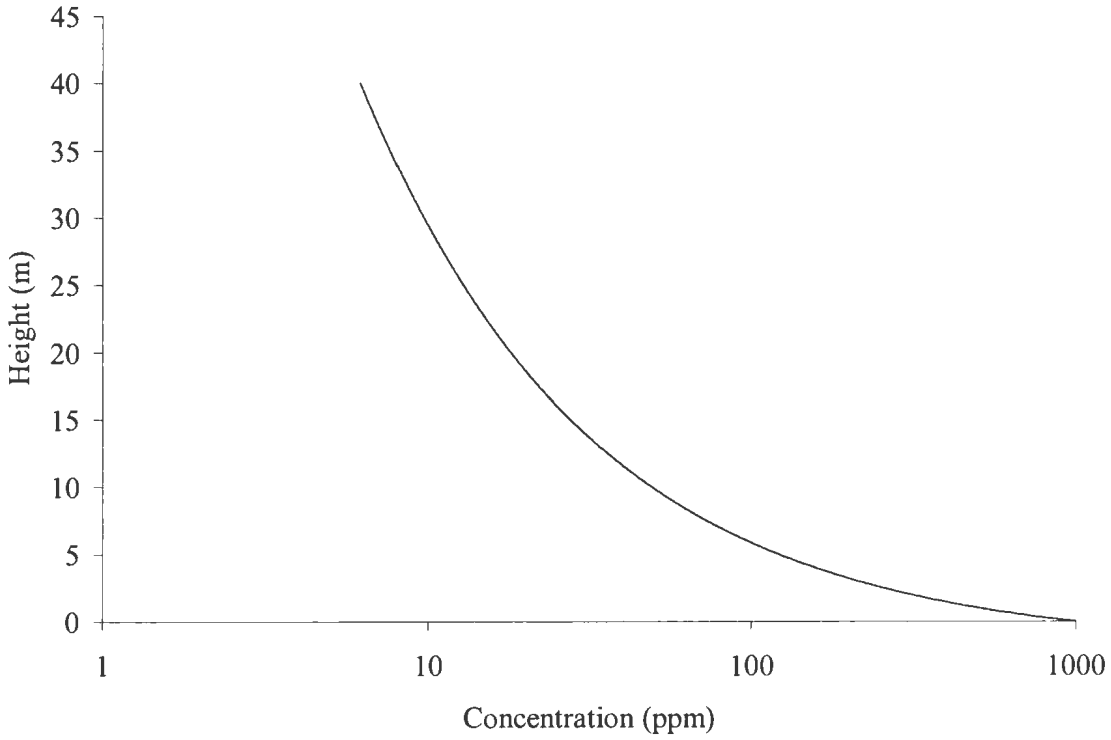

(c)

Figure 5.7 Simulation results of the submerged oil buoyant jet modelling with no gas

As mentioned earlier, naphthalene is used as a representative stressor in the present study. The concentration of naphthalene in a typical crude oil is approximately 1000 ppm (Neff, 2002). The ratio of surfacing plume concentration to initial concentration, $\frac{C}{C_o}$, from the bubble buoyant jet simulation is 9.2×10^{-4}. This ratio is 6.2×10^{-3} for the oil jet. This results in a naphthalene concentration in the surface oil slick of 0.92 ppm (~ 0.007 mol/m^3) and 6.17 ppm (~0.04 mol/m^3) for the bubble plume and oil plume, respectively.

The oil loss due to evaporation and natural dispersion processes, oil spreading, chemical emission, water column concentration, and pore water concentration profiles are shown in Figure 5.8. For the sake of demonstration, the point estimates of physicochemical and multimedia environmental data are used to obtain these curves for the oil and gas mixture scenario. The slick growth ceases as its thickness reaches 0.01 cm, resulting in a final area of 7.01×10^5 m^2 at 7.25 h (see Figure 8a). The decrease in oil volume is shown in Figure 5.8 (b). Initially, the volume of oil slick lost is primarily due to the evaporation process. At an elapsed time of 24 h since the oil has surfaced, 81% of the total volume lost is due to the evaporation process. The dispersion-emulsification formulation eventually drives the residual oil into the water column, thus giving the surface slick a finite lifetime of approximately 174 h.

During the growth period, the water concentration profile follows the shape of the emission curve in Figure 5.8(c). Once the growth has ceased, the concentration increases without an increase in the emission rate. A residence time analysis could explain this peculiar behavior of the concentration profile. In Chapter 4 it has been shown that advection and growth are the most important transport processes. The early cessation of growth transport causes the concentration increase in the simulations. The rise in concentration eventually stops due to the constant decrease in the emission rate (see Figure 5.8c). A simulation that includes predefined fixed dimensions of a water compartment results in the concentration profile having only one peak (see Figure 5.8d). Thus, the two peaks in the concentration profile are attributed to area growth in the simulations.

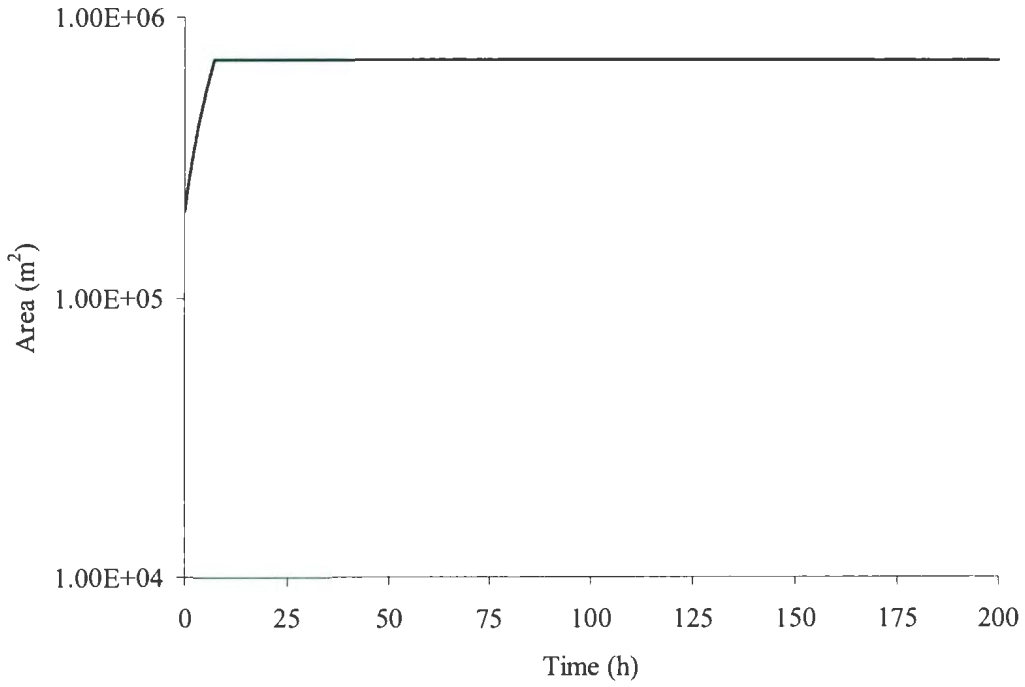

(a)

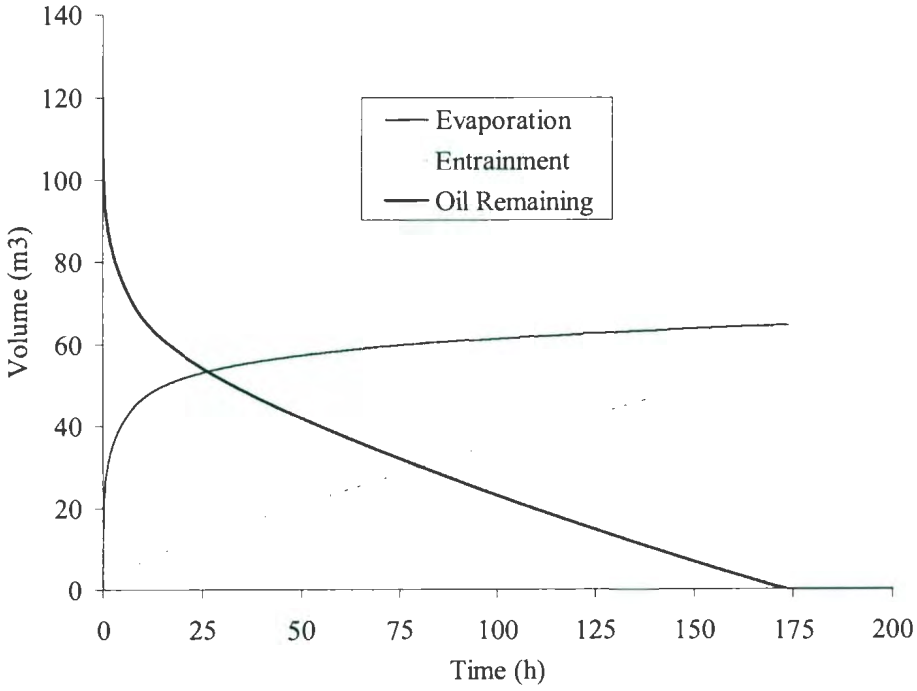

(b)

Figure 5.8 Multimedia fate of Hibernia oil in the marine environment

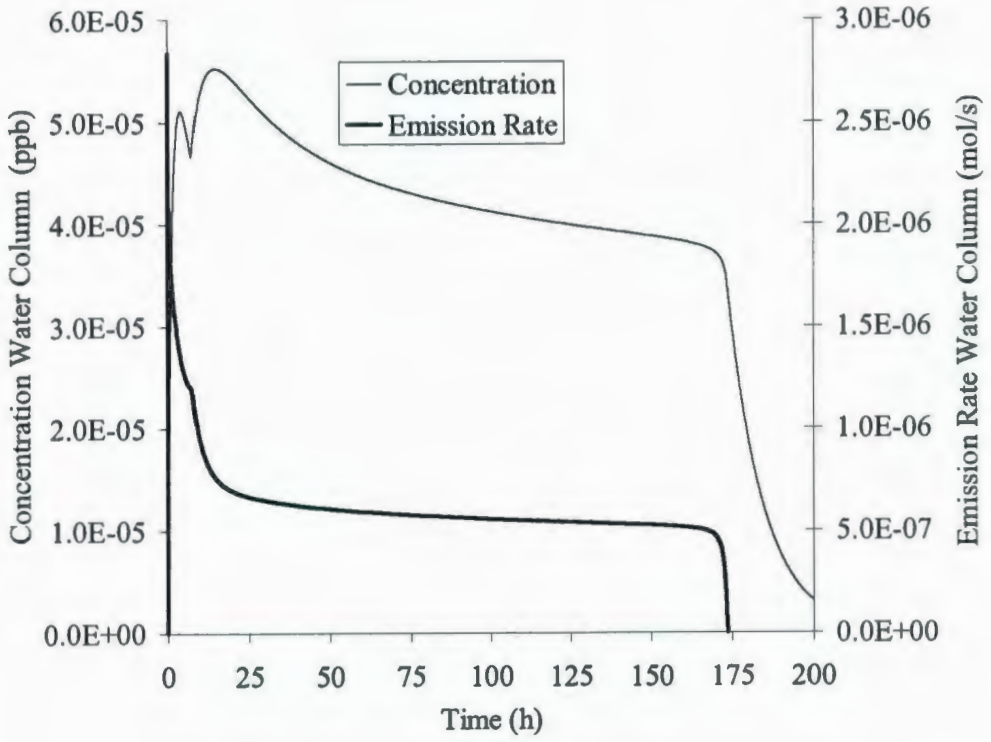

(c)

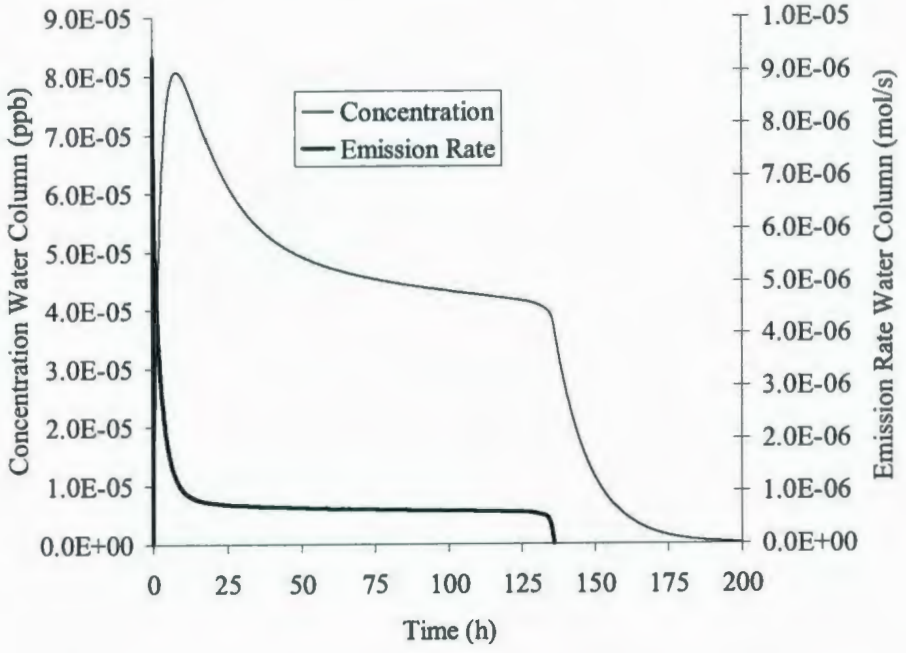

(d)

Figure 5.8 Multimedia fate of Hibernia oil in the marine environment

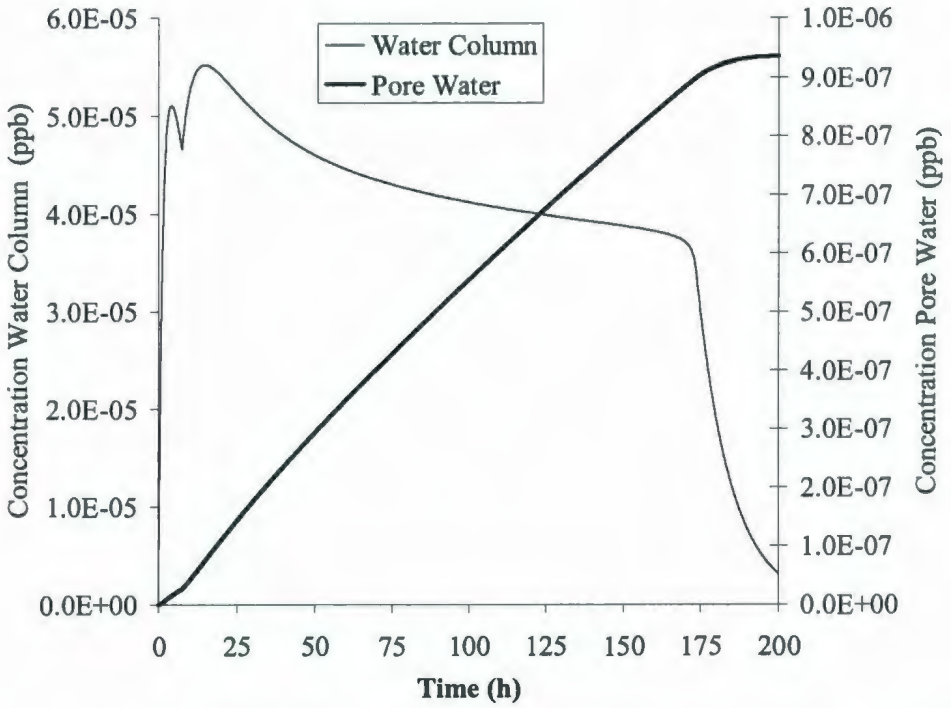

(e)

Figure 5.8 Multimedia fate of Hibernia oil in the marine environment

The water column and pore water concentration profiles are shown in Figure 5.8(e). The water compartment shows a rapid decrease of its burden after the chemical input is stopped. The response of the sediment compartment to the chemical emission is slower than that of the water compartment. The magnitudes of water column concentrations are higher than the pore water concentrations (see Figure 5.8e). Thus, water column concentrations are used in the exposure analysis.

Two averaging time periods of 96 h and 200 h are used to calculate EC. The probability of exposure is considered to be unity. As naphthalene log $K_{OW} < 5$, so BF is also considered to be unity in Equation (5.10). A bootstrapping method as explained in

section 5.3.1 is used to calculate $EC_{95\%}$. Both the shorter and longer averaging times give $EC_{95\%}$ values of the same order of magnitude (Table 5.8). The $EC_{95\%}$ value averaged over 96 h is considered as the representative exposure concentration. A bootstrapping method is also employed to calculate $PNEC_{5\%}$, as described in section 5.3.2. The uncertainty is reported as standard deviation (SD) and coefficient of variation (CV) in Table 5.8. The uncertainty associated with $PNEC_{5\%}$ is higher than the uncertainty in $EC_{95\%}$ estimates. The reason is that only 19 data points are sampled in bootstrapping for the calculation of $PNEC_{5\%}$, whereas 999 data points are used for the calculation of $EC_{95\%}$ estimates.

Equations (5.16) and (5.17) are used to calculate the point estimate and standard deviation for RQ and the results are reported in Table 5.8. From the RQ lognormal variable, 10,000 samples are generated and for each sample point the risk is estimated using Equation (5.18). The risk associated with naphthalene for the oil and gas mixture release scenario is practically zero. The cumulative frequency of risk and frequency distribution function for the oil buoyant jet release case is shown in Figure 5.9. The median risk (50^{th} percentile) for the oil release (case 2) is approximately 21.7 per trillion with 95% lower (LCL) and upper confidence levels (UCL) of 21.3 per trillion and 22.1 per trillion, respectively. The 95th percentile risk and associated 95% confidence intervals are reported in Table 5.8. A positive skewness in the risk data is representative of lognormal distribution (Equation (5.18)).

Table 5.8 Risk characterization—results of two case studies

Parameter	Symbol	Distribution	Mean*		SD	CV
Predicted No Effect Concentration, 5th percentile	$PNEC_{5\%}$	Lognormal	5.22		1.25	0.24
Exposure Concentration, 95th percentile	$EC_{95\%}$	Lognormal	Case 1+			
			96h	6.32×10^{-5}	8.72×10^{-7}	0.014
			200h	5.47×10^{-5}	4.73×10^{-7}	0.009
			Case 2++			
			96h	5.1×10^{-4}	3.83×10^{-6}	0.008
			200h	6.10×10^{-4}	4.1×10^{-6}	0.007
Risk Quotient	RQ	Lognormal	Case 1+			
			1.13×10^{-5}		2.7×10^{-6}	0.24
			Case 2++			
			1.04×10^{-4}		2.53×10^{-5}	0.24
Risk ($x10^{-12}$)						
	50th Percentile (95% LCL, UCL)		21.7 (21.3,22.1)			
	95th Percentile (95% LCL, UCL)		108.4 (105.2,111.6)			

*All concentrations are in μg/ L
+Oil and gas mixture release scenario
++Oil release scenario with no gas

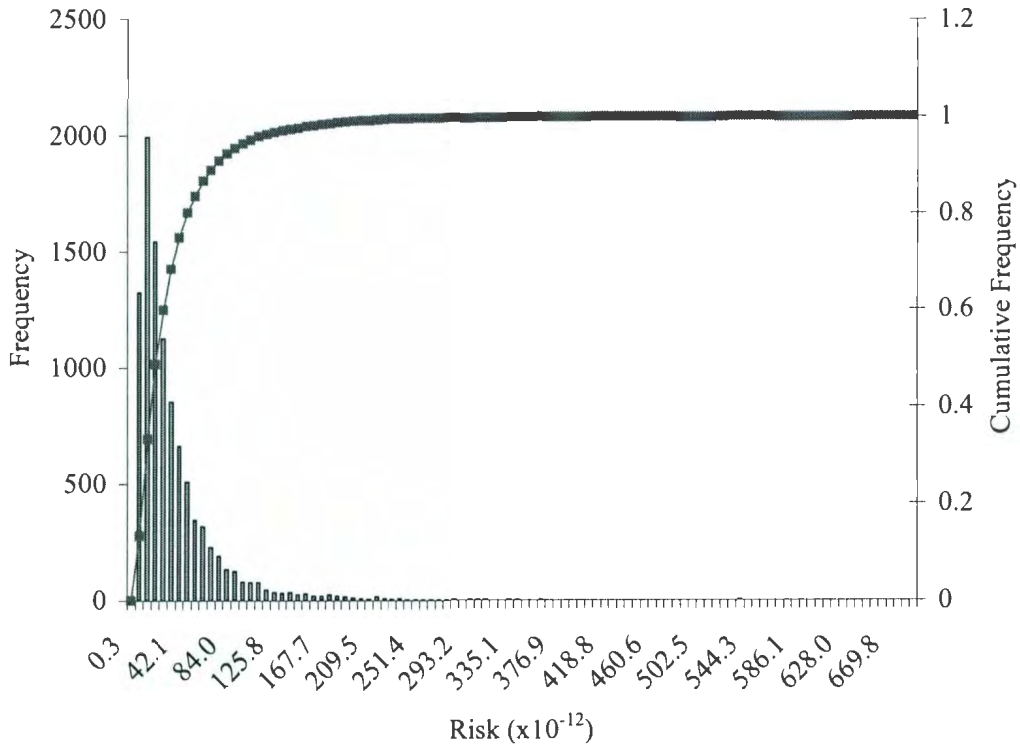

Figure 5.9 Frequency distribution of risk for naphthalene

Chapter 6

Conclusions and Recommendations

The research conducted in the current study has quantified the structural and ecological risks associated with failure of a rigid marine riser. This chapter presents a summary of the conclusions drawn from this work. Recommendations for future research are also provided. Finally, the novelty of the completed research is described.

6.1 Summary and Conclusions

It is concluded that the present study gives a holistic view of an integrated methodology that quantifies the structural and ecological risks of a marine riser. The methodology for riser fatigue reliability design was discussed in detail in Chapter 3. This study concludes that the non-linearity associated with Morison-type wave loading can be effectively accounted for in the expected fatigue damage by using a ratio of non-linear to linear response. Approximate formulae, which have already been successfully tested in the time domain analysis, are very time-efficient in calculating the fatigue life of a riser. They become more attractive for dynamic response modelling when the associated uncertainty is accounted for in reliability based design.

To perform probabilistic fatigue analysis for a riser, uncertainties were studied for both stress and resistance. Stress uncertainty arises due to scatter in S-N curve data and the random variable that quantifies modelling error. Uncertainty in the strength arises due to modelling error associated with Miner's rule. These uncertainties are well documented in the literature and are assumed as lognormally distributed. The lognormal quantification

of uncertainty results in the formulation of a closed form solution. The closed form solution is particularly useful in swift calculations of 'notional' failure probability (P_f).

The behavior of the hazard rate function of lognormal distribution is rationalized for predicting fatigue life. It has been shown that the hazard function increases in the fatigue failure regime and begins to decrease far away from the failure regime.

In addition to the closed form solution, a simulation method was also used to study the problem. Instead of using the direct Monte Carlo simulation, a simple algorithm was used to avoid a large uncertainty associated with the small P_f values and a small number of simulations.

The proposed methodology was applied to evaluate fatigue reliability of a multi-bore riser for a floating production system. In simulations, nine sea states were used in terms of the significant wave height; the associated average time period and other wave characteristics were calculated using the Pierson-Moskowitz spectrum. The service/fatigue life for the riser in the demonstrated example was calculated as 39 years at an acceptable *reliability index* of 2.

A fugacity-based methodology was presented in Chapter 4 to predict the oil fate for a batch spill scenario on the sea surface. In the proposed methodology, the oil weathering processes were coupled with a level IV (dynamic) fugacity-based model. A two-compartment system, namely, water and sediment, was used to explore the fate of oil in a marine environment. The application of the methodology was presented by a case study involving a Statfjord oil spill scenario. The study showed that the water compartment response to the chemical input was faster than the sediment compartment

because the advection process was the dominant process and was only present in the water column. The residence time analysis supports the conclusion that advection was the most important transport process with the lowest residence time of 5 h. The water column concentrations were observed to be higher than the pore water concentrations.

The fugacity-based oil fate methodology was extended to account for an underwater release of contaminants (oil/gas mixtures) from a broken riser. The developed exposure assessment methodology accounts for the hydrodynamics of an underwater blowout, weathering processes, and a fugacity-based multimedia fate of oil. Exposure assessment in a complex marine environment is a challenging task. The developed methodology provides a step toward handling this complex exposure assessment problem. Although mathematical models used in the current assessment methodology have been validated elsewhere with experimental data, the models along with specified assumptions are simple approximations to the oil fate in a real environment.

The diversity of marine life makes ERA even more challenging. The toxic data available for the organisms of an ecosystem were considered as representative of the whole system and were utilized in the characterization of ecological effects. Uncertainties accounted for the exposure and effect analyses provide the probabilistic basis for the risk characterization.

Two case studies of practical importance were presented to demonstrate the application of the methodology. The first case included an oil/gas mixture release from the riser. The second case simulated the oil release with no gaseous mixture. The release duration was considered as 30 min for both cases. The oil surfaced and remained

unignited in the simulations. The source strength measured the extent of the radial spread of the surface slick for the 30 min release duration. This extent of lateral spread was used as an initial condition in the oil weathering simulations. The oil quantity released in case 1 was approximately 13% of the oil quantity released in case 2.

Initially, the volume of oil slick lost was governed by the evaporation process; however, dispersion-emulsification formation then drove the leftover oil to the water column. A fugacity-based level IV model was employed to model the oil fate in the water and sediment compartments. Naphthalene was considered as an indicator to carry out the ERA. In case study 1, the calculated risk is essentially zero, whereas in case study 2 the 95^{th} percentile of risk was approximately 108×10^{-12}.

6.2 Recommendations

Based on this research, the following recommendations are suggested for future research:

1. The present research dealt with a risk assessment framework including structural and ecological risks associated with the failure of a rigid marine riser. The results of the risk assessment should be combined with a decision-making process for effective design of a marine riser.
2. The fatigue analysis in this study was based on Morison-type wave loading. However, it may be useful to include vortex-induced vibrations in the fatigue analysis. The reliability-based approach then can be utilized in predicting the design life.

3. Approximate formulae have been utilized in modelling the dynamic response of a vertical marine riser. The approximate formulae of main statistical parameters of random response for a steel catenary riser can also be established. Such an analytical formulation will be an effective and time efficient dynamic approach for reliability based design.
4. The proposed methodology for multimedia fate modelling should be validated through laboratory and/or field data.
5. With the availability of new data, more organisms may be included in developing the stressor-response relationship for an ecological risk study.
6. The exposure analysis was performed only for an indicator pollutant, naphthalene, in the water column and pore water. A chemical specific approach can be used to measure the concentration of other hydrocarbons present in the oil. The overall ecological risk of different chemicals can be combined assuming independent probabilities (as done in the CHARM model). In addition, oil can be used as a 'mixture of compounds' and its toxicity as a whole can be used to estimate ecological risk. A risk estimate associated with a mixture of various hydrocarbons would perhaps be more meaningful from a decision-making viewpoint.
7. The parameter of fish migration rate is important in estimating the probability of exposure to the contaminants. The current study has assumed a conservative value of unity for this parameter in the calculations of exposure concentration. However, when more information becomes available about fish migration rates, it can be utilized for more realistic estimates of exposure probabilities.

8. Secondary effects, such as an increased mortality of predators due to the consumption of affected marine life, could be included in the ERA study.
9. Unlike drilling waste discharges, where a contaminant discharge is one of the routine offshore procedures, contaminant loss from a riser is an accidental event. This accidental event may pose an acute human health risk due to the consumption of contaminated seafood. Thus, the current study may be extended to human health risk assessment.
10. The fire and explosion risks to an offshore production platform also need to be quantified in addition to ecological risk in case of an ignited oil release.

6.3 Statement of Originality

The novelty of the present work can be viewed from the following perspectives:

1. The integrated risk assessment approach provides a holistic view that is essentially needed for the improved design and operation of a marine riser.
2. The proposed reliability-based methodology bridges the gap between simple design models based on a factor of safety approach, and time consuming and computationally extensive numerical models.
3. By quantifying uncertainties with a lognormal distribution in stress and strength, a closed form failure probability expression has been derived in Equation (3.43). The derived expression is essentially equivalent to the Wirsching (1984) time-to - fatigue failure lognormal format.
4. Non-stationarity and the deviation of peak response from the Rayleigh distribution are accounted for in the expected fatigue damage expression.

5. The validity of a lognormal format in calculating time to fatigue failure is discussed. It was proved that the hazard rate function kept on increasing during the fatigue failure regime.
6. Although in the past a fugacity-based approach was employed in modelling the distribution of hydrocarbons in a marine environment from the perspective of drilling waste discharges, the fugacity-based approach was not utilized for an oil spill scenario. In the current study the fate of a highly concentrated oil slick is modelled using the weathering algorithms. A fugacity-based approach is utilized in the multimedia fate modelling of low-concentration oil fractions that enter into the water column from the oil slick due to one of the weathering processes—natural dispersion.
7. Unlike a conventional fugacity-based approach, the growth of the water compartment is allowed to account for an oil spreading mechanism (Equations 4.15 and 4.16).
8. Generalized residence time expressions for the advection, growth, and inter-media transport processes are derived.
9. A new methodology has been developed to characterize the chemical exposure to marine life associated with an underwater oil and gas mixture release from a broken riser. In this context the hydrodynamics of the underwater mixture release are combined with weathering and fugacity models. A general expression to calculate an initial oil slick spread due to an underwater oil release from shallow to moderate depths is developed and presented in Equation (5.6).

10. A conventional area growth equation for the surface tension-viscous regime has been revised in terms of the change in area as a function of actual area. This new convenient form of the area growth expression is combined with other weathering algorithms in a set of differential equations. Finally, the developed methodology for exposure analysis is incorporated in the U.S. EPA ecological risk assessment framework.

REFRENCES

Abramowitz, M. and Stegun, I.A. 1970. *Handbook of Mathematical Functions with Formulas, Graphs, and Mathematical Tables*. National Bureau of Standards, Washington DC, USA.

Akar, P.J., and Jirka, G. H. 1994. Buoyant Spreading Processes in Pollutant Transport and Mixing, Part 1: Lateral Spreading with Ambient Current Advection. *Journal of Hydraulic Research*, 32:815-831.

Alaee, M., Whittal, R. M., and Starchan, W. M. J. 1996. The Effect of Water Temperature and Composition on Henry's Law Constant for Various PAH's. Chemosphere, 32 (6): 1153-1164.

API. 1999. Fate of Spilled Oil in Marine Waters. American Petroleum Institute. Publication Number 4691.

API RP1111. 1998. Design, Construction, Operation, and Maintenance of Offshore Hydrocarbon Pipelines. American Petroleum Institute.

Asante-Duah, D.K. 1993. *Hazardous Waste Risk Assessment*. Lewis Publishers, Ann Arbor.

ASCE (Committee on Fatigue and Fracture Reliability). 1982. Fatigue Reliability (a series of papers). *Journal of the Structural Division*, ASCE, 108: 3-88.

ASCE. 1996. State-of-the-Art Review of Modelling Transport and fate of Oil Spill. *Journal of Hydraulic Engineering*, 122: 594-609.

Assakkaf, I.A., and Ayyub, B.M. 2000. Load and Resistance Factor Design Approach for Fatigue of Marine Structures. 8th ASCE Speciality Conference on Probabilistic Mechanics and Structural Reliability, PMC 2000-169.

Ayyub, B.M. 2003. *Risk Analysis in Engineering and Economics*. Chapman and Hall/CRC, Florida, USA.

Ayyub, B. M., Assakkaf, I. A., Kihl, D. P., and Sieve, W. M. 2002. Reliability-Design Guidelines for Fatigue of Ship Structures. *Naval Engineers Journal,* 114.

Ayyub, B. M., and Haldar, A. 1984. Practical Structural Reliability Techniques. *Journal of Structural Engineering*, ASCE, 110(8): 1707-1724.

Bai, Y. 2001. *Pipelines and Risers*. Elsevier, Amsterdam.

Barltrop, N.D.P, and Adams, A.J. 1991. *Dynamics of Fixed Marine Structures*. 3rd Ed., Butterworth-Heinemann Ltd., Oxford.

Bates, K., Young, W. and Sutton, A. 1997. Proposed Environmental Quality Standards for Naphthalene in Water. Environment Agency R&D Technical Report P54.

Bendat, J.S. 1958. *Principles and applications of random noise theory*. Wiley, New York.

Bobra, M.A. and Chung, P.T. 1986. A Catalogue of Oil Properties. Report EE-77, Consultchem, Ottawa, Canada.

Bogdanoff, J.L. 1978. A New Cumulative Damage Model. *Journal of Applied Mechanics*. 45: 246-250.

Booth, L. G., and Sarkar, S. 1998.Monte Carlo Approximation of Bootstrap Variances. *Amercian Statist*, 52, 354-357.

Breitung, K. 1984. Asymptotic Approximations for Multinormal Integrals. *Journal of Engineering Mechanics, ASCE*. 110(3): 357-366.

Broding, W.C., Diederich, F.W., and Parker, P.S. 1964. Structural Optimization and Design Based on a Reliability Design Criterion. *Journal of Spacecraft*. 1: 56-61.

Brouwers, J.J.H. 1982. Analytical Methods for Predicting the Response of Marine Risers. Royal Netherlands Academy of Arts and Sciences, Series b, Netherlands, 85: 381-400.

Brouwers, J.J.H. and Verbeek, P.H.J. 1983. Expected Fatigue Damage and Expected Extreme Response for Morison-Type Wave Loading. *Applied Ocean Research*. 5: 129-133.

Buchanan, I, and Hurford, N. 1988. Methods for Predicting the Physical Changes in Oil Spilt at Sea. *Oil and Chemical Pollution*, 4: (4) 311-328.

Bury, K. 1999. *Statistical Distributions in Engineering*. Cambridge University Press, Cambridge, UK.

Byers, W. G., Marley, M. J., Mohammadi, J., Nielsen, R. J., and Sarkani, S. (1997). Fatigue Reliability Reassessment Procedures: State-OF- The-Art Paper. *Journal of Structural Engineering*, 123: 277-285.

Canadian Council of Ministers of Environment (CCME). 1997. A Framework for Ecological Risk Assessment: Technical Appendices, PN 1274.

Chakrabarti, K.S. 1990. *Nonlinear Methods in Offshore Engineering*. Elsevier Publishers, Amsterdam, The Netherlands.

Chen, H. Z., Li, D., Li, X. 2007. Mathematical Modeling of Oil Spill on the Sea and Application of the Modeling in Daya Bay. Journal of Hydrodynamics, Ser. B, 19(3): 282-291.

CIN (2004). Chemical Hazard Assessment and Risk Management User Guide Version 1.4.

Clark, E. K., Gobas, F. A. P. C., and Mackay, D. 1990. Model of Organic Chemical Uptake and Clearance by Fish from Food and Water. *Environmental Science Technology*, 24: 1203-1213.

CMPT. 1999. *A Guide to Quantitative Risk Assessment for Offshore Installations*. The Centre for Marine and Petroleum Technology. Publication 99/100.

CONCAWE. 1983. Characteristics of Petroleum and its Behavior at Sea. Report No. 8/83.

Covello, V.T., and Merkhofer, W.M. 1992. Risk Assessment Methods: Approaches for Assessing Health and Environmental Risks. Plenum Press, New York.

European Environment Agency (EEA). 1999. Environmental Risk Assessment - Approaches, Experiences and Information Sources. Environmental Issue Report No 4, ISBN: 92-9167-080-4.

Exxon Corporation. 1985. Fate and Effects of Oil in the Sea. Exxon Background Series.

Faltinsen, O.M. 1990. Sea Loads on Ships and Offshore Structures. Cambridge, UK.

Fannelop, T. K., and Sjoen, K. 1980. Hydrodynamics of Underwater Blowouts. AIAA 8th Aerospace Sciences Meeting, Paper 80-0219, California, USA.

Fannelop, T. K., Horchberg, S., and Kuffer, J. 1991. Surface Current and Recirculating Cells Generated by Bubble Curtains and Jets. *Journal of Fluid Mechanics*, 229: 629-657.

Fay, J. A. 1969. The Spread of Oil Slicks on a Calm Sea. In: *Oil on the Sea*, Hoult, D. P., Ed., pp. 53-63. Plenum Press, NY.

Frick, W. E.1984. Non-empirical Closure of the Plume Equations. *Atmospheric Environment*, 18: 653-662.

Frick, W. E., Baumgartner, D. J., and Fox, C. G. 1994. Improved Prediction of Bending Plumes, *Journal of Hydraulic Research*, 32 (6): 935-950.

FOCS. 2002. Hydrocarbons and their Effects on Aquatic Organisms in Relation to Offshore Oil and Gas Exploration and Oil Well Blowout Scenarios in British Columbia, 1985. Fisheries and Oceans Canada Science, Vancouver, BC.

Haimes, Y. Y., Barry, T., and Lambert, J. H. 1994.When and How Can You Specify a Probability Distribution. When You Don't Know Much? *Risk Analysis* 14 (5):661-706.

Hancq, A.D., Walters, J.A., and Beuth, L. J. 2000. Development of an Object-Oriented Fatigue Tool. Engineering with Computers, 16: 131-144.

Hasofer, A., and Lind, N. 1974. An Exact and Invariant First-Order Reliability Format. Journal of the Engineering Mechanics Devision, ASCE, 100: 111-121.

Hoult, D. P. 1972. Oil Spreading on the Sea. Annual Review of Fluid Mechanics, Van Dyke, ed., pp. 341-368.

Huda, M. K., Tkalich, P., and Gin, K. Y. H. 1999. A 3-D Multiphase Oil Spill Model. Proceedings of the Conference, Oceanology International '99 Pacific Rim, Singapore. 143-150.

Hughes, O.F. 1983. *Ship Structural Design: a Rationally-based, Computer-aided, Optimization Approach.* Wiley, New York, USA.

Husain, T., Sadiq, R., Mukhtasor, and Khan, A. A. (2001). Framework for Ecological Risk Assessment: Deterministic and Uncertainty Analyses. In: *The Gulf Ecosystem:*

Health and Sustainability, Khan, M.Y., Munawar, M., Price, A.R.G., ED., pp. 199-218. Elsevier Publishers.

Ji, Z.-G., Johnson, W.R., Marshall, C.F. 2004. Deepwater Oil-Spill Modeling for Assessing Environmental Impacts. Fifth International Conference on Environmental Problems in Coastal Regions Incorporating oil spill Studies, COASTAL ENVIRONMENT V, Alicante, Spain. WIT Press, Southampton, UK, pp. 349-358.

Johansen, O. 2000. DeepBlow – A Lagrangian Plume Model for Deep Water Blowouts. *Spill Science and Technology Bulletin*, 6:103-111

Karman, C. C., Johensen, S., Schobben, H. P. M., and Scholten, M. C. T. 1996. Ecotoxicological Risk of Produced Water Discharged from Oil Production Platforms in the Statfjord and Gilffaks Field, In Produced Water 2: *Environmental Issues and Mittigation Technologies,* Reed, M., and Johnsen, S., ED., pp.127-134, Plennum Press, NY.

Karman, C. C. and Reerink, H.G. 1998. Dynamic Assessment of the Ecological Risk Assessment of the Discharge of Produced Water from Oil and Gas Producing Platforms. *Journal of Hazardous Materials*, 61: 43-51.

Kirk, C.L., Etok, E. U., and Cooper, M.T. 1979. Dynamic and Static Analysis of a Marine Riser. *Applied Ocean Research*. 1: 125-135.

Lee, J. H. W., and Cheung, V. 1990. Generalized Lagrangian Model for Buoyant Jets in Current. *Journal of Environmental Engineering, ASCE*, 116 (6): 1085-1105.

Leira, B. 1998. Reliability Aspects of Marine Riser and Subsea Pipeline Design. in: Soares, C.G. (Ed.), *Risk and Reliability in Marine Technology*, Rotterdam, The Netherlands, 273-313.

Lin, Y.K. 1967. *Probabilistic Theory of Structural Dynamics*. McGraw-Hill, New York, USA.

Lutes, D. L., Corazao, M., Hu, S.J. and Zimmerman, J. 1984. Stochastic Fatigue Damage Accumulation. *Journal of Structural Engineering*. ASCE, 110: 2585-2601.

Mackay, D., Buist. I, Mascarenhas. R, and Paterson, S. 1980. Oil Spill Processes and Models. Environmental Protection Service, Environment Canada.

Mackay, D., Joy, M., and Paterson, S. 1983. A Quantitative Water, Air, Sediment Interaction (QWASI) Fugacity Model for Describing the Fate of Chemicals in Lakes. *Chemosphere*, 12: 277-291.

Mackay, D., and McAuliffe, C. D. 1989. Fate of Hydrocarbons discharged at Sea. *Oil and Chemical Pollution*, 5: (1) 1-20.

Mackay, D. 1991. *Multimedia Environmental Models: The Fugacity Approach*. Lewis Publishers, USA.

Mackay, D., Paterson, S., and Shiu, W. Y. 1992. Generic Models for Evaluating the Regional Fate of Chemicals, *Chemosphere*, 24: 695-717.

MacLeod, M., Fraser., A., Mackay, D. 2002. Evaluating and Expressing the Propagation of Uncertainty in Chemical Fate and Bioaccumulation Models. *Environmental Toxicology and Chemistry*, 21: 700-709.

Maddox, N. R., and Wildenstein, A. W. 1975. A Spectral Fatigue Analysis for the Offshore Structures. Proceedings of the Offshore Technology Conference 2261.

Maddox, N. R. 1975. A Deterministic Fatigue Analysis for Offshore Structures. *Journal of PetroleumTtechnology*, July, 901-912.

Melchers, R.E. 1987. *Structural Reliability Analysis and Prediction*. Ellis Horwood Limited, West Sussex, UK.

McDougall, T. J. 1978. Bubble Plumes in Stratified Environments. *Journal of Fluid Mechanics,* 85: 655-672.

Milgram, J. H. 1983. Mean Flow in Round Bubble Plumes. *Journal of Fluid Mechanics*. 133: 721-731.

Millero, F. J., and Poisson, A. 1981. International One-Atmosphere Equation of State for Seawater. *Deep Sea Research*, 28 A: 625-629.

Miner, M. A., 1945 "Cumulative Damage in Fatigue", *Journal of Applied Mechanics.*, 12: A159.

MMS. 1997. Fate and Behavior of Deepwater Subsea Oil Well Blowouts in the Gulf of Mexico. Mineral Management Service. Project Number: 287.

Moe, G., and Crandall, S. H. 1978. Extremes of Morison-Type Wave Loading on a Single Pile. *Journal of Mechanical Design, ASME*, 100: 100-104.

Mooney, M. J. 1951. The Viscosity of a Concentrated Suspension of Spherical Particles. *Journal of Colloid Science*, 6: 162-170.

Morooka, C.K., Coelho, F.M., Shiguemoto, D. A., Franciss, R., and Matt, C. G. C. 2006. Dynamic Behavior of a Top Tensioned Riser in Frequency and Time Domain. Proceedings of the 16th International Offshore and Polar Engineering. San Francisco, CA, United States.

Mukhtasor, Sadiq, R., Husain, T., Veitch, B., and Bose, N. 2001. Acute Ecological Risk Associated with Soot Deposition: A Persian Gulf Case Study. *Journal of Ocean Engineering,* 28: 1295-1308.

Mukhtasor, Husain, T., Veitch, B., and Bose, N. 2004. An Ecological Risk Assessment Methodology for Screening Discharge Alternatives of Produced Water. *Human and Ecological Risk Assessment,* 10 (3): 505-524.

Neff, M. J. 2002. *Bioaccumulation in Marine Organisms: Effects of Contaminants from Oil Well Produced Water.* Elsevier, Amsterdam, The Netherlands.

Nilsen and Hanson. 1995. Reliability Analysis Design of a 15" Dynamic Flexible Gas Export Riser. Proceedings of the International Offshore and Polar Engineering Conference, Hague, Netherlands.

Nolte, K.G., and Hansford, J.E. 1976. Closed Form Expressions for Determining the Fatigue Damage of Structures Due to Ocean Waves. OTC, Paper 2606.

National Research Council (NRC). 1985. Oil in the Sea: Inputs, Fates, and Effects. National Academy Press, Washington, DC.

Palm, W.J. 2001. *Introduction to Matlab 6 for Engineers*. McGraw-Hill, 1st Ed., Singapore.

Pesticide Action Network (PAN). http://www.pesticideinfo.org/Detail_Chemical.jsp?Rec_Id=PC35114#Ecotoxicity, accessed on July 2007.

Paris, P., and Erdogan, F. 1963. A critical analysis of crack propagation laws. *Journal of Basic Engineering*, ASME, 85: 528-534.

PERD. 1993. Reliability of Offshore Structural Systems: Theory, Computation and Guidelines for Application. Program of Energy Research and Development. Project Number: 62243.2.93.

Rackwitz, R., and Fiessler, B. 1978. Structural Reliability Under Combined Random Load Sequences. *Computers and Structures*, 9: 489-494.

Reed, M. 1989. The Physical Fates Component of the Natural Resource Damage Assessment Model System. *Oil and Chemical Pollution*, 5: (2-3) 99-123.

Reed, M., Emilsen, M. H, Hetland, B., Johansen, O., Buffington, S., and Hoverstad, B. 2006. Numerical Model for Estimation of Pipeline Oil Spill volumes. Environmental Modelling and Software, 21: 178-189.

Robertson, J., L., M, Smart, D., and Al-Hassan, T. 1995. Offshore North Sea Pipeline and Riser Loss of Contaminent Study (PARLOC): Applications and Limitations in the Assessment of Operating Risks. Proceedings OMAE, Copenhagen.

Rubinstein, R. Y. 1981. Simulation and the Monte Carlo method. John Wiley and Sons Inc., New York, USA.

Sadiq, R. 2001. Drilling Waste Discharges in the Marine Environment: A Risk Based Decision Methodology. Ph.D. Dissertation, Faculty of Engineering, Memorial University of Newfoundland, Canada.

Sadiq, R., Husain, T., Veitch, B., and Bose, N. 2003. Distribution of Arsenic and Copper in Sediment Pore Water: An Ecological Risk Assessment Case Study for Offshore Drilling Waste Discharges. *Risk Analysis,* 23 (6): 1309-1321.

Sarpkaya, T. 1981. *Mechanics of Wave Forces on Offshore Structures*. Van Nostrand Reinhold Co., New York.

Scorer, R.S. 1978. *Environmental Aerodynamics*. Ellis Horwood, UK.

Sebastiao. P, and Soares, C. G. 1995. Modelling the Fate of Oil Spills at Sea. Spill Science and Technology Bulletin, 2: 121-131.

Sebastiao. P, and Soares, C. G. 1998. Weathering of Oil Spills Accounting for Oil Components. In: *Oil and Hydrocarbon Spills, Modelling, Analysis and Control*, Garacia-Martinez, R., and Brebbia, C.A., Ed., pp. 63-72. WIT Press, Southampton, UK.

Serta, O.B., Sphaier, S.H., and Fernandes, A.C. 2000. Fatigue Design of Risers: An Improved Methodology Incorporating a Transverse Hydrodynamic Force model. Proccedings of the 10th Internation Offshore and Polar Engineering Conference, Seattle, USA, 2: 49-52.

Shooman, M.L. 1968. Probabilistic Reliability: An Engineering Approach. McGraw-Hill, New York, USA.

Souza, G.F.M., and Goncalves, E. 1997. Fatigue Performance of Deep Water Rigid Marine Riser. 7th International Offshore and Polar Engineering Conference, Honolulu, USA, 2: 144-151.

Stiver, W., and Mackay, D. 1984. Evaporation Rates of Spills of Hydrocarbons and Petroleum Mixtures. *Environmental Science and Technology*, 18: (11) 834-840.

Sweet, A.L. 1990. On the Hazard Rate of the Lognormal Distribution. *IEE Transactions on Reliability*. 39: 325-328.

Sweetman, J. A., Cousins, T, I., Seth, R., Jones, C. K., and Mackay, D. 2002. A Dynamic Level IV Multimedia Environmental Model: Application to the Fate of Polychlorinated Biphenyls in the United Kingdom Over a 60-Year Period. *Environmental Toxicology and Chemistry*, 21: (5) 930-940.

Tucker, T.C. and Murtha, J.P. 1973. Non-Deterministic Analysis of a Marine Riser. 5th Annual Offshore Technology Conference. Houston, USA, Paper 1770.

Tvedt, L. 1990. Distribution of Quadratic Forms in Normal Space: Application to Structural Reliability. *Journal of Engineering Mechanics, ASCE.* 116(6): 1183-1197.

U.S. EPA. 1998. Guidelines for Ecological Risk Assessment, Risk assessment Forum. U.S. Environmental Protection Agency, EPA-630-R-98-002F, Washington DC, USA.

U.S. EPA. 1999. Environmental Assessment of Proposed Effluent Limitations Guidelines and Standards for Synthetic-Based Drilling Fluids and other Non-Aqueous Drilling Fluids in the oil and Gas Extraction Point Source Category, U.S. Environmental Protection Agency, EPA-821-B-98-019, Washington DC, USA.

Verbeek, P.H.J. and Brouwers, J.J.H. 1986. Approximate Formulae for Response of Slender Risers in Deep Water. *International Journal of Shipbuilding Progress.*1: 22-37.

Waldman, G.D., Fannelop T., K., and Johnson, R. A. 1972. Spreading and Transport of Oil Slicks on the Open Ocean. OTC 1548.

Wirsching, P. H., and Light, M. C. 1980. Fatigue Under Wide Band Random Stresses. *Journal of the Structural Division, ASCE,* 106: 1593-1607.

Wirsching, P.H. 1984. Fatigue Reliability for Offshore Structures. *Journal of Structural Engineering*, ASCE, 110: 2340-2356.

Wirsching, P.H. and Chen, Y.N. 1988. Considerations of Probability-Based Design for Marine Structures. *Marine Structures*. 1: 23-45.

Yang, W. C., and Wang, H. 1977. Modelling of Oil Evaporation in Aqueous Environment. *Water Research*, 11: 879-887.

Yapa, P. D., and Zheng, L. 1997. Simulation of Oil Spills from Underwater Accidents I: Model Development. *Journal of Hydraulic Research*, 35(5): 673-687.

Yapa, P. D., and Zheng, L. 1997a. Simulation of Oil Spills from Underwater Accidents II: Model Verification. *Journal of Hydraulic Research*, 35(5): 673-687.

Yapa, P.D., Zheng, L., and Nakata, K. 1999. Modeling Underwater Oil/Gas Jets and Plumes. *Journal of Hydraulic Engineering*, 125: 481-491.

Zheng, L., Yapa, P.D., and Chen, F. 2002. A Model for Simulating Deepwater Oil and Gas Blowouts – Part I: Theory and Model Formulation. *Journal of Hydraulic Research*, 41 (4): 339-351.

Appendix I

Selected Properties of a Lognormal Distribution and Hazard Rate Function

If k independent lognormal variables X_i, with parameters μ_i and σ_i, are multiplied such as:

$$T = \prod_{i=1}^{k} b_i X_i^{ai} \tag{A 1.1}$$

then T will also follow the lognormal distribution, by virtue of the reproductive property of the lognormal distribution, with the following parameters:

$$\mu = \sum_{i=1}^{k} \ln(b_i) + \sum_{i=1}^{k} a_i \mu_i \tag{A 1.2}$$

$$\sigma^2 = \sum_{i=1}^{k} a_i^2 \sigma_i^2 \tag{A1.3}$$

where

μ = mean of a lognormal distribution

σ^2 = variance of a lognormal distribution

a_i = constant

b_i = constant

The mean $\mu_1'(X)$, variance $\mu_2(X)$, and coefficient of variance $cv(X)$, of a lognormal variable (X) can be given respectively by:

$$\mu_1'(X) = \exp\left(\mu + \frac{\sigma^2}{2}\right) \tag{A 1.4}$$

$$\mu_2(X) = \exp\left(2\mu + \sigma^2\right)\left[\exp(\sigma^2) - 1\right] \tag{A 1.5}$$

$$cv(X) = \sqrt{\exp(\sigma^2) - 1} \tag{A 1.6}$$

A well fitted statistical distribution with the life data of a product can be used to model the time to failure. In this context, the *hazard function* becomes a unique and significant characteristic of a life model. The hazard function expresses the conditional likelihood of failure during the time interval t to $t + dt$ as $dt \to 0$, mathematically:

$$P(t < T \le t + dt \mid T > t) = \frac{P(t < T \le t + dt)}{P(T > t)} \tag{A 1.7}$$

The condition in the above expression is that the failure has not occurred prior to time t. The conditional probability equation can also be written as:

$$h(t) = \frac{f_T}{R_e} \tag{A 1.8}$$

and

$$R_e = \int_t^{\infty} f_T dt \tag{A 1.9}$$

where

f_T = failure probability density function

R_e = reliability function

The possible general shape of $h(t)$ for the structure wear is given by a "bathtub curve" (see Figure A 1.1). The bathtub curve is comprised of three regimes: i) burn-in, ii) useful life, and iii) wear-out.

Burn-in failure is characterized by decreasing failure rate. This kind of failure is observed during the early life of the structure and is caused by manufacturing defects, poor quality control, etc. The useful life regime is characterized by constant failure rate and failure occurs at random during the useful life of the structure. The wear-out region is characterized by increasing failure rate. It corresponds to the end of the structure's life due to degradation processes (such as fatigue, corrosion, etc.).

If the lognormal distribution is advocated as a life model, then substitution of the lognormal probability density and reliability functions into Equation (A 1.8) yields the following expression:

$$h(t) = \frac{\frac{1}{t\sigma}\phi\left(\frac{\ln(t)-\mu}{\sigma}\right)}{\Phi\left(-\frac{\ln(t)-\mu)}{\sigma}\right)} \qquad \text{(A 1.9)}$$

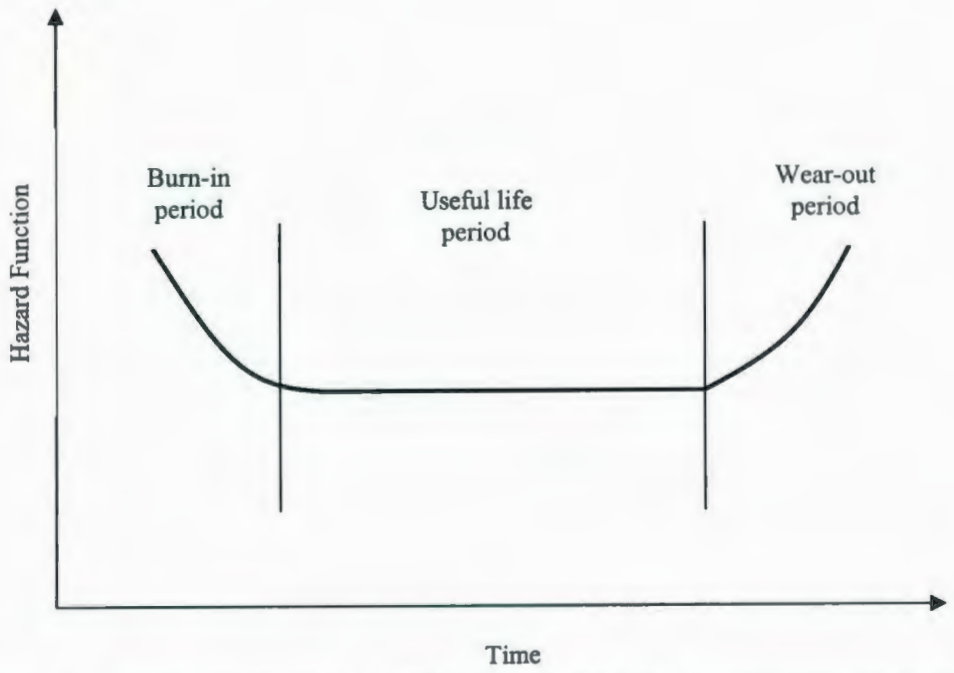

Figure A 1.1 Typical variation of hazard function with age of structure—a bathtub curve

Appendix II

Implementation of Special Functions in MATLAB

The implementation of special functions used in Equations (3.18) and (3.46) in MATLAB is discussed here. Equation (3.18) involves three functions: Gamma function, $\Gamma(x)$; lower Gamma function, $\gamma(a,x)$; and upper Gamma function, $\Gamma(a,x)$. The Gamma function $\Gamma(x)$ is prescribed mathematically as:

$$\Gamma(x) = \int_0^{\infty} t^{(x-1)} \exp(-t)dt \qquad \text{(A 2.1)}$$

It is calculated in MATLAB by calling the built in function 'gamma (x)'. The lower Gamma function $\gamma(a,x)$ can be given as:

$$\gamma(a,x) = \int_0^{x} t^{(a-1)} \exp(-t)dt \qquad \text{(A 2.2)}$$

The function $\gamma(a,x)$ is implemented in MATLAB using the function 'gammainc (x,a)'.

The gammainc (x,a) is defined as:

$$\text{gammainc(x,a)} = 1 \,/\, \text{gamma(a)} * \int_0^{x} t^{(a-1)} \exp(-t)dt \qquad \text{(A 2.3)}$$

Therefore, the MATLAB coding for calculating $\gamma(a,x)$ is:

L = gamma(a)*gammainc(x,a) (A 2.4)

where L represents lower gamma function.

Finally, the upper gamma function $\Gamma(a,x)$ can be implemented in MATLAB as:

U = gamma(a)*L (A 2.5)

where U denotes upper gamma function.

For the lognormal distribution the probability of failure in Equation (3.46) is calculated in MATLAB using the error function (erf) as follows:

$$P_f = \frac{1}{2}\left[1 + erf\left(\frac{\ln \hat{D} - \mu_{\ln \hat{\Delta}}}{\sigma_{\ln \hat{\Delta}}\sqrt{2}}\right)\right] \qquad \text{(A 2.6)}$$

Appendix III

Area Growth for the *Surface Tension-Viscous* Phase

The radius of a spill (R_s) in the *surface tension-viscosity* phase is given as (Fay, 1971; Hoult , 1972; and Waldman *et al.*, 1972):

$$R_s = 1.6\left(\frac{s_t}{\rho}\right)^{\frac{1}{2}} \nu^{-\frac{1}{4}} t^{\frac{3}{4}} \qquad \text{(A 3.1)}$$

where

s_t = oil-water interfacial tension $[N/m]$

ρ = density of sea water $[Kg/m^3]$

ν = kinematic viscosity $[m^2/s]$

t = time $[s]$

$\left(\frac{s_t}{\rho}\right)^{\frac{1}{2}} \nu^{-\frac{1}{4}} = 0.094 \ (m/s^{3/4})$ (Fannelop and Sjoen, 1980)

Equation (A 3.1) becomes:

$$R_s = 0.15(m/s^{3/4})t^{\frac{3}{4}} \qquad \text{(A 3.2)}$$

where the constant 0.15 has dimensions of $(m/s^{3/4})$. The dimensions of a constant warrant a dimensionally homogeneous equation.

The area of a circular spill is:

$$A_s = \pi\left(0.15(m/s^{3/4})t^{\frac{3}{4}}\right)^2 \qquad \text{(A 3.3)}$$

$$A_s = 0.0707(m^2/s^{3/2})t^{\frac{3}{2}} \quad \text{(A 3.4)}$$

The rate of change of the slick area is prescribed as:

$$\frac{dA_s}{dt} = 0.106(m^2/s^{3/2})t^{\frac{1}{2}} \quad \text{(A 3.5)}$$

or

$$\left[\frac{dA_s}{dt}\right]^3 = 0.0012(m^6/s^{9/2})t^{\frac{3}{2}} \quad \text{(A 3.6)}$$

or alternatively,

$$\left[\frac{dA_s}{dt}\right]^3 = 0.0168(m^4/s^3)\left(0.0707(m^2/s^{3/2})t^{\frac{3}{2}}\right) \quad \text{(A 3.7)}$$

The bracket term on the right hand-side of the above equation is the slick area as given by Equation (A 3.4).

$$\left[\frac{dA_s}{dt}\right]^3 = 0.0168(m^4/s^3)A_s \quad \text{(A 2.8)}$$

Finally, the spreading expression in terms of change in area as a function of the actual area is expressed as:

$$\frac{dA_s}{dt} = 0.256(m^{4/3}/s)A_s^{\frac{1}{3}} \quad \text{(A 3.9)}$$

Appendix IV

Initial Condition for a Bubble Jet

McDougall (1978) prescribed the following expressions to calculate the initial radius (b_o) and vertical velocity (w_o) of a bubble jet:

$$b_o = 2\alpha_o z_o \left[\begin{array}{l} 0.6 + 0.01719\left(\frac{z_o}{AH}\right)^{\frac{1}{3}} - 0.002527\left(\frac{z_o}{AH}\right)^{\frac{2}{3}} + \\ \frac{z_o}{H}\left(-0.04609 + 0.00003131A^{-1}\right) + \ldots \end{array} \right] \tag{A 4.1}$$

$$w_o = w_b(\beta^2+1)\alpha_o z_o \left(\frac{AH}{z_o}\right)^{\frac{1}{3}} \left[\begin{array}{l} 1.99 - 0.3195\left(\frac{z_o}{AH}\right)^{\frac{1}{3}} + 0.06693\left(\frac{z_o}{AH}\right)^{\frac{2}{3}} + \\ \frac{z_o}{H}\left(0.4536 - 0.0105A^{-1}\right) + \ldots \end{array} \right] \tag{A 4.2}$$

$$A = \frac{Q_{gas} P_a (\beta^2+1)}{4\pi\alpha_o^2 \rho_a H^2 \left[w_b(\beta^2+1)\right]^3} \tag{A 4.3}$$

$$H = water\ depth + 10.2\ [m] \tag{A 4.4}$$

in which subscript 'o' corresponds to initial values, α_o = initial shear entrainment coefficient (a value of 0.083 is used after Yapa and Zheng, 1997), z_o = vertical coordinate of a point close to the source ($\cong 0.025H$), P_a = atmospheric pressure, and the remainder of the parameters are as defined in Table 5.1.

McDougall (1978) used the Gaussian profile in developing the equations that calculate the initial values of radius and velocity. For the Lagrangian modelling approach, the initial radius and velocity values obtained from the Gaussian profile are converted to the equivalent top-hat radius and velocity profiles as explained in Chapter 5.

The initial bubble fraction (ε_o) within the bubble core is calculated by the following expression:

$$\varepsilon_o = \frac{Q_{gas} P_a}{\rho_a g (H - z_o) \pi \beta^2 b_o^2 (w_b + w_o)} \tag{A 4.5}$$

Similarly, for the initial oil fraction (f_o) in the liquid part:

$$f_o = \frac{Q_{oil}}{\pi b_o^2 w_o (1 - \beta^2 \varepsilon_o)} \tag{A 4.6}$$

the parameters used in Equations (A 4.5) and (A 4.6) are defined elsewhere in Chapter 5.

Appendix V

Finite Difference Discretization

Mass

$$\Delta m_{l(k)} = \rho_a Q_e \Delta t \tag{A 5.1}$$

$$m_{l(k+1)} = m_{l(k)} + \Delta m_{l(k)} \tag{A 5.2}$$

Temperature, salinity, concentration and density

$$I_{(k+1)} = \frac{m_{l(k)} I_{(k)} + \Delta m_{l(k)} I_a - \rho_a K 2\pi h_{(k)} (I_{(k)} - I_a)\Delta t}{m_{l(k+1)}} \tag{A 5.3}$$

$$\rho_{l(k+1)} = \rho(T_{k+1}, S_{k+1}, C_{k+1}) \tag{A 5.4}$$

$$\rho_{b(k+1)} = \frac{\rho_a g(H - z_{k+1}) + P_a}{R_g T_a} \tag{A 5.5}$$

Velocities (momentum equation)

horizontal

$$u_{(k+1)} = \frac{(m_{l(k)} + m_{b(k)}) u_{(k)} + u_a \Delta m_{l(k)}}{m_{l(k+1)} + m_{b(k+1)}} \tag{A 5.6}$$

lateral

$$v_{(k+1)} = \frac{(m_{l(k)} + m_{b(k)}) v_{(k)}}{m_{l(k+1)} + m_{b(k+1)}} \tag{A 5.7}$$

vertical

$$w_{(k+1)} = \frac{\left(\frac{\rho_a - \rho_l}{\rho_l}\right)_{(k+1)} m_{l(k+1)} g + \left(\frac{\rho_a - \rho_b}{\rho_b}\right)_{(k+1)} m_{b(k+1)} g}{m_{l(k+1)}} \tag{A 5.8}$$

Thickness and radius

$$h_{(k+1)} = \frac{\vec{V}_{(k+1)}}{\vec{V}_{(k)}} h_{(k)} \tag{A 5.9}$$

$$b_{(k+1)} = \sqrt{\frac{m_{l(k+1)}}{\rho_{l(k+1)} \pi (1 - \beta^2 \varepsilon) h_{(k+1)}}} \tag{A 5.10}$$

Location and orientation

$$x_{(k+1)} = x_k + u_{(k+1)} \Delta t \tag{A 5.11}$$

$$y_{(k+1)} = y_k + v_{(k+1)} \Delta t \tag{A 5.12}$$

$$z_{(k+1)} = z_k + w_{(k+1)} \Delta t \tag{A 5.13}$$

$$\Delta s_{(k+1)} = \left| \vec{V}_{(k+1)} \right| \Delta t \tag{A 5.14}$$

$$\phi_{(k+1)} = \tan^{-1} \frac{w_{(k+1)}}{\sqrt{\left(u_{(k+1)}^2 + v_{(k+1)}^2 \right)}} \tag{A 5.15}$$

$$\theta_{k+1} = \tan^{-1} \frac{v_{k+1}}{u_{k+1}} \tag{A 5.16}$$

$$\left| \vec{V}_{(k+1)} \right| = \sqrt{u_{(k+1)}^2 + v_{(k+1)}^2 + w_{(k+1)}^2} \tag{A 5.17}$$